博士学位論文

Molecular biological studies on temporal and spatial regulation of translation during oocyte maturation in mouse
（マウスの卵成熟過程における翻訳の時空間制御の分子生物学的研究）

武井　夏海

北海道大学大学院生命科学院

2021年3月

CONTENTS

ACKNOWLEDGMENTS

I express my sincere appreciation to Associate Prof. Tomoya Kotani for his invaluable advice and encouragement throughout the course of this study. I am deeply grateful to Drs. Masakane Yamashita, Asato Kuroiwa and Atsushi Kimura for helpful suggestion, discussion and practical guidance. I also heartily thank Mr. Shohei Kawamura for his help to progress this study. This work was partly performed in the Cooperative Research Project Program of the Medical Institute of Bioregulation, Kyushu University. Thanks are also duo to the members of the Kotani laboratory and all member of the laboratories of Reproductive and Developmental Biology for their cooperation and encouragement.

ABBREVIATION

3’UTR, 3’ untranslated region
AP, alkaline phosphatase
APC/C, anaphase-promoting complex/cyclosome
Bb, balbiani body
BCIP, 5-bromo-4-chloro-3-indolyl phosphate
CPE, cytoplasmic polyadenylation element
CPEB, CPE-binding element
CSF, cytoplasmic factor
DAZL, deleted in azoospermia-like
DDW, double distilled water
DIG, digoxigenin
DNP, dinitrophenyl
EB, extraction buffer
EBM, exon junction complex binding motif
Emi2, early meiotic inhibitor 2
FISH, fluorescence *in situ* hybridization
FMRP, fragile x mental retardation protein
FPKM, fragments per kilobase per million
GV, germinal vesicle
GVBD, germinal vesicle broke down
His, histidine
HRP, horseradish peroxidase
IP, immunoprecipitation
LDS, lithium dodecyl sulfate
MAKP, mitogen-activated protein kinase
MI, metaphase I
MIH, maturation-inducing hormone
MII, metaphase II
MO, morpholino oligo nucleotide
MPF, maturation/M-phase-promoting factor
NBT, nitro blue tetrazolium
OA, okadaic acid
PAT, poly(A) test
PB1, first polar body

PBE, pumilio-binding element
PGC, primordial germ cell
Plk, polo-like kinase
PMI, prometaphase I
PUF, Pumilio1 and Fem-3 mRNA-binding factor
Pum1, pumilio1
RT-PCR, reverse transcription PCR
SAC, spindle assembly checkpoint
Tdrd3, tudor domain containing protein 3
TSA, tyramide signal amplification
UBA, ubiquitin binding domain

GENERAL INTRODUCTION

Vertebrate oocytes are arrested at prophase of meiosis I (PMI) and accumulate translationally repressed mRNAs in the cytoplasm in order to promote meiosis and development (de Moor et al., 2005; Masui and Clarke, 1979; Winata and Korzh, 2018). These oocytes are unable to be fertilized and called immature oocytes. In response to hormones, immature oocytes resume the meiosis and are arrested at metaphase II (MII). This process is called oocyte maturation and is necessary to acquire fertility. After resumption of meiosis, such morphological changes as germinal vesicle breakdown (GVBD), chromosome condensation, spindle formation and first polar body extrusion are occurred. For proper progression of these events during oocyte maturation, not only the modification of proteins deposited in oocytes, but also the temporal translation of dormant mRNAs is required. However, the molecular and cellular mechanisms of temporal regulation of mRNA translation during oocyte maturation remain largely unknown. My aim in this thesis is to address the question how the translation of dormant mRNAs is regulated in periods specific to individual mRNAs.

In meiosis I, hundreds of mRNAs including those encoding key components of cell cycle such as cyclin B1, a regulatory subunit of maturation/M-phase-promoting factor (MPF), are regulated at the translational level in frog, zebrafish and mouse oocytes (Sagata et al., 1989; Furuno et al., 1994; Tanaka and Yamashita, 1995; Hochegger et al., 2001; Kondo et al., 2001; Chen et al., 2011; Gaffre et al., 2011; Horie and Kotani, 2016; Kotani et al., 2013; Luong et al., 2020). cyclin B1 is synthesized after initiation of oocyte maturation and immediately function in meiosis I. In contrast to these mRNAs, the translation of more than one thousand mRNAs, such as *Wee1* and *Emi2* mRNAs, was shown to be activated in meiosis II (Nakajo et al., 2000; Madgwick et al., 2006; Inoue et al., 2007; Tung et al., 2007; Suzuki et al., 2010; Chen et al., 2011; Luong et al., 2020). The timing of the translation is important to correctively progress meiosis. For instance, it was shown that precocious synthesis of cyclin B1 induced precocious activation of MPF, resulting in defects in spindle formation and chromosome segregation in frog and mouse oocytes (Davydeko et al., 2013; Kotani and Yamashita, 2002).

One of the mechanisms promoting translational activation of dormant mRNAs has been shown to rely on *cis*-acting elements. The *cis*-acting element-mediated cytoplasmic polyadenylation of mRNAs drives translational activation of mRNAs (McGrew et al., 1989; Sheets et al., 1994). The cytoplasmic polyadenylation element (CPE) locates on the 3' untranslated region (3'UTR) of thousands of mRNAs in oocytes

(Chen et al., 2011), and CPE-binding protein (CPEB) functions in both repression and direction of the cytoplasmic polyadenylation (Barkoff et al., 2000; de Moor and Richter, 1999; Gebauer et al., 1994; Tay et al., 2000). In addition, deleted in azoospermia-like (DAZL) protein has been shown to be a translational repressor and activator in moues oocytes (Chen et al., 2011; Yang et al., 2020). The DAZL protein increases during oocyte maturation and cooperates with CPEB1 in regulating translation of maternal mRNAs, which is mediated by the DAZL-binding element on their 3'UTR. In addition, CPEB4 replaces CPEB1 to sustain cytoplasmic polyadenylation in frog oocytes in meiosis II (Igea and Mendez, 2010). Although, more than one thousand maternal mRNAs contain these elements, individual mRNAs are translated at different timings during oocyte maturation, suggesting that the other mechanisms regulate the timings of translation of distinct mRNAs. However, the detailed mechanisms by which translational timings of various dormant mRNAs are coordinated remain unclear.

A previous study reported that cyclin B1 mRNA forms RNA granules in immature oocytes of zebrafish and mouse (Kotani et al., 2013). These RNA granules disassemble at the timing of translational activation during oocyte maturation (Kotani et al., 2013; Nukada et al., 2015; Horie and Kotani, 2016). In addition, the formation of cyclin B1 RNA granules required the binding of pumilio1 (Pum1), which is a sequence-specific RNA binding protein and highly conserved in eukaryotes. Pum was shown to repress the translation of target mRNAs in a spatially and temporally regulated manner (Murata and Wharton, 1995; Asaoka-Taguchi et al., 1999). Binding of Pum1 was shown to be required for the RNA granule formation, implying that Pum1 regulates the translational timing of target mRNAs through formation and disassembly of granules (Kotani et al., 2013).

To address detailed mechanisms of temporal regulation of translation, I first established a method to detect mRNAs with high-sensitivity and high-resolution using tyramide signal amplification (TSA) system in chapter I. In chapter II, I identified *Mad2* (also as known *Mad2/1*) mRNA as one of the Pum1-target mRNAs in mouse. Mad2 has been shown to function as a component of spindle assembly checkpoint in meiosis I of mouse oocytes (Homer et al., 2005), and the translation of *Mad2* mRNA was regulated during oocyte maturation in a way similar to that of cyclin B1 mRNA. I described the mechanisms of translational regulation, which were mediated by RNA granules and Pum1 in meiosis I.

The mechanisms of translational regulation in meiosis II remain unclear, compared with that in meiosis I. EMI2 is one of the proteins expressed in meiosis II. EMI2 protein is a component of cytostatic factor and contributes to arrest the meiosis at metaphase II

during oocyte maturation. Previous studies showed that reduction of EMI2 released oocytes from MII arrest and the expression of EMI2 in MI induced MI arrest (Shoji et al., 2006; Madgwick et al., 2006; Inoue et al., 2007; Suzuki et al., 2010), indicating that the translation of *Emi2* mRNA is strictly regulated during oocyte maturation. Previous study using *Xenopus* oocytes has shown that the temporal translation of *Emi2* mRNA was regulated by the 3'UTR (Tung et al., 2007). Although the timing of EMI2 expression is important for progression of oocyte maturation and embryonic development, the mechanisms of translational regulation largely remain to be elucidated. In chapter III, I focused on the mechanisms of translational regulation of *Emi2* mRNA to understand the temporal regulation of translation in meiosis II. *Emi2* mRNA was shown to form RNA granules, and the translational activation of *Emi2* mRNA was coincided with the disassembly of RNA granules, resembling the regulation of cyclin B1 mRNA. Furthermore, the specific protein which regulates the temporal translation of *Emi2* mRNA was identified. I present that the specific proteins which are components of each RNA granule contribute to the regulation of temporal translation.

Chapter I

High-sensitivity and high-resolution *in situ* hybridization of mRNAs in vertebrate ovaries

INTRODUCTION

Localization of mRNAs at subcellular regions plays fundamental roles in spatial and temporal gene expression in many organisms from yeast to mammals (Kloc et al., 2002; Johnston, 2005; Martin and Ephrussi, 2009; Buxbaum et al., 2015; Kotani et al., 2017). The standard methods for studying mRNA expression and localization in cells, tissues and organs are *in situ* hybridization techniques (Harrison et al., 1973; Cox et al., 1984). Conventional *in situ* hybridization methods are generally based on probing each target mRNA with RNA probes labeled with biotin, digoxigenin (DIG) or fluorescein, followed by the detection of probes by specific antibodies and enzymatic reactions. However, detection of mRNA localization remains difficult because the expression levels of many mRNAs are low and the expression of such mRNAs in a single cell cannot be detected by conventional methods.

Amplification of signals in conventional *in situ* hybridization methods by using a tyramide signal amplification (TSA) system has facilitated the identification of mRNAs localized at specific subcellular regions in embryos and cultured cells (Lecuyer et al., 2007; Wilk et al., 2016; Mingle et al., 2005; Mingle et al., 2009; Raap et al., 1995). Those studies revealed that thousands of mRNAs are localized at subcellular regions during embryogenesis and in third instar larval tissues in *Drosophila* (Lecuyer et al., 2007; Wilk et al., 2016) and that all seven mRNAs examined are localized within the cytoplasm of cultured chicken cells (Mingle et al., 2005). In addition, cell biological and biochemical analyses have shown that approximately 50 mRNAs are localized in cell protrusions during migration of cultured mouse cells (Mili et al., 2008) and that 5-10% of mRNAs are localized to microtubules in *Xenopus* eggs and human cultured cells (Blower et al., 2007). Accumulated evidence has shown that localization of mRNAs is a main regulatory mechanism of gene expression in cells. In contrast to *Drosophila* embryos and cultured mammalian cells which enable detection of mRNAs in whole-mount *in situ* hybridization, techniques for detection of mRNAs with high sensitivity and high resolution have not been established for vertebrate adult tissues and organs because of their large size, which prevents detection of mRNAs in deep layers when using distinct organs in whole.

A single-molecule fluorescent *in situ* hybridization (smFISH) method is based on probing each mRNA with 50-100 singly labeled oligonucleotide probes of length 20 bases (Raj et al., 2008). This technique can be combined with frozen and paraffin sections (Itzkovitz et al., 2011; Chandrakesan et al., 2015). However, preparation of 50-100 different oligonucleotides and labeling them with fluorophores are laborious and

resource intensive, particularly for detecting a large number of different target mRNAs. RNAscope is a novel *in situ* hybridization method, which is based on a series of hybridization events with approximately 20 pairs of branched oligonucleotide probes and enables detection of mRNAs with high-sensitivity (Wang et al., 2012). However, preparation of 20 pairs of branched oligonucleotide probes for target mRNAs is not inexpensive. Establishment of a method such as *in situ* hybridization with the TSA system combined with paraffin sections allows convenient and cost-effective preparation of probes, which are the same with those used in conventional *in situ* hybridization methods, and enables highly sensitive detection of RNAs by using differently labeled tyramide molecules in single cells at subcellular levels while preserving tissue and cell morphology.

In this study, I examined the expression and subcellular localization of mRNAs known to play important roles in oogenesis and embryogenesis. I first examined the expression of *Pou5f1/Oct4* mRNA in mouse ovaries by making paraffin sections and performing *in situ* hybridization using the TSA system. Although the expression of this transcript in the adult ovary has not been reported, I clearly showed *Pou5f1/Oct4* mRNA expression in mouse oocytes. I then examined the subcellular localization of *mos*, *cyclin B1* and *dazl* mRNAs in zebrafish ovaries. During zebrafish oogenesis, *mos*, *cyclin B1* and *dazl* mRNAs are accumulated as translationally repressed forms and are known to be localized at the animal or vegetal polar cytoplasm of the oocyte (Kondo et al., 1997; Kondo et al., 2001; Yasuda et al., 2010; Yasuda et al., 2013; Kotani et al., 2013; Horie and Kotani, 2016; Maegawa et al., 1999; Suzuki et al 2009). Double fluorescence *in situ* hybridization with the TSA system showed some similarities and many differences in distribution patterns of these mRNAs at subcellular levels in the oocyte cytoplasm. My method also showed detailed distribution patterns of *Cyclin B1* and *Dazl* mRNAs in mouse ovaries. Thus, my method enables detection of mRNAs in vertebrate tissues and organs with high-sensitivity and high-resolution while maintaining tissue and cell morphology in a cost-effective manner and can facilitate studies of the localization of RNAs at subcellular levels.

MATERIALS AND METHODS

Animals

All animal experiments in this study were approved by the Committee on Animal Experimentation, Hokkaido University. ICR mice (CLEA-Japan Inc.) were maintained

on a 14 h light/ 10 h dark cycle at 25℃ with free access to food and water.

Isolation and fixation of ovaries

Zebrafish ovaries were dissected from adult females in zebrafish Ringer's solution (116 mM NaCl, 2.9 mM KCl, 1.8 mM $CaCl_2$, and 5 mM HEPES; pH 7.2). The ovaries were further dissected into several pieces (5-10 mm in diameter) with forceps under a SZ-ST dissecting microscope (Olympus). Mouse ovaries were dissected from 8-week-old females in phosphate buffered saline (PBS: 137 mM NaCl, 2.7 mM KCl, 10 mM Na_2HPO_4, and 2 mM KH_2PO_4; pH 7.2). Ovaries of zebrafish and mice were fixed with 4% paraformaldehyde in PBS (4% PFA/PBS) for 3 h to overnight at 4˚C and then washed with PBS three times.

Slide coating

For paraffin sections, glass slides were coated with gelatin as follows. Gelatin powder (Wako Pure Chemical Industries, Ltd.) was dissolved in double distilled water (DDW) at 60˚C. Microscope glass slides (Matsunami Glass Industries, Ltd.) were incubated with 0.5% gelatin in DDW containing 0.05% $CrK(SO_4)_2$ for 15 min. Then the slides were dried and stored. Reagents used in this study are listed in Table 1.

Paraffin sections

For paraffin embedding, the samples were dehydrated first with an amphipathic solvent and then with hydrophobic solvents as follows. Unless otherwise mentioned, incubation steps were performed at room temperature. Fixed ovaries of zebrafish (Fig. 1A) and mice (Fig. 1B) were dehydrated with 70%, 80%, 90%, 95%, and 99% ethanol each for 15 min with gentle shaking. Incubation with 99% ethanol was performed twice. Then the samples were incubated with isoamyl acetate (Wako Pure Chemical Industries, Ltd.) for 15 min with gentle shaking. This process was performed twice. Samples can be held for several days in this solvent. Before embedding, the samples were incubated with Lemosol (Wako Pure Chemical Industries, Ltd.) for 15 min with gentle shaking. This process was performed twice. Notably, incubation with isoamyl acetate makes samples to be easily cut into thin sections, particularly in the case of zebrafish oocytes, which contain large amounts of yolks. Alternatively, isoamyl acetate and Lemosol incubation can be replaced by incubation with xylene. Then the samples were placed in paraffin (Fisher Scientific; melting point, 56-57˚C) previously melted at about 60˚C in a dish and incubated at about 60˚C for 15 min on a NHP-1 hot plate (Iuchi). This process was repeated three times by transferring the samples to different dishes containing melted

paraffin, using glass pipets or forceps. Finally, the samples were embedded in freshly prepared paraffin and immediately cooled on ice until the paraffin was completely set.

The embedded zebrafish ovaries were cut into 5-µm-thick sections for detecting mRNA distribution in stage I oocytes and 9-12-µm-thick sections for detecting signals in later stage oocytes using a LR-85 microtome (Yamato Kohki Industrial Co., Ltd.). The embedded mouse ovaries were cut into 8-10-µm-thick sections. The sections were floated on DDW prepared on gelatin-coated glass slides. The slides were then incubated on a HI1220 flattening table (Leica Biosystems) at 42˚C to flatten the sections until the slides were completely dried.

Solution preparation

For *in situ* hybridization, stock solutions were prepared as follows. 20× saline-sodium citrate (20× SSC: 3 M NaCl, 300 mM sodium citrate; pH 7.0) was autoclaved and stored. Torula RNA (Sigma) was dissolved in DDW at 50˚C and purified by phenol-, phenol-chloroform-, and chloroform-extraction. The RNA was precipitated, dissolved in DDW (10 mg/ml) and stored at -20˚C. 20× Denhardt's solution was prepared by dissolving Ficol-400 (0.4%), polyvinylpyrrolidone (0.4%) and bovine serum albumin (0.4%) in DDW and was stored at -20˚C.

Probe preparation

Digoxigenin (DIG)- and fluorescein-labeled RNA probes were prepared by *in vitro* transcription with RNA polymerases and plasmid vectors containing target transcript sequences. One µg of linearized plasmid DNAs was used as a template, and RNA probes were synthesized with SP6, T7 or T3 RNA polymerase (Roche) and DIG or Fluorescein RNA Labeling Mix (Roche) for 2-3 h at 37˚C. After precipitation with ethanol and lithium chloride, the RNA probes were dissolved in DDW. After determining the concentrations, the RNA probes were diluted (50 ng/µl) with probe dilution buffer (50% formamide, 5× SSC, 0.1% Tween-20) containing torula RNA (5 mg/ml) and were stored at -20˚C.

In this study, I prepared 8 DIG-labeled antisense and sense RNA probes for the full lengths of mouse *Pou5f1/Oct4* and zebrafish *cyclin B1* gene transcripts and for the parts of zebrafish *dazl* and mouse *Dazl* gene transcripts (Table 2). In addition, I prepared 6 fluorescein-labeled antisense and sense RNA probes for the full lengths of zebrafish *mos*, zebrafish *cyclin B1*, and mouse *Cyclin B1* gene transcripts (Table 2).

Rehydration and proteinase K stimulation

The sections of ovaries on glass slides were incubated with xylene for 5 min to remove paraffin. This process was performed once more. After removing xylene with 99% ethanol, the sections were rehydrated with 70% ethanol and PBS each for 2 min. The incubation with PBS was performed twice. When tissues of interest possess endogenous peroxidase activity, samples can be incubated with 1% H_2O_2 for 15-60 min to quench the activity. In this study, I did not quench the samples of ovaries. Then the sections were treated with 1% Triton-X100 in PBS for 5 min. After washing with PBS twice, the sections were treated with 0.2N HCl for 5 min. After washing again with PBS twice, the sections were incubated with 1 μg/ml Proteinase K (Sigma) in PBS at 37˚C for 5 min. The sections were washed again with PBS twice and fixed with 4% PFA/PBS for 5 min, followed by incubation with 100 mg/ml glycine in PBS for 15 min. The incubation with glycine was performed twice. Then the sections were incubated with a prehybridization buffer for sections (70% formamide, 2× SSC) for 60 min.

Hybridization

The sections of ovaries were hybridized with a mixture of 0.25-2 ng/μl of the fluorescein- and/or DIG-labeled RNA probes in hybridization mix solution (70% formamide, 20 mM Tris-HCl; pH 8.0, 2.5 mM EDTA, 1X Denhardt's solution, 30 mM NaCl, 1 mg/ml torula RNA) containing 10% dextran sulfate at 45˚C overnight in a moisture chamber. During this incubation, the sections were covered with Parafilm. The probe concentrations depended on the probes and expression levels of transcripts (see the Results section). After incubation, the parafilm was removed in 5× SSC at 50˚C. The sections were then washed with 50% formamide in 2× SSC at 50˚C for 30 min. After incubation with TNE (10 mM Tris, 500 mM NaCl, 1 mM EDTA; pH 7.5) at 37˚C for 10 min, the sections were incubated with 20 μg/ml RNase A (Sigma) in TNE at 37˚C for 30 min to reduce nonspecific background signals (Cox et al., 1984). Then the sections were washed with TNE at 37˚C for 10 min, 2× SSC at 50˚C for 20 min, and 0.2× SSC at 50˚C for 20 min. The incubation with 0.2× SSC was performed twice. Then, the sections were incubated with TNT (100 mM Tris, 150 mM NaCl, 0.5% Tween-20; pH 7.5) at least for 5 min.

Detection of DIG- and fluorescein-labeled RNA probes

Single *in situ* hybridization of mRNA encoding *Pou5f1/Oct4* in mouse ovaries was performed as follows. After hybridization with the DIG-labeled *Pou5f1/Oct4* RNA probes as described above, the sections were blocked with a blocking buffer (0.5%

blocking reagent (PerkinElmer, Inc), 100 mM Tris, 150 mM NaCl; pH 7.5) for 30 min in a moisture chamber. Then the sections were treated with anti-DIG-horseradish peroxidase (HRP) antibody (Roche) (1:500 dilution in blocking buffer) for 30 min in a moisture chamber. After washing with TNT three times, the sections were treated with tyramide-dinitrophenyl (DNP) (PerkinElmer, Inc.) (1:50 dilution in 1× Plus Amplification Diluent (PerkinElmer, Inc.), followed by dilution with an equal volume of DDW) for 20 min in a moisture chamber. After washing again with TNT three times, the samples were treated for 30 min with anti-DNP-alkaline phosphatase (AP) antibody (PerkinElmer, Inc.) (1:500 dilution in blocking buffer) in a moisture chamber. The samples were washed with TNT three times. After washing with a staining buffer (100 mM Tris, 100 mM NaCl, 50 mM $MgCl_2$; pH 9.5), the samples were reacted with mixture of 225 μg/ml of nitro blue tetrazolium (NBT) and 175 μg/ml of 5-bromo-4-chloro-3-indolyl phosphate (BCIP) in staining buffer in a moisture chamber. The reaction was stopped with a stop solution (10 mM Tris, 1 mM EDTA; pH 8.0). The samples were then mounted with glycerol and observed under an Axioskop microscope (Carl Zeiss).

Double fluorescence *in situ* hybridization of mRNAs encoding Mos and Cyclin B1 in zebrafish ovaries was performed as follows. After hybridization with fluorescein-labeled *mos* RNA probes and DIG-labeled *cyclin B1* RNA probes, the sections were blocked with the blocking buffer for 30 min in a moisture chamber. The sections were then treated with anti-Fluorescein-HRP antibody (Roche) (1:200 dilution in blocking buffer) for 30 min in a moisture chamber. After washing with TNT three times, the sections were treated with tyramide-Cy3 (PerkinElmer, Inc.) (1:50 dilution in 1× Plus Amplification Diluent, followed by dilution with an equal volume of DDW) for 20 min in a moisture chamber. The samples were washed again with TNT three times and then treated with 1% H_2O_2 in PBS for 15-60 min for inactivating HRP. When the amount of target transcripts was large and HRP could not be inactivated by this treatment, the samples were dehydrated with methanol, treated with 1% H_2O_2 in methanol for 30 min, and rehydrated with PBS. After washing with PBS twice, the sections were blocked with blocking buffer for 30 min in a moisture chamber. Then the samples were incubated with anti-DIG-HRP antibody (Roche) (1:500 dilution in blocking buffer) for 30 min in a moisture chamber. After washing with TNT three times, the sections were treated with tyramide-Fluorescein (PerkinElmer, Inc.) (1:50 dilution in 1× Plus Amplification Diluent, followed by dilution with an equal volume of DDW) for 20 min in a moisture chamber. The samples were then washed with TNT three times.

Double fluorescence *in situ* hybridization of mRNAs encoding Cyclin B1 and Dazl

in zebrafish and mouse ovaries was performed as follows. After hybridization with fluorescein-labeled *cyclin B1* RNA probes and DIG-labeled *dazl* RNA probes, the sections were blocked with blocking buffer for 30 min in a moisture chamber. The sections were then treated with anti-DIG-HRP antibody (Roche) (1:500 dilution in blocking buffer) for 30 min in a moisture chamber. After washing with TNT three times, the sections were treated with tyramide-DNP (1:50 dilution in 1× Plus Amplification Diluent, followed by dilution with an equal volume of DDW) for 20 min in a moisture chamber. After washing three times with TNT, the samples were treated overnight with anti-DNP-Alexa 488 antibody (Molecular Probes) (1:500 dilution in blocking buffer) in a moisture chamber. The samples were washed with TNT three times and then dehydrated with methanol, treated with 1% H_2O_2 in methanol for 30 min for inactivating HRP, and rehydrated with PBS. After washing with PBS twice, the sections were blocked with the blocking buffer for 30 min in a moisture chamber. Then the samples were incubated with anti-Fluorescein-HRP antibody (1:200 dilution in blocking buffer) for 30 min in a moisture chamber. After washing with TNT three times, the sections were treated with tyramide-Cy3 (1:50 dilution in 1× Plus Amplification Diluent, followed by dilution with an equal volume of DDW) for 20 min in a moisture chamber. The samples were then washed with TNT three times.

Hoechst staining and mounting

To detect nuclei, the samples were incubated with 10 μg/ml Hoechst 33258 for 10 min. After being mounted with a Prolong Antifade Kit (Molecular probes) or Fluoro-KEEPER Antifade Reagent (Nacalai Tesque), the samples were observed under a LSM5LIVE confocal microscope (Carl Zeiss).

Hematoxylin and eosin (HE) staining

To observe tissue and cell morphology, the sections of mouse and zebrafish ovaries were stained with hematoxylin and eosin. After rehydration as described above, the sections were washed with running water for 5 min and incubated with hematoxylin staining solution for 2 min. After being washed with running water 30 min, the sections were incubated with eosin staining solution 30 seconds. The sections were then washed with running water 3 min, dehydrated with 70%, 80%, 90%, 95%, and 99% ethanol each for 1 min and incubated with xylene for 1 min. The samples were then mounted with a mounting medium MGK-S (Matsunami Glass Industries, Ltd.) and observed under the Axioskop microscope.

RESULTS

Detection of *Pou5f1/Oct4* mRNA in the mouse ovary

Vertebrate oocytes of many species are arrested at prophase I of the meiotic cell cycle and accumulate large numbers of maternal factors including mRNAs during their growth. *Pou5f1/Oct4* mRNA encodes a transcriptional factor essential for mouse embryogenesis (Scholer et al., 1989; Nichols et al., 1998). This transcript is also necessary for maintenance or acquisition of pluripotency in embryonic stem (ES) cells or induced pluripotent stem (iPS) cells (Jaenisch and Young, 2008). The expression of *Pou5f1/Oct4* mRNA is less abundant in oocytes (Wu et al, 2013) and has not been detected by *in situ* hybridization methods. I examined the expression of *Pou5f1/Oct4* mRNA in mouse adult ovaries by making paraffin sections and performing *in situ* hybridization with or without the TSA system. Hybridization of 10 μm-thick mouse ovary sections with 1 ng/μl of the antisense *Pou5f1/Oct4* RNA probe showed no signal (Fig. 2A) as in the sections hybridized with 1 ng/μl of the sense *Pou5f1/Oct4* RNA probe (Fig. 2B) in a conventional *in situ* hybridization method without the TSA system. In contrast, the same hybridization procedure detected the expression of *Pou5f1/Oct4* mRNA in oocytes when the signals were amplified with the TSA system (Fig. 2C). Hybridization with the sense *Pou5f1/Oct4* RNA probe showed no signal (Fig. 2D). The tissue and cell morphology of mouse ovaries was observed by HE staining (Fig. 3). My method is highly reproducible because similar results were constantly obtained from three independent experiments (data not shown). These results indicate that *in situ* hybridization with the TSA system is highly sensitive and that *Pou5f1/Oct4* mRNA is specifically expressed in oocytes of mouse ovaries.

Subcellular localization of *mos* and *cyclin B1* mRNAs in the zebrafish ovary

I next examined the localization of *mos* and *cyclin B1* mRNAs simultaneously in zebrafish adult ovaries by making paraffin sections and performing double fluorescence *in situ* hybridization with the TSA system. *mos* mRNA encodes a kinase activating the mitogen-activated protein kinase (MAPK) pathway (Sagata et al., 1989), and *cyclin B1* mRNA encodes a regulatory subunit of maturation/M-phase-promoting factor (MPF) (Nurse, 1990). These mRNAs are accumulated in the animal polar cytoplasm of zebrafish oocytes as a translationally repressed form (Kondo et al., 2001; Yasuda et al., 2010; Kotani et al., 2013; Horie and Kotani, 2016; Suzuki et al., 2009; Tay et al., 2000).

Hybridization of 12 μm-thick zebrafish ovary sections with 1 ng/μl of the fluorescein-labeled antisense *mos* RNA probe and 0.25 ng/μl of the DIG-labeled

antisense *cyclin B1* RNA probe, followed by amplification of signals using the TSA system, showed bright signals at the animal polar cytoplasm beneath the micropyle, a structure through which a sperm enters into the oocyte cytoplasm (Fig. 4A-C). In contrast, hybridization with the same concentrations of sense probes showed no signal (data not shown). Since the expression level of *mos* mRNA is low, hybridization with low concentrations of the *mos* RNA probe (less than 1 ng/μl) resulted in low levels of signals. In contrast, a reduction in the concentration of *cyclin B1* RNA probe (less than 1 ng/μl) did not affect the levels of specific signals but reduced nonspecific signals probably due to the high levels of *cyclin B1* mRNA expression. In conclusion, the low concentration of the *cyclin B1* RNA probe (0.25 ng/μl) resulted in highly specific and less background signals. High resolution imaging of these two mRNAs showed that both mRNAs formed large granules in the animal polar cytoplasm of oocytes (Fig. 4D-F). However, the granules of *mos* mRNA were different from those of *cyclin B1* mRNA. The *mos* RNA granules barely co-localized with the *cyclin B1* RNA granules (3.9%, n = 282). Similar subcellular localization patterns of *mos* and *cyclin B1* mRNAs were observed in all oocytes of two independent experiments (data not shown). The tissue and cell morphology of zebrafish ovaries was observed by HE staining (Fig. 3B-D). These results clearly showed the different distribution of *mos* and *cyclin B1* mRNAs although both mRNAs are localized at the same cytoplasmic regions. These results also showed the advantage of my method that enabled staining of distinct mRNAs without overlapping signals in the detection of distinct probes.

Subcellular localization of *cyclin B1* and *dazl* mRNAs in the zebrafish ovary

To further validate my method, I analyzed the expression of *cyclin B1* and *dazl* mRNAs in zebrafish oocytes. *dazl* mRNA encodes a zebrafish homolog of Deleted in Azoospermia (DAZ), an RNA-binding protein thought to be involved in primordial germ cell (PGC) development (Maegawa et al, 1999; Houston and King, 2000; Hashimoto et al., 2004). Hybridization of 5-12 μm-thick zebrafish ovary sections with 0.25 ng/μl of the fluorescein-labeled antisense *cyclin B1* RNA probe and 1 ng/μl of the DIG-labeled antisense *dazl* RNA probe, followed by amplification of signals using the TSA system, showed that *cyclin B1* mRNA was distributed throughout the cytoplasm except for the Balbiani body (Bb) marked by *dazl* mRNA in stage Ia oocytes (Fig. 5A). No obvious physiological structure of *cyclin B1* mRNA was observed in this stage. In contrast, *dazl* mRNA was localized at the Bb (Fig. 5A) as reported previously by using a conventional *in situ* hybridization method without the TSA system (Kosaka et al., 2007; Marlow and Mullins, 2008). The Bb is a universal and transient structure consisting of

mitochondria, Golgi apparatus, endoplasmic reticulum, and certain RNAs (Kloc et al., 2014). In later stage (stage Ib) oocytes, the Bb is dispersed, leading to specification of the vegetal polar region and establishment of the animal-vegetal axis in oocytes (Marlow and Mullins, 2008; Gupta et al., 2010; Heim et al., 2014). *cyclin B1* mRNA was detected as granular structures throughout the cytoplasm of stage Ib oocytes (Fig. 5B, red signals). In this period, *dazl* mRNA moved to the vegetal cortex of oocytes (Fig. 5B, green signals). No obvious structure of *dazl* mRNA was observed in stage I oocytes. At stage II, *cyclin B1* mRNA becomes localized at the animal polar cytoplasm as persisting granular structures (Fig. 5C, arrowheads). In this stage, *dazl* mRNA was localized at the vegetal polar cytoplasm as granular structures (Fig. 5C, arrows). Large numbers of *cyclin B1* RNA granules were localized at the animal polar cytoplasm in stage III (Fig. 5D, arrowheads) and fully grown, stage IV oocytes (Kotain et al., 2013; Horie and Kotani, 2016; Nukada et al., 2015). The localization and granular structure of *dazl* mRNA were maintained in stage III and IV oocytes, but the granules were broadly distributed in the vegetal polar cytoplasm (Fig. 5D, arrows). In all stages, no signal was detected with the control sense probes (data not shown). Similar distribution patterns of *cyclin B1* and *dazl* mRNAs during oocyte development were obtained from three independent experiments (data not shown).

Double staining of *cyclin B1* and *dazl* mRNAs showed interesting aspects of the mRNA distribution and localization in oocytes. First, *cyclin B1* and *dazl* mRNAs were distributed in completely different regions in the cytoplasm of stage Ia oocytes (Fig. 5A) and localized at different poles in later stages (Fig. 5C and D). Second, in the period of Bb dispersion, *cyclin B1* mRNA was distributed in the region where the Bb was localized and was partially co-localized with *dazl* mRNA in this region (Fig. 5B, insets). In contrast, *dazl* mRNA was not dispersed throughout the cytoplasm and maintained its aggregation while moving to the vegetal cortex (Fig. 5B). Finally, *cyclin B1* mRNA seemed to form granular structures from stage Ib (Fig. 5B), while *dazl* mRNA seemed to form such structures from stage II (Fig. 5C).

Subcellular localization of *Cyclin B1* and *Dazl* mRNAs in the mouse ovary

I next examined the distribution and localization of *Cyclin B1* and *Dazl* mRNAs in mouse adult ovaries. Hybridization of 8-10 μm-thick mouse ovary sections with 1 ng/μl of the fluorescein-labeled antisense *Cyclin B1* RNA probe and 1 ng/μl of the DIG-labeled antisense *Dazl* RNA probe, followed by amplification of signals using the TSA system, showed that *Cyclin B1* and *Dazl* mRNAs were distributed as granules in the cytoplasm of fully grown mouse oocytes (Fig. 6), as was observed for the zebrafish.

However, in contrast to the zebrafish, *Cyclin B1* and *Dazl* RNA granules were not localized in different regions but were similarly distributed in the cytoplasm. Interestingly, *Cyclin B1* and *Dazl* mRNAs were found to be assembled into different granules, and these granules were distributed close to each other (Fig. 6, insets). No signal was detected with the control sense probes (data not shown). Similar distribution patterns of *Cyclin B1* and *Dazl* mRNAs were obtained from three independent experiments (data not shown). My method thus showed similarity and difference of the two mRNAs in distribution pattern and region-specific localization in zebrafish and mouse oocytes. In addition, my method also enables detection of the subcellular localization of RNAs in mouse testes (Satoh et al., 2019, data not shown).

DISCUSSION

Detection and subcellular localization of mRNAs in adult tissues and organs

Because of the limitations of techniques, the detection and analysis of subcellular localization of mRNAs remain difficult. In this study, I produced 16 different RNA probes for the detection of mRNAs and showed the expression and subcellular localization of distinct RNAs in mouse and zebrafish adult ovaries. My method detects the mRNAs with high-sensitivity because *Pou5f1/Oct4* mRNA could be detected in mouse oocytes (Fig. 2), which was not detected by a conventional method. In addition, my method provides high-resolution imaging while maintaining tissue and cell morphology and is useful for simultaneous detection of two different mRNAs at subcellular levels. Double staining of *mos* and *cyclin B1* mRNAs in zebrafish oocytes demonstrated the distributions of these mRNAs as different granules even both mRNAs were localized in the same regions (Fig. 4). Since one can make biotin- or DNP-labeled RNA probes for detection of mRNAs of interest, the expression and localization of three and four mRNAs would be simultaneously analyzed by this method.

A previous study showed that zebrafish *cyclin B1* mRNA is initially distributed throughout the cytoplasm of oocytes (stages I and II) and becomes localized at the animal polar cytoplasm after stage III, when DIG-labeled RNA probes were recognized by an AP-coupled anti-DIG antibody, followed by detection of signals by precipitation of AP substrates (Kondo et al., 2001). Fluorescence *in situ* hybridization with the TSA system has revealed the localization of *cyclin B1* mRNA at the animal polar cytoplasm as RNA granules (Kotani et al., 2013; Horie and Kotani, 2016; Nukada et al., 2015), and this study revealed changes in *cyclin B1* mRNA distribution and localization during

oocyte development; i.e., *cyclin B1* mRNA was initially distributed throughout the cytoplasm of oocytes in stage I and subsequently moved to the animal pole in stage II (Fig. 5A-C), and a granular structure was first found in stage Ib oocytes and persisted in later stages (Fig. 5B-D). An explanation for the difference in distribution of *cyclin B1* mRNA in stage II oocytes is that precipitation of AP substrates tends to be diffused throughout the cytoplasm, while tyramide is associated with peptides in close proximity to POD-coupled antibodies. This difference was also demonstrated in the case of mRNAs expressed in *Drosophila* embryos (Lecuyer et al., 2007). Collectively, my method enables detection of the precise subcellular localization of mRNAs in vertebrate adult tissues and organs.

The localization of *dazl* mRNA during oogenesis in the zebrafish has been shown in previous studies in which the signals of RNA probes were detected by precipitation of AP substrates (Kosaka et al., 2007; Marlow and Mullins, 2008). My fluorescence *in situ* hybridization with the TSA system showed similar localization patterns of *dazl* mRNA (Fig. 5). However, details of the distribution pattern were different. Previous studies showed that *dazl* mRNA was diffusely localized in the vegetal polar cytoplasm of later stage oocytes, probably due to diffusion of AP substrate precipitation in this region (Maegawa et al., 1999; Kosaka et al., 2007; Marlow and Mullins, 2008). My method revealed that *dazl* mRNA forms granular structures at the vegetal pole, and these granules were broadly distributed in the vegetal cytoplasmic region of later stage oocytes (Fig. 5C and D). This finding suggests that *dazl* mRNA does not diffusely distribute throughout the vegetal polar cytoplasm as single RNA-protein complexes but assembles into large structures in this region. My observations will contribute to elucidation of the regulation of *dazl* mRNA during oocyte development and after fertilization.

Detection of *Cyclin B1* and *Dazl* mRNAs in mouse oocytes is difficult due to their low expression levels in a single oocyte. A previous study from our laboratory showed the distribution of *Cyclin B1* mRNA in the mouse oocyte cytoplasm as granules by single fluorescence *in situ* hybridization with the TSA system (Kotani et al., 2013). In this study, double fluorescence *in situ* hybridization of *Cyclin B1* and *Dazl* mRNAs revealed that these two mRNAs were assembled into different granules and that these granules were distributed in similar regions in fully grown oocytes (Fig. 6). These results demonstrate for the first time the different subcellular distributions of mRNAs in the cytoplasm of mammalian oocytes.

Conserved and species-specific regulation of mRNAs in zebrafish and mouse oocytes

My results demonstrated similarity and difference of the mRNA regulations in zebrafish and mouse species. Granular structures of mRNAs have been suggested to function in regulating the timing of translational activation of the mRNAs (Kotani et al., 2013; Horie and Kotani, 2016). mRNAs encoding Cyclin B1 and Dazl appeared to form granular structures in both zebrafish and mouse oocytes, suggesting translational regulation of these mRNAs.

In contrast to the conservation in physiological structure, localization of these mRNAs appeared to be different in the zebrafish and mouse. This may be due to differences in the functions of Dazl protein. During zebrafish embryogenesis, maternally provided *dazl* mRNA and its protein product have been suggested to function in PGC development (Hashimoto et al., 2004) as in the case of *Xenopus* (Houston and King, 2000). Localization of *dazl* mRNA at the vegetal polar cytoplasm of oocytes is one of the important processes for PGC development after fertilization (Kosaka et al., 2007; Hashimoto et al., 2004). Although the zygotically expressed mouse *Dazl* gene has been shown to function in spermatogenesis (Reijo et al., 1995; Ruggiu et al., 1997), maternally provided *Dazl* mRNA and its protein product might function in oocyte maturation but not in embryogenesis. A recent study has shown that translation of *Dazl* mRNA is activated at the early period of oocyte maturation, which is similar to the period of translational activation of *Cyclin B1* mRNA (Chen et al., 2011). Synthesized Cyclin B1 protein activates MPF, and MPF promotes oocyte maturation by phosphorylating substrates of the catalytic subunit of Cdc2 (Hampl and Eppig, 1995; Ledan et al., 2001; Polanski et al., 1998), while synthesized Dazl protein promotes translational activation of other mRNAs, protein products of which are essential for promoting progression of oocyte maturation (Chen et al., 2011; Sousa et al., 2016). Distributions of *Cyclin B1* and *Dazl* mRNAs in similar regions in mouse oocytes might be important for translational activation of these mRNAs at a similar timing.

I have described a high-sensitivity and high-resolution *in situ* hybridization method that enables detection of the distribution and localization of RNAs at subcellular levels in large organs such as the ovary and testis. This method is applicable to many organisms and various tissues and organs and should facilitate studies of gene expression at the level of RNA regulation, which is functionally and mechanistically important for promoting various biological processes in diverse species.

Chapter II

Changes in subcellular structures and states of Pumilio1 regulate the translation of target *Mad2* and *Cyclin B1* mRNAs

INTRODUCTION

Diverse biological processes including meiosis, embryonic development and neuronal plasticity are promoted by translational activation of dormant mRNAs at appropriate timings and places (Buxbaum et al., 2015; Martin and Ephrussi, 2009; Mendez and Richter, 2001; Mili and Macara, 2009). This temporal control of translation has been most extensively studied in oocyte meiosis. Fully grown vertebrate oocytes are arrested at prophase I of meiosis and accumulate thousands of translationally repressed mRNAs in the cytoplasm (Kotani et al., 2017; Masui and Clarke, 1979; Winata and Korzh, 2018). In response to specific cues such as hormones, oocytes resume meiosis and are arrested again at metaphase II. This process is termed oocyte maturation and is necessary for oocytes to acquire fertility. For proper progression of oocyte maturation, hundreds of dormant mRNAs are translationally activated in periods specific to distinct mRNAs (Chen et al., 2011; Luong et al., 2020), which are generally categorized as early meiosis I, late meiosis I and meiosis II. Of these, cyclin B1 mRNA, which encodes the regulatory subunit of maturation/M-phase-promoting factor (MPF), is translated in the early period of meiosis I, and the newly synthesized cyclin B1 proteins in this period are prerequisite for the progression of meiosis (Davydenko et al., 2013; Kondo et al., 2001; Kotani and Yamashita, 2002; Ledan et al., 2001; Polanski et al., 1998).

Translational activation of the dormant mRNAs including cyclin B1 has been shown to be directed by the cytoplasmic polyadenylation of mRNAs, which is mediated by the cytoplasmic polyadenylation element (CPE) in their 3' UTR (McGrew et al., 1989; Sheets et al., 1994). The CPE-binding protein (CPEB) functions in both repression and direction of the cytoplasmic polyadenylation (Barkoff et al., 2000; de Moor and Richter, 1999; Gebauer et al., 1994; Tay et al., 2000). Although many dormant mRNAs contain CPEs, they are translated in different periods during oocyte maturation, indicating that there must be additional mechanisms to determine the timings of translational activation of distinct mRNAs. However, the molecular and cellular mechanisms by which translational timings of hundreds of mRNAs are coordinated remain unclear.

Pumilio1 (Pum1) is a sequence-specific RNA-binding protein that belongs to the Pumilio and Fem-3 mRNA-binding factor (PUF) family, which is highly conserved in eukaryotes from yeast to human (Spassov and Jurecic, 2003; Wickens et al., 2002). Pum was identified in *Drosophila* as a protein that is essential for posterior patterning of embryos (Lehmann and Nussleinvolhard, 1987) and it was shown to repress the translation of target mRNAs in a spatially and temporally regulated manner (Asaoka-Taguchi et al., 1999; Murata and Wharton, 1995). In *Xenopus*, zebrafish and mouse

oocytes, Pum1 has been shown to bind to cyclin B1 mRNA and determine the timing of translational activation of cyclin B1 mRNA during oocyte maturation (Kotani et al., 2013; Nakahata et al., 2003; Ota et al., 2011a; Pique et al., 2008). Pum1 knockout mice were shown to be viable but defective in spermatogenesis (Chen et al., 2012) and oogenesis (Mak et al., 2016). Pum1-deficient mice also showed neuronal degeneration in the brain through an increase in Ataxin1 protein (Gennarino et al., 2015). In the mouse testis and brain, Pum1 was shown to target more than one thousand mRNAs (Chen et al., 2012; Zhang et al., 2017). The amount of proteins synthesized from these Pum1-target mRNAs, but not the amount of mRNAs, was increased in Pum1-deficient mice, indicating that Pum1 represses the translation of target mRNAs (Chen et al., 2012; Zhang et al., 2017). Despite the importance of Pum function in diverse systems, how Pum regulates the translation of target mRNAs remains to be elucidated.

In addition to sequence-specific RNA-binding proteins, our laboratory demonstrated that formation and disassembly of cyclin B1 RNA granules determine the timing of translational activation of mRNA, i.e., granular structures of this mRNA formed in immature, germinal vesicle (GV)-stage oocytes were disassembled at the timing of translational activation of mRNA, and stabilization and dissociation of these granules prevented and accelerated the mRNA translation, respectively (Kotani et al., 2013). Binding of Pum1 was shown to be required for the RNA granule formation, implying that Pum1 regulates the translational timing of target mRNAs through formation and disassembly of granules (Kotani et al., 2013).

P granules are cytoplasmic granules that consist of mRNAs and RNA-binding proteins and have been shown to behave as liquid droplets with a spherical shape in *C. elegans* embryos (Brangwynne et al., 2009). In addition, several RNA-binding proteins that are assembled into stress granules were shown to produce liquid droplets in vitro and in cultured cells (Lin et al., 2015; Molliex et al., 2015). Although phase changes in these liquid droplets into solid-like assemblies have been linked to degenerative diseases (Li et al., 2013; Weber and Brangwynne, 2012), more recent studies have demonstrated the assembly of solid-like substructures within stress granules (Jain et al., 2016; Shiina, 2019), suggesting physiological roles of the solid-like assemblies.

In this study, I identified *Mad2* mRNA as one of the Pum1-target mRNAs in mouse oocytes and found that *Mad2* and cyclin B1 mRNAs were distributed as distinct granules in the cytoplasm. Interestingly, Pum1 was assembled into aggregates exhibiting highly clustered structures, and these aggregates surrounded *Mad2* and cyclin B1 RNA granules. The Pum1 aggregates dissolved in an early period after resumption of meiosis possibly by phosphorylation, resulting in translational activation of *Mad2* and cyclin B1

mRNAs in early meiosis I. These results provide an aggregation-dissolution model for temporal and spatial control of mRNA translation. Since Pum1 aggregates resembled solid-like assemblies, the results suggest the physiological importance of phase changes of proteins in RNA regulation.

MATERIALS AND METHODS

Animals

All animal experiments in this study were approved by the Committee on Animal Experimentation, Hokkaido University. ICR mice (CLEA-Japan Inc.) were maintained on a 14 h light/ 10 h dark cycle at 25℃ with free access to food and water.

Preparation of ovaries and oocytes

Mouse ovaries were dissected from 8-week-old females in M2 medium (Sigma). Oocytes were retrieved from ovaries by puncturing the ovaries with a needle in M2 medium containing 10 μM milrinone, which prevents resumption of oocyte maturation. To induce oocyte maturation, the isolated oocytes were washed three times and incubated with M2 medium without milrinone at 37˚C. Alternatively, oocyte maturation was induced by injection of 5 U of hCG 48 h after injection of 5 U of pregnant mare serum gonadotropin into 3-week-old females. For reverse transcription PCR (RT-PCR) and poly(A) test (PAT) assays, ovaries and oocytes were extracted with Trizol reagent (Invitrogen) and total RNA was used for RT-PCR and RNA ligation-coupled RT-PCR. For *in situ* hybridization analysis, mouse ovaries were fixed with 4% paraformaldehyde in PBS (137 mM NaCl, 2.7 mM KCL, 10 mM Na_2HPO_4, and 2 mM KH_2PO_4, pH 7.2) (4% PFA/PBS) overnight at 4˚C. Oocytes isolated from ovaries were transferred into oviducts after fixation with 4% PFA/PBS for 10 min at 4˚C. The oviducts were then fixed with 4% PFA/PBS overnight at 4˚C. For immunoblotting analysis, 30 oocytes were washed with PBS and extracted with lithium dodecylsulfate (LDS) sample buffer (Novex) at 0, 10, and 18 h after resumption of oocyte maturation. For immunoprecipitation (IP)/RT-PCR analysis, mouse ovaries were homogenized with an equal volume of ice-cold extraction buffer (EB: 100 mM β-glycerophosphate, 20 mM HEPES, 15 mM $MgCl_2$, 5 mM EGTA, 1 mM dithiothreitol, 100 μM (*p*-amidinophenyl)methanesulfonyl fluoride, 3 μg/ml leupeptin; pH 7.5) containing 1% Tween 20 and 100 U/ml RNasin Plus RNase Inhibitor (Promega). After centrifugation at 15,000 g for 10 min at 4˚C, the supernatant was collected and used for IP.

Zebrafish ovaries were dissected from adult females in zebrafish Ringer's solution (116 mM NaCl, 2.9 mM KCl, 1.8 mM $CaCl_2$, and 5 mM HEPES; pH 7.2). Zebrafish oocytes were manually isolated from ovaries with forceps under a dissecting microscope. Oocyte maturation was induced by treatment with 1 μg/ml of 17α,20β-dihydroxy-4-pregnen-3-one, a maturation-inducing hormone (MIH) in fish. For ultracentrifugation analysis, fully grown immature oocytes and oocytes 3 h after MIH stimulation (matured oocytes) were homogenized with an equal volume of ice-cold EB containing 0.2% Tween20. After ultracentrifugation at 90,000 g for 30 min at 4˚C, the supernatant and precipitates were collected and used for immunoblot analysis.

RT-PCR and quantitative PCR

Total RNA extracted from mouse ovaries or 50 immature oocytes was used for cDNA synthesis using the Super Script III First Strand Synthesis System (Invitrogen). The full length of *Mad2* mRNA was amplified with the cDNA and primer sets specific to *Mad2*, m*Mad2*-f1 (5'-GTA GTG TTC TCC GTT CGA TCT AG-3') and m*Mad2*-r1 (5'-GTA TCA CTG ACT TTT AAA GCT TGA TTT TTA-3'). The amounts of short and long *Mad2* mRNAs were quantified by using a real-time PCR system with SYBR green PCR Master Mix (Applied Biosystems) according to the manufacturer's instructions. The short and long *Mad2* transcripts were amplified with the cDNA and primer sets to both types of *Mad2,* m*Mad2*-f2 (5'-GAA TAG TAT GGT GGC CTA CAA-3') and m*Mad2*-r2 (5'-TTC CCT CGT TTC AGG CAC CA-3'), and primer sets specific to long *Mad2*, m*Mad2*-f3 (5'-CTG GAC CAG GAT ATA AAG AAG CG-3') and m*Mad2*-r3 (5'-GCT GTC CTC CCT GCC TCT CT-3'). The signals obtained with distinct primer sets were normalized by standard curves obtained with plasmid DNAs encoding the short or long *Mad2* gene.

Section *in situ* hybridization

Section *in situ* hybridization and fluorescent *in situ* hybridization (FISH) with the tyramide signal amplification (TSA) Plus DNP system (PerkinElmer) were performed according to the procedure described in Chapter I. Briefly, fixed ovaries or oviducts containing oocytes isolated from ovaries were dehydrated, embedded in paraffin, and cut into 7-μm-thick sections. Digoxigenin (DIG)-labeled antisense RNA probes for the full length of short *Mad2* and sequences specific to long *Mad2* were used for detection of *Mad2* gene transcripts. No signal was detected with sense probes. After hybridization and washing, samples were incubated with an anti-DIG-horseradish peroxidase (HRP) antibody (1:500 dilution; Roche, cat. no. 11 633 716 001) for 30 min. To detect *Mad2*

transcripts by alkaline phosphatase (AP) staining, reaction with tyramide-dinitrophenyl (DNP) (PerkinElmer) was performed according to the manufacturer's instructions. The samples were then incubated with an anti-DNP-AP antibody (1:500 dilution; PerkinElmer, cat. no. NEL746A) for 30 min, followed by reaction with NBT and BCIP according to the manufacturer's instructions. To detect *Mad2* transcripts by fluorescence microscopy, reaction with tyramide-Fluorescein (PerkinElmer) was performed according to the manufacturer's instructions. To detect nuclei, samples were incubated with 10 μg/ml Hoechst 33258 for 10 min. After being mounted with a Prolong Antifade Kit (Molecular probes), the samples were observed under an LSM 5 LIVE confocal microscope (Carl Zeiss) at room temperature using a Plan Apochromat 63x/1.4 NA oil differential interference contrast lens and LSM 5 DUO 4.2 software (Carl Zeiss).

Double *in situ* hybridization of *Mad2* and cyclin B1 transcripts was performed as follows. A fluorescein-labeled antisense RNA probe for cyclin B1 was used for detection of the cyclin B1 gene transcript. Seven-μm-thick sections of mouse ovaries were hybridized with a mixture of *Mad2* and cyclin B1 antisense RNA probes. Then the samples were incubated with an anti-Fluorescein-HRP antibody (1:200 dilution; Roche, cat. no. 11 426 346 910) for 30 min. Reaction with tyramide-Cy3 (PerkinElmer) was performed according to the manufacturer's instructions. For inactivating HRP, samples were incubated with 1% H_2O_2 in PBS for 15 min. Detection of the DIG-labeled antisense *Mad2* RNA probe was performed as described above. After staining with Hoechst 33258, the samples were mounted and observed under the LSM5LIVE confocal microscope. The number of *Mad2* and cyclin B1 RNA granules was quantified using ImageJ software, which enables detection of granules according to size (larger than 0.2 μm) and intensity at the center of granules. Similar results were obtained using a fluorescein-labeled antisense RNA probe for *Mad2* and a DIG-labeled RNA probe for cyclin B1.

Immunoblotting

Mouse oocyte extracts were separated by SDS-PAGE with Bolt Bis-Tris Plus Gels (Novex), blotted onto an Immobilon membrane using a Bolt Mini Blot Module (Novex), and probed with an anti-human Pum1 goat antibody (1:1000 dillution; Bethyl Laboratories, Inc., cat. no. A300-201A), an anti-human cyclin B1 rabbit antibody (1:100 dillution; Santa Cruz Biotechnology, Inc., cat. no. sc-752), an anti-hamster cyclin B1 mouse monoclonal antibody (1:1000 dilution; V152, Abcam, cat. no. ab72), and an anti-human Mad2 rabbit antibody (1:1000 dillution; Bethyl Laboratories, Inc., cat. no. A300-301A). The supernatant and precipitates of zebrafish oocyte extracts were separated by

SDS-PAGE, blotted onto an Immobilon membrane, and probed with an anti-*Xenopus* Pum1 mouse monoclonal antibody (1:1000 dillution; Pum2A5, Nakahata et al., 2001) and an anti-GM130 mouse monoclonal antibody (1:250 dillution; BD Biosciences, cat. no. 610822). The intensity of signals was quantified using ImageJ software.

Poly(A) test (PAT) assay

RNA ligation-coupled RT-PCR was performed according to the procedure reported previously (Kotani et al., 2013). Four hundred ng of total RNA extracted from pools of 250 mouse oocytes was ligated to 400 ng of P1 anchor primer (5'-P-GGT CAC CTT GAT CTG AAG C-NH_2-3') in a 10-µl reaction using T4 RNA ligase (New England Biolabs) for 30 min at 37˚C. The ligase was inactivated for 5 min at 92˚C. Eight µl of the RNA ligation reaction was used in a 20-µl reverse transcription reaction using the Superscript III First Strand Synthesis System with a P1' primer (5'-GCT TCA GAT CAA GGT GAC CTT TTT TTT-3'). Two µl of the cDNA was used for the 1st PCR with the P1' primer and an m*Mad2*-f4 primer (5'-GAC CCC ATA TTG AAA TAC ATG C-3') or mcyclin B1-f1 primer (5'-CCA CTC CTG TCT TGT AAT GC-3') for 45 cycles. One µl of the 1st PCR reaction was used for the 2nd PCR with the IRD800-P1' primer (5'-IRD800-GCT TCA GAT CAA GGT GAC CTT TTT TTT-3') and an m*Mad2*-f5 primer (5'-GAG CTC ACA ACG CAG TTG-3') or mcyclin B1-f2 primer (5'-CCT GGA AAA GAA TCC TGT CTC-3') for 20 cycles. The PCR product was resolved on a 3% TAE gel and observed by using Odessay (M&S TechnoSystem). I confirmed that the increase in PCR product length was due to elongation of the poly(A) tails by cloning the 2nd PCR products and sequencing them.

RT-PCR analysis after IP (IP/RT-PCR)

Eighty µl of mouse ovary extracts was incubated with 4 µl of 1.0 µg/ml anti-human Pum1 goat antibody (Bethyl Laboratories, cat. no. A300-201A) or 4 µl of 1.0 µg/ml control goat IgG for 1 h at 4˚C. The extracts were then incubated with protein A-Sepharose beads (GE Healthcare) for 3 h at 4˚C and washed five times with EB containing 1% Tween 20. After extraction of mRNAs from the beads with Trizol reagent, RT-PCR was performed using primer sets specific to *Mad2*, m*Mad2*-f6 (5'-GTG ACC ATT GTT AAA GGA ATC CAT CCC-3') and m*Mad2*-r1, to cyclin B1, mcyclin B1-f3 (5'-AGT CCC TCA CCC TCC CAA AAG C-3') and mcyclin B1-r1 (5'-AAA GCT TTC CAC CAA TAA ATT TTA TTC AAC-3'), to *β-actin*, m*β-actin* -f1 (5'-AGT CCC TCA CCC TCC CAA AAG C-3') and m*β-actin* -r1 (5'-GGT CTC AAG TCA GTG TAC AGG C-3'), and to *α-tubulin*, m*α-tubulin*-f1 (5'-CTT TGT GCA CTG

GTA TGT GGG T-3') and m*α-tubulin*-r1 (5'-ATA AGT GAA ATG GGC AGC TTG GGT-3'). The intensity of signals was quantified using ImageJ software.

Immunofluorescence

Fixed ovaries were dehydrated, embedded in paraffin, and cut into 7-μm-thick sections. After rehydration, samples were microwaved for 10 min with 0.01 M citric acid (pH 6.0) containing 0.05% Tween 20, followed by cooling down for 40 min. After incubation with a TNB blocking solution (PerkinElmer) for 1 h at room temperature, the samples were incubated with anti-human Pum1 goat antibody (1:100 dilution; Novus Biologicals, cat. no. NB100-259) at 4˚C for overnight. The samples were then incubated with anti-goat IgG-Alexa Fluor Plus 647 antibody (1:200 dilution; Invitrogen, cat. no. A32849) at room temperature for 1 h. After staining with Hoechst 33258, the samples were mounted and observed under the LSM 5 LIVE confocal microscope. No signal was detected in the reaction without the anti-Pum1 antibody. To further confirm the specificity of signals, a GST-fused N-terminus fragment of mouse Pum1 (amino acids 1-399) (GST-Pum1NN) was expressed in *Escherichia coli* and gel-purified. Before immunostaining of mouse ovary sections, 3 μg of anti-Pum1 antibody was incubated with 18 μg of GST-Pum1NN in PBS (300 μl reaction) for overnight at 4˚C. To simultaneously detect Pum1 and cyclin B1 and *Mad2* mRNAs, the samples were immunostained with the Pum1 antibody as described above after detection of the cyclin B1 and *Mad2* RNA probes in *in situ* hybridization analysis. The intensities of signals were measured by ImageJ software. Monte Cario simulation was performed with ImageJ software by creating random dots and measuring distance to Pum1 aggregates. The dimension of the images used was 5000 x 5000 nm.

mRNA injection and immunostaining

Sequences encoding the full length and parts of mouse Pum1 (ΔQN, ΔN and ΔC) were cloned into pCS2-GFP-N to produce Pum1 fused with GFP at the N terminus of Pum1. mRNAs encoding GFP, GFP-Pum1, GFP-Pum1ΔQN, GFP-Pum1ΔN, and GFP-Pum1ΔC were synthesized with an mMESSAGE mMACHINE SP6 kit (Life Technologies) and dissolved in distilled water. Ten pg of the mRNAs was injected into fully grown mouse oocytes using an IM-9B microinjector (Narishige) under a Dmi8 microscope (Leica) in M2 medium containing 10 μM milrinone. After being incubated for 4 h at 37˚C, the oocytes were fixed with 2% PFA/PBS containing 0.05% Triron-X100 for 1 h at 4˚C for *in situ* hybridization analysis or were washed four times with M2 medium without milrinone for induction of oocyte maturation. At the appropriate

time points after resumption of meiosis, the distribution of proteins fused with GFP was observed under the LSM 5 LIVE confocal microscope. To simultaneously detect GFP-Pum1 and cyclin B1 or *Mad2* mRNA, the fixed oocytes were attached on slide glasses using Smear Gell (GenoStaff). The oocytes were immunostained with anti-GFP mouse antibody (1:200 dilution; Roche, ca. no. 1 814 460) followed by anti-mouse IgG-Alexa Fluor 488 antibody (1:200 dilution; Molecular Probes) after hybridization and washing of the cyclin B1 or *Mad2* RNA probe in *in situ* hybridization analysis.

To analyze the effects of permeabilization on GFP-Pum1 aggregates, the oocytes injected with mRNA encoding GFP or GFP-Pum1 were incubated for overnight at 37˚C with M2 medium containing 10 μM milrinone. After observation under the LSM 5 LIVE confocal microscope, the oocytes were transferred to M2 medium containing 0.012% digitonin and 10 μM milrinone. The oocytes were then observed under the confocal microscope at the appropriate time points.

To analyze the effects of GFP-Pum1ΔC on oocyte maturation, the oocytes injected with mRNA encoding GFP or GFP-Pum1ΔC were incubated for 9 and 18 h at 37˚C with M2 medium and then fixed with 4% PFA/PBS for 1 h at 37˚C. The samples were permeabilized with PBS containing 0.1% Triton-X100 for 20 min, followed by incubation with a blocking/washing solution (PBS containing 0.3% BSA and 0.01% Tween 20) for 1 h at room temperature. The samples were then incubated with Cy3-conjugated anti-β-tubulin antibody (1:150 dilution; Sigma, cat. no. C4585) for 30 min at room temperature, washed with washing solution, and mounted with VECTASHIELD Mounting Medium with DAPI (Funakoshi). The samples were observed under the LSM 5 LIVE confocal microscope.

To analyze the stability of Mad2 in immature and mature oocytes, 2.5 pg of mRNA encoding GFP-Mad2 was injected into GV- and MII-stage oocytes. After being incubated for 2 h at 37˚C, the oocytes were treated with puromycin and observed under the Nikon Ti-E inverted microscope equipped with the Nikon A1Rsi special imaging confocal laser scanning system.

FRAP analysis

FRAP measurements were performed according to the procedure reported previously (Kimura and Cook, 2001; Tsutsumi et al., 2016). A Nikon Ti-E inverted microscope equipped with a Nikon A1Rsi special imaging confocal laser scanning system (Nikon) was used for the measurements. A small area (approximately 10 μm diameter circle) was positioned in a region of the oocyte cytoplasm and bleached using 100% 488 nm laser with 5 scans. Images were then collected using 1.0% laser power every 5.0 s for

5.0 min. The relative fluorescence intensity in the bleached area was normalized using the intensity in the control area measured subsequently after measurement of the bleached area. The normalized intensities were analyzed using a fitting equation for a double exponential association model. A smaller bleached area (5 μm diameter circle) gave equivalent results. To observe details of changes in GFP-Pum1 aggregates after photobleaching, similar experiments were performed using a high-resolution microscope, Zeiss LSM 980 with Airyscan 2 Multiplex (Carl Zeiss).

Puromycin treatment and Pum1 antibody injection

To inhibit protein synthesis, oocytes were treated with 20 μM puromycin in M2 medium and incubated at 37˚C. The oocytes were collected at appropriate time points after incubation with puromycin for immunoblotting analysis. Two pg of anti-Pum1 antibody (Bethyl Laboratories, cat. no. A300-201A) was injected into fully grown mouse oocytes using the microinjector in M2 medium containing 10 μM milrinone. The oocytes were then washed three times and incubated for 18 h at 37˚C with M2 medium containing 1 μM milrinone. To analyze the distribution of GFP-Pum1, 10 pg of the GFP-Pum1 mRNA was co-injected with 2 pg of anti-Pum1 antibody into fully grown mouse oocytes, followed by washing and incubation of oocytes as described above. The distribution of GFP-Pum1 was observed under the LSM 5 LIVE confocal microscope.

Phosphatase treatment

The dephosphorylation experiments were performed according to the procedure reported previously (Pahlavan et al., 2000). Briefly, samples of 30 oocytes in phosphatase buffer (New England Biolabs) containing 1% SDS, 100 μM (*p*-amidinophenyl)methanesulfonyl fluoride, and 3 μg/ml leupeptin were incubated with 17.5 U alkaline phosphatase (New England Biolabs) at 37˚C for 1 h. The reaction was stopped by adding the equal volume of lithium dodecyl sulfate (LDS) sample buffer. The samples were then analyzed by immunoblotting.

Okadaic acid, BI2536, centrinone, U0126 and roscovitine treatment

To inhibit activities of protein phosphatase 1 and 2A, oocytes were treated with 2.5 μM okadaic acid (OA) in M2 medium containing 10 μM milrinone and incubated at 37˚C. OA was dissolved in DMSO as stocks and diluted in M2 medium before use. As a control, oocytes were treated with DMSO. The oocytes were collected at 16 h after incubation for immunoblotting analysis. To analyze the distribution of GFP-Pum1, fully grown mouse oocytes were injected with 10 pg of the GFP-Pum1 mRNA and incubated in M2 medium

containing 10 μM milrinone at 37˚C for 4 h, followed by treatment with OA as described above. The distribution of GFP-Pum1 was observed under the LSM 5 LIVE confocal microscope. Activities of Plk1 and Plk4 were inhibited by treating the oocytes with 100 nM BI2536 and 5 μM centrinone, respectively, according to the procedure reported previously (Bury et al., 2017). Activities of MAPK and MPF were inhibited by treating the oocytes with 50 μM U0126 and 50 μM roscovitine, respectively, according to the procedure reported previously (Nabti et al., 2014).

RESULTS

Expression of Mad2 is translationally regulated during mouse oocyte maturation

Mad2 has been shown to function as a component of spindle assembly checkpoint proteins to accurately segregate chromosomes in meiosis I of mouse oocytes (Homer et al., 2005). However, how Mad2 is accumulated in oocytes remains unknown. To clarify the mechanism of Mad2 accumulation in meiosis I, I first analyzed the expression of *Mad2* mRNA in mouse oocytes. Using purified RNAs from ovaries, I isolated two splicing variants of *Mad*2 mRNA by RT-PCR analysis (Fig. 7A). RT-PCR and quantitative PCR analyses of oocytes isolated from ovaries showed that the short version of *Mad2* mRNA was dominant in oocytes (Figs. 7A and B). In addition, *in situ* hybridization analysis of ovary sections with the tyramide signal amplification (TSA) system detected the expression of short, but not long, *Mad2* mRNA in oocytes (Fig. 7C). FISH analysis showed that short *Mad2* mRNA was distributed in the oocyte cytoplasm by forming RNA granules (Fig. 7D). In contrast, long *Mad2* mRNA was not detected by FISH analysis (data not shown). These results suggest that short *Mad2* mRNA is crucial for the synthesis of protein in oocytes.

I then analyzed the expression of Mad2 protein in oocytes. Immunoblot analysis showed that the amount of Mad2 as well as that of cyclin B1 increased after resumption of meiosis (Fig. 7E). Consistent with this, poly(A) test (PAT) assay showed that poly(A) tails of *Mad2* mRNA were elongated 4 h after resumption of meiosis as in the case of cyclin B1 (Fig. 7F). Inhibition of protein synthesis with puromycin prevented the accumulation of Mad2 in oocytes even when meiosis had resumed (Fig. 7G). To rule out a possibility that Mad2 protein becomes stabilized after resumption of meiosis, I analyzed stability of Mad2 by expressing GFP-Mad2 followed by puromycin treatment. The rate of destruction of GFP-Mad2 in immature oocytes was similar to that in mature oocytes (Fig. 7H), indicating that the stability of Mad2 is not changed. Taken together,

the results indicate that Mad2 protein is accumulated in an early period of oocyte maturation by the translational activation of dormant mRNA stored in oocytes.

Mad2 mRNA is a Pum1-target mRNA and forms granules distinct from cyclin B1 RNA granules

I then assessed the mechanism by which the translation of *Mad2* mRNA is temporally regulated. Since *Mad2* mRNA was translated in a period similar to that for cyclin B1 mRNA and contains several putative Pumilio-binding elements (PBEs) in its 3'UTR (Fig. 8A), I investigated whether Pum1 binds to *Mad2* mRNA by using an IP/RT-PCR. *Mad2* and cyclin B1 mRNAs, but not *α-tubulin* and *β-acti*n mRNAs, were detected in precipitations with an anti-Pum1 antibody, while neither of them was detected in precipitations with control IgG (Fig. 8B), indicating that Pum1 targets *Mad2* mRNA as well as cyclin B1 mRNA. From these results, I speculated that both mRNAs were assembled into the same granules. However, double FISH analysis showed that the two mRNAs formed distinct granules (Fig. 8C). The granules containing *Mad2* mRNA were rarely overlapped with those containing cyclin B1 mRNA (0.18%, n = 2748). Formation of distinct granules of *Mad2* and cyclin B1 mRNAs resembles formation of *Map2*, *CaMKIIα* and *β-actin* RNA granules in neurons, in which distinct mRNAs were assembled into different granules (Mikl et al., 2011).

Time course analysis showed that the number of *Mad2* RNA granules was decreased at 4 h (prometaphase I) and that the granules had almost completely disappeared at 18 h (metaphase II) after resumption of meiosis, being consistent with the changes in cyclin B1 RNA granules (Fig. 8D and E) (Kotani et al., 2013). The amount of *Mad2* mRNA was not changed in oocytes at 18 h after resumption of meiosis (Fig. 8F), indicating that the decrease in the number of *Mad2* RNA granules is caused by granule disassembly. These results suggest that translation of *Mad2* mRNA is temporally regulated through formation and disassembly of RNA granules, similar to the cytoplasmic regulation of cyclin B1 mRNA (Kotani et al., 2013).

Pum1 forms aggregates that surround target mRNAs

To further assess the mechanism by which translation of *Mad2* and cyclin B1 mRNAs is temporally and spatially regulated by Pum1, I analyzed the distribution of Pum1 in the oocyte cytoplasm. Immunofluorescence analysis showed that Pum1 was ununiformly distributed in the cytoplasm of immature oocytes and appeared to form aggregates in highly clustered structures (Fig. 9A). This signal was specific to Pum1 since no signal was detected when the antibody was absorbed with N-terminus region of Pum1 (amino

acids 1-399) (data not shown), which includes the region recognized by the antibody (amino acids 225-275). Simultaneous detection of Pum1 protein and cyclin B1 and *Mad2* mRNAs showed that clusters of Pum1 aggregates covered cyclin B1 and *Mad2* RNA granules (Fig. 9B and C). In most cases, Pum1 aggregates surrounded and partially overlapped with cyclin B1 and *Mad2* RNA granules at the periphery (Fig. 9C; 95.1%, n = 268 for cyclin B1; 98.4%, n = 124 for *Mad2*), while in remaining cases Pum1 aggregates were localized at the center of granules in addition to the periphery (Fig. 9C; 4.9% for cyclin B1; 1.6% for *Mad2*). These distribution patterns were specific to *Mad2* and cyclin B1 mRNAs since 1) the average distance between randomly distributed dots and Pum1 aggregates was 1.8-fold longer than the experimental distance between the center of RNA granules and Pum1 aggregates ($p < 0.001$) (Monte Cario simulation; 100 permutations) and 2) *α-tubulin* mRNA was not surrounded by Pum1 and instead it uniformly distributed in the cytoplasm (Fig. 9D).

To assess the molecular mechanisms of Pum1 aggregation, I then examined the distribution of GFP-Pum1 and mutant forms of Pum1 by injecting mRNA into mouse oocytes. GFP-Pum1 was distributed in a way similar to that of endogenous Pum1, i.e., it appeared to form highly clustered aggregates (Fig. 10A and B) and surrounded cyclin B1 and *Mad2* RNA granules (Fig. 10C). Pum1 contains a glutamine/asparagine (Q/N)-rich domain (Fig. 10D), also identified as a prion-like domain (Fig.10E; Lancaster et al., 2014), which is thought to promote highly ordered aggregation of proteins (Lancaster et al., 2014; Salazar et al., 2010). GFP-Pum1 that lacks the Q/N-rich domain (GFP-Pum1ΔQN) (Fig. 10D) was distributed uniformly throughout the oocyte cytoplasm (Fig. 10A). Taken together, the results indicate that Pum1 assembles into highly clustered aggregates by the Q/N-rich domain, and these aggregates cover target mRNAs.

I then analyzed the distribution of Pum1 lacking the N-terminus (GFP-Pum1ΔN) or lacking the C-terminus, which contains the PUF domain responsible for binding to target mRNAs (Zhang et al., 1997) (GFP-Pum1ΔC: Fig. 10D). GFP-Pum1ΔN formed aggregates similar to those of GFP-Pum1 (Fig. 10F). In contrast, GFP-Pum1ΔC formed aggregates larger than those of GFP-Pum1 (Fig. 10F), indicating that the C-terminus PUF domain is involved in regulating the size of aggregates.

Pum1 shows insoluble and immobile properties in immature oocytes

I then examined the properties of endogenous Pum1 by ultracentrifugation. Since I was unable to obtain appropriate amounts of materials by using mouse oocytes, I used zebrafish oocytes for this analysis. Zebrafish Pum1 has been shown to target cyclin B1 mRNA (Kotani et al., 2013) and it contains the Q/N-rich domain also identified as a

prion-like domain (Fig. 10E). Ultracentrifugation analysis showed that most of the endogenous Pum1 (64.8% ± 3.4%, n = 3) was concentrated in an insoluble fraction in immature oocytes (Fig. 11A), supporting the results of immunofluorescence showing that endogenous Pum1 forms aggregates (Fig. 9).

I next examined the properties of GFP-Pum1 in mouse oocytes by FRAP analysis. As a control, GFP-Pum1ΔQN was analyzed. After photobleaching, the fluorescence of GFP-Pum1 and GFP-Pum1ΔQN gradually recovered (Fig. 11B). The fluorescence recovery curves were fitted to a double exponential association model (data not shown). The half time of recovery ($t_{1/2}$) of the first fraction of GFP-Pum1 was rapid, while that of the second fraction of GFP-Pum1 was slow (Fig. 11C, left), suggesting that a part of Pum1 forms large complexes. Moreover, a critical finding was that a significant fraction of GFP-Pum1 (40.7% ± 8.6%, n = 12) showed immobility (not recovering after photobleaching), while only a small fraction of GFP-Pum1ΔQN (13.6% ± 5.5%, n = 14) was static (Fig. 11B and C, right). Thereby, the Q/N-rich region promotes the assembly of Pum1 into highly ordered aggregates in an immobile state. To analyze the details of Pum1 recovery after photobleaching, I observed changes in GFP-Pum1 in aggregates using a high-resolution microscope. The intensity of GFP-Pum1 in aggregates recovered slowly and only partially (Fig. 11D), supporting the notion that Pum1 aggregates exhibit an immobile property.

I further analyzed the properties of Pum1 by permeabilizing oocytes with digitonin. A recent study demonstrated that liquid-like droplets of RNA-binding proteins were rapidly shrunk and dissolved within 2 to 3 min after this treatment, while stable assemblies of RNA-binding proteins that exhibit solid-like properties were maintained in cultured cells (Shiina, 2019). After permeabilization with digitonin, GFP rapidly diffused out of the oocytes (Fig. 11E and F). In contrast, the structure and intensity of GFP-Pum1 aggregates persisted after permeabilization (Fig. 11E and F). Collectively, the immunofluorescence, ultracentrifugation, FRAP and permeabilization analyses suggest that Pum1 assembles into aggregates in a solid-like state in immature oocytes. The study by Shiina (Shiina, 2019) demonstrated that GFP-Pum1 forms solid-like substructures of RNA granules in cultured cells, being consistent with my results in oocytes.

Pum1 aggregates are dissolved prior to translational activation of target mRNAs

I next examined whether the distribution and properties of Pum1 changed during oocyte maturation. Time course analysis of GFP-Pum1 showed that the Pum1 aggregates disappeared after resumption of meiosis (Fig. 12A). Most of the aggregates of GFP-

Pum1 had disappeared 4 h after resumption of meiosis, at which time poly(A) tails of *Mad2* and cyclin B1 mRNA were elongated (Fig. 7F) and the granules of both RNAs had disappeared (Fig. 8C), suggesting a link between translational activation of target mRNAs and Pum1 dissolution. Consistent with these observations, the ultracentrifugation assay showed that a large part of endogenous Pum1 became soluble (69.0% ± 4.4%, n = 3) in mature oocytes, compared with the soluble fraction in immature oocytes (35.2% ± 3.4%, n = 3) (Fig. 11A). In contrast, a Golgi matrix protein GM130 remained insoluble in mature oocytes (Fig. 11A). FRAP analysis in mouse oocytes indicated that the $t_{1/2}$ of GFP-Pum1 was not significantly different between immature and mature oocytes (Fig. 12B and C, left). In contrast, the percentage of immobile fractions of GFP-Pum1 was significantly reduced in mature oocytes (18.8% ± 6.8%, n = 6) compared with that in immature oocytes (40.7% ± 8.6%, n = 12) (Fig. 12B and C, right). Taken together, the results indicate that Pum1 aggregates dissolve during oocyte maturation and suggest the relationship between changes in the property of Pum1 and temporal regulation of target mRNA translation.

Stabilization of Pum1 aggregates prevents the translation of target mRNAs

I next assessed whether the change in the property of Pum1 was involved in the translational regulation of target mRNAs. By observing the distributions of truncated forms of Pum1 after resumption of meiosis, I found that the large aggregates of GFP-Pum1ΔC were stable and persisted until 18 h (Fig. 13A). In contrast, GFP-Pum1ΔQN no longer formed aggregates (Fig. 13B), and the aggregates of GFP-Pum1ΔN were dissociated within 4 h (Fig. 13C). Consistent with the observations after resumption of meiosis, GFP-Pum1, Pum1ΔQN, and Pum1ΔN did not affect the progression of oocyte maturation, while GFP-Pum1ΔC prevented polar body extrusion (Fig. 13A and Fig. 14A). Temporal synthesis of proteins is required for proper spindle formation in meiosis I (Davydenko et al., 2013; Kotani and Yamashita, 2002; Polanski et al., 1998; Susor et al., 2015). In oocytes expressing GFP-Pum1ΔC, meiosis I spindles were defective, while correct meiosis II spindles were formed in oocytes expressing GFP at 18 h after resumption of meiosis (Fig. 14B).

RNA granules of *Mad2* and cyclin B1 were disappeared in oocytes expressing GFP and GFP-Pum1, Pum1ΔQN and Pum1ΔN at 4 h after resumption of meiosis (Fig. 14C and D), as in the case of non-injected oocytes (Fig. 8D and E). In contrast, both RNA granules were maintained in oocytes expressing GFP-Pum1ΔC, although the number of cyclin B1 RNA granules ware slightly decreased (Fig. 14C and D). The aggregates of GFP-Pum1ΔC, but not GFP alone, surrounded cyclin B1 RNA granules (Fig. 14E). The

amounts of GFP-Pum1 and mutant forms of Pum1 were 1.6-1.8-fold larger than that of endogenous Pum1 (Fig. 14F). Synthesis of Mad2 and cyclin B1 was attenuated in oocytes expressing GFP-Pum1ΔC, while the amounts of both proteins were not changed in oocytes expressing GFP and GFP-Pum1, Pum1ΔQN and Pum1ΔN (Figs. 14G and H). These results suggest that insoluble GFP-Pum1ΔC inhibited translational activation of Pum1-target mRNAs by stabilizing Pum1 aggregates and RNA granules, resulting in failure in spindle formation and polar body extrusion.

Cyclin B1 synthesis after resumption of meiosis has been shown to promote bipolar spindle formation in meiosis I via activating MPF in meiosis I (Polanski et al., 1998). At 9 h after resumption of meiosis, bipolar structures of meiosis I spindles were observed in oocytes expressing GFP (94% of oocytes, n = 17) as in the case of non-injected oocytes (89% of oocytes, n = 9), while meiosis I spindles were still in round shapes without poles in oocytes expressing GFP-Pum1ΔC (60% of oocytes, n = 15) (Fig. 14I), being consistent with the attenuation of cyclin B1 synthesis (Fig. 14G and H). Injection of cyclin B1 mRNA carrying the SV40 3'UTR, which lacks PBE, at 1 h after resumption of meiosis completely rescued the formation of bipolar spindles (100% of oocytes, n = 8) (Fig. 14I). The results indicate that the inhibition of protein synthesis by expression of GFP-Pum1ΔC is indeed a cause of abnormal progression of meiosis. Since Pum1 targets thousands of mRNAs in the testis and brain (Chen et al., 2012; Zhang et al., 2017), syntheses of many proteins responsible for correct spindle formation would be attenuated in oocytes expressing GFP-Pum1ΔC.

I then examined the effects of Pum1 inhibition on the progression of oocyte maturation by injecting the anti-Pum1 antibody. To effectively analyze the effect of the anti-Pum1 antibody, I incubated oocytes with 1 μM milrinone, which partially prevents resumption of meiosis. Under this condition, 50-100% of the oocytes underwent germinal vesicle breakdown (GVBD) (Fig. 15A and B) in a manner dependent on protein synthesis since puromycin treatment prevented GVBD (Fig. 15A). Injection of the anti-Pum1 antibody, but not control IgG, prevented GVBD, dissolution of GFP-Pum1 aggregates, and synthesis of cyclin B1 and Mad2 (Fig. 15B-E). The injected anti-Pum1 antibody was distributed within the cytoplasm in a way similar to that of endogenous Pum1 (Fig. 15F). These results strongly suggest that the anti-Pum1 antibody inhibited the dissolution of endogenous Pum1 aggregates and thereby prevented the translational activation of Pum1-target mRNAs.

Pum1 phosphorylation is linked with the dissolution of aggregates

I finally assessed the mechanism by which Pum1 aggregates are dissolved. As observed

in *Xenopus* and zebrafish (Ota et al., 2011a; Saitoh et al., 2018), the electrophoretic mobility of Pum1 was reduced in mature mouse oocytes (Fig. 16A, left). This reduction was recovered by phosphatase treatment (Fig. 16A, right), indicating that Pum1 is phosphorylated during mouse oocyte maturation. Treatment of immature oocytes with okadaic acid (OA), a protein phosphatase 1 and 2A (PP1 and PP2A) inhibitor, induced Pum1 phosphorylation and rapid dissolution of Pum1 aggregates (Fig. 16B-D). These results suggest that kinases responsible for Pum1 phosphorylation are present and at least partially active in immature oocytes and that the dissolution of Pum1 is promoted by phosphorylation. Polo-like kinase (Plk) 1 and 4 were shown to be present in immature mouse oocytes (Bury et al., 2017; Pahlavan et al., 2000). Interestingly, inhibition of Plk4, but not that of Plk1, prevented the dissolution of Pum1 aggregates (Figs. 16C-D and 17A). Inhibition of Plk4 also prevented the phosphorylation of Pum1, though Pum1 seemed still partially phosphorylated (Fig. 16B, bottom). Thereby, Plk4 is a kinase promoting the dissolution of Pum1 aggregates and Pum1 phosphorylation in oocytes treated with OA. No effect on the dissolution of Pum1 was observed when activation of Mitogen-activated protein kinase (MAPK) was inhibited, while aggregate disolution was delayed but not prevented when the activity of MPF was inhibited (Fig. 17A), suggesting that MPF, which consists of pre-existing cyclin B2 and Cdc2 kinase (Daldello et al., 2019), is partially involved in Pum1 aggregate dissolution. Together, these results provide a link between phosphorylation of Pum1 and dissolution of Pum1 aggregates.

I further analyzed the effects of OA treatment on *Mad2* and cyclin B1 RNA granules and translational activation of these mRNAs. *Mad2* and cyclin B1 RNA granules dissapeared almost completely at 2 h after treatment with OA (Fig. 16E and F). In contrast, inhibition of Plk4 prevented the disassemby of both RNA granules (Fig. 16E and F). In addition, OA treatment induced synthesis of Mad2 and cyclin B1, while both proteins were not synthesized in oocytes treated with OA and Plk4 inhibitor (Fig. 16G and Fig. 17B). Taken together, Plk4 rapidly promotes phosphorylation of Pum1, dissolution of Pum1 aggregates, disassembly of *Mad2* and cyclin B1 RNA granules, and translational activation of both mRNAs when PP1 and PP2A activities are inhibited.

To assess a possibility that the anti-Pum1 antibody injected into oocytes prevented phosphorylation of Pum1, I analyzed Pum1 phosphorylation state in this experiment. Pum1 phosphorylation was observed in oocytes injected with control IgG, while it was prevented in oocytes injected with the anti-Pum1 antibody (Fig. 15G). The results support the importance of Pum1 phosphorylation for dissolution of Pum1 aggregates and translational activation of target mRNAs.

DISCUSSION

Extensive biochemical studies have demonstrated the importance of *cis*-acting mRNA elements and *trans*-acting RNA-binding proteins in the regulation of temporal translation (Radford et al., 2008). However, their cytoplasmic and molecular mechanisms remain largely unknown. My results provide an aggregation-dissolution model for temporal and spatial control of mRNA translation, i.e., Pum1 aggregates in clustered structures ensure translational repression of target mRNAs by stably maintaining their granular structures, and the dissolution of aggregates possibly by phosphorylation permits the disassembly of granules and translational activation of mRNAs. Given that many dormant mRNAs stored in oocytes contain PBEs (Chen et al., 2011) and Pum1 targets more than one thousand mRNAs in the testis and brain (Chen et al., 2012), Pum1 would target a large number of mRNAs in oocytes. In addition, clusters of Pum1 aggregates might be comprised of granules of these target mRNAs and related proteins and thereby allow their coordinated regulation. My results will be a basis for understanding how translational timings of hundreds of mRNAs are coordinately regulated.

Phase changes of Pum1 and translational regulation of target mRNAs

Recent studies have demonstrated that many of the RNA-binding proteins harbor prion-like domains and that some of these proteins have the ability to assemble RNA granules (Decker et al., 2007; Gilks et al., 2004; Reijns et al., 2008). These RNA-binding proteins were shown to promote liquid-liquid phase separation, resulting in the assembly of protein-RNA complexes into droplets (Elbaum-Garfinkle et al., 2015; Lin et al., 2015; Molliex et al., 2015; Nott et al., 2015). These droplets are thought to function as partitions that effectively maintain stability and/or translational repression of mRNAs. In contrast, phase transition of the liquid droplets into solid-like structures such as amyloid fibrils has been thought to contribute to pathological diseases such as amyotrophic lateral sclerosis (ALS) (Li et al., 2013; Weber and Brangwynne, 2012). However, more recently, solid granules were found to assemble during muscle regeneration in a physical state (Vogler et al., 2018). In addition, core regions of stress granules were shown to exhibit solid-like properties (Jain et al., 2016; Shiina, 2019). Although these findings suggest the involvement of solid granules in RNA regulation, the physiological importance of the phase changes of protein aggregation from liquid to solid states and vice versa remains unclear.

In this study, I demonstrated that Pum1 assembled into aggregates in highly

clustered structures through the Q/N-rich region and these aggregates showed insoluble and immobile properties in immature oocytes (Figs. 9, 10 and 11). After initiation of oocyte maturation, the Pum1 aggregates dissolved into a soluble and mobile state (Figs. 11A and 12). The mutant form of Pum1 that lacks the C-terminal PUF domain, Pum1ΔC, formed stable aggregates and these structures persisted after initiation of oocyte maturation (Fig. 10 F and Fig. 13A). Pum1ΔC is expected to be unable to bind to target mRNAs but to have the ability to form assemblies via the Q/N-rich region. Since an RNA molecule was shown to buffer the assembly of RNA-binding proteins that harbor prion-like domains into a solid-like aggregates (Maharana et al., 2018), it is possible that the lack of RNA-binding ability of Pum1ΔC resulted in the assembly of large and stable aggregates as in the case of RNA-binding proteins such as TDP43 and FUS. Pum1ΔC would stabilize endogenous Pum1 aggregates via the Q/N-rich region-mediated assembly into or around endogenous Pum1 aggregates and thereby prevent the translational activation of Pum1-target mRNAs (Figs. 13 and 14). The anti-Pum1 antibody also prevented dissociation of Pum1 aggregates and synthesis of cyclin B1 and Mad2 (Fig. 15). This antibody would stabilize Pum1 aggregates by inhibiting Pum1 phosphorylation (Fig. 15G) as discussed below, although I could not rule out a possibility that the antibody affected the conformation or composition of Pum1 assemblies. Collectively, my results suggest a physiological significance of phase changes of protein aggregation in translational repression and activation of target mRNAs.

Regulation of the subcellular structures and states of Pum1 by phosphorylation and dephosphorylation

P granules are the germinal granules in *C. elegans* that are important for fate decision of germline cells. Live imaging of embryos demonstrated that P granules behave as dynamic liquid droplets (Brangwynne et al., 2009). Intriguingly, disassembly of P granules after fertilization was shown to require MBK-2 kinase, while subsequent assembly of P granules at the posterior region of embryos required protein phosphatase 2A (PP2A) (Gallo et al., 2010; Wang et al., 2014). MEG-1 and MEG-3 were found to be the substrates of MBK-2 and PP2A in the granules (Wang et al., 2014). These results demonstrated that the dynamics of liquid RNA granules is regulated by phosphorylation and dephosphorylation of assembled proteins.

My results suggest the importance of protein phosphorylation and dephosphorylation for changes in structures and states of Pum1 aggregates. SDS-PAGE analysis demonstrated that Pum1 was phosphorylated during mouse oocyte maturation (Fig.

16A). Interestingly, treatment of oocytes with OA, an inhibitor of PP1 and PP2A, rapidly dissociated Pum1 aggregates and induced Pum1 phosphorylation (Fig. 16B-D). Since PP2A was shown to be localized in the cytoplasm of GV-stage mouse oocytes, while PP1 was dominantly localized in the nucleus (Smith et al., 1998), PP2A would be a phosphatase involved in Pum1 dephosphorylation and the maintenance of Pum1 aggregates. Even when the activity of PP1 and PP2A was inhibited by OA, Pum1 phosphorylation was attenuated and the aggregates persisted in the presence of a Plk4 inhibitor (Fig. 16B-D), suggesting that Plk4 is a kinase responsible for Pum1 phosphorylation and aggregate dissolution. However, other kinases would phosphorylate Pum1, since inhibition of Plk4 activity delayed, but did not completely prevent, the disolution of Pum1 aggregates and Pum1 phosphorylation after initiation of oocyte maturation (unpublished data). To date, only Nemo-like kinase 1 (Nlk1) has been shown to phosphorylate Pum1 (Ota et al., 2011b). My results suggest the participation of MPF in dissolution of Pum1 aggregates (Fig. 17A). Involvement of Nlk1, MPF and other kinases in phosphorylation of Pum1 and dissolution of aggregates remains to be investigated. Puf3, one of the PUF family proteins in yeast, was shown to be phosphorylated at more than 20 sites throughout the entire region (Lee and Tu, 2015). In addition, our group previously showed that Pum1 was phosphorylated at multiple sites in an early period of oocyte maturation in zebrafish (Saitoh et al., 2018). These results suggest that many sites including those in the Q/N-rich domain might be phosphorylated, resulting in Pum1 aggregate dissolution.

The anti-Pum1 antibody injected into GV-stage oocytes prevented the Pum1 phosphorylation, aggregate disolution and synthesis of cyclin B1 and Mad2 (Fig. 15). Since this antibody recognizes amino acid residues from 225 to 275 of Pum1, phosphorylation around this region might be crucial to trigger disolution of Pum1 aggregates. Our group previously showed that overexpression of GFP-Pum1ΔC prevented disassembly of RNA granules and phosphprylation of endogenous Pum1 in zebrafish oocytes (Saitoh et al., 2018). Collectively, these results suport the notion that phosphorylation of Pum1 is a critical step to promote dissolution of Pum1 aggregates, disassembly of RNA granules, and translational activation of Pum1-target mRNAs.

Subcellular structures of Pum1 and homogenous RNA granules

An intriguing finding in this study is that Pum1-target *Mad2* and cyclin B1 mRNAs formed distinct granules in the oocyte cytoplasm, instead of making granules containing both mRNAs (Fig. 8). Pum1 was found to produce highly clustered structures that surrounded both *Mad2* and cyclin B1 RNA granules (Fig. 9). These structures partially

resemble those of germ granules in *Drosophila* embryos, in which mRNAs form homogenous RNA clusters and are spatially positioned within the granules, while RNA-binding proteins are evenly distributed throughout the granules (Trcek et al., 2015). These findings suggest the existence of a common mechanism by which each mRNA could be organized into homogenous particles. However, in contrast to my findings, the structures of germ granules were not changed during early stages of embryogenesis and were independent of the control of mRNA translation and degradation (Trcek et al., 2015). Therefore, the function of spacially organized structures of germ granules in *Drosophila* embryos seems to be different from the function of subcellular structures of Pum1 and RNA granules in mouse oocytes.

My results showed that Pum1 aggregates surrounded and overlapped *Mad2* and cyclin B1 RNA granules at the periphery but were rarely localized at the center of granules (Fig. 9). Given that Pum1 was shown to bind directly to PBE in the 3'UTR of target mRNAs including cyclin B1 (Kotani et al., 2013; Nakahata et al., 2003; Ota et al., 2011; Pique et al., 2008), Pum1-target mRNAs may compose highly ordered structures within granules, in which the 3' ends of mRNAs are localized at the periphery of granules as in the case of a long noncoding RNA, *Neat1*, in paraspeckle nuclear bodies (Souquere et al., 2010; West et al., 2016). In the small fraction of cyclin B1 and *Mad2* RNA granules, Pum1 was localized at the center of granules. Since this type of localization was found in large granules, the central localization may result from co-localization of several granules that are surrounded by Pum1. Structural analysis of the RNA granules will be an interesting issue to be explored.

Details of the molecular mechansims by which Pum1 is assembled into aggregates remain unknown. One possible model is that Pum1 binds to a target mRNA via the PUF domain and subsequently assembles into aggregates via the Q/N-rich region. Another possibility is that Pum1 contains two populations; one population binds to target mRNAs and the other functions as structual scaffolds without binding to mRNAs. In addition to the homogenous assembly of Pum1, heterogenous assembly with other RNA-binding proteins may produce aggregates. In any case, the resulting Pum1 aggregates in clustered structures would make compartments that function as regulatory units with related proteins assembled together. These units enable to coordinately regulate the translation of assembled mRNAs. In various cells besides oocytes, many mRNAs are known to be transported and localized at subcellular regions through binding of RNA-binding proteins to mainly 3'UTRs (Martin and Ephrussi, 2009; Milli and Macara, 2009; Russo et al., 2008). Recent studies demonstrated the accumulation of translationally repressed mRNAs at protrusions of fibroblast cells and synapses of

neuronal cells in a static state (Buxbaum et al., 2014; Moissoglu et al., 2019). Since Pum1 functions in diverse systems and other RNA-binding proteins that harbor prion-like domains may function in a manner similar to that of Pum1, my results will contribute to an understanding of the nature of temporal and spatial control of translation in many cell types of diverse organisms.

Chapter III

Translational regulation of *Emi2* mRNA in meiosis II: Control of different timings of translation by assembling distinct RNA-binding proteins

INTRODUCTION

Temporally regulated translation of mRNAs stored in the cell cytoplasm is an important mechanism for promoting various biological phenomena including oocyte meiosis and embryonic development. During oogenesis, oocytes accumulate thousands of translationally repressed mRNAs and are arrested at prophase of meiosis I (Masui and Clarke 1979; Winata and Korzh, 2018). Fully grown oocytes are called immature oocytes or GV-stage oocytes. After resumption of meiosis through hormonal stimulations, more than one thousand mRNAs begin to be translated at timings specific to distinct mRNAs (Chen et al., 2011; Kotani et al., 2017). Oocytes are arrested again at metaphase of meiosis II (MII) until fertilization.

The 3'UTR of many dormant mRNAs contains the cytoplasmic polyadenylation element (CPE), which is recognized by CPE-binding protein (CPEB). CPEBs are critical regulators of the cytoplasmic polyadenylation in oocyte (Richer, 2007). Changes in the length of poly(A) tails have been shown to control mRNA stabilization and translation (McGrew et al., 1989; Vassalli et al., 1989; Sheets rt al., 1994; Stutz et al., 1998). Although a large number of dormant mRNAs contain CPEs in their 3'UTRs, they are translated in different periods during oocyte maturation; Translation of hundreds dormant mRNAs is activated in meiosis I, and translation of more than one thousand dormant mRNAs is activated in meiosis II (Chen et al., 2011; Conti and Franciosi, 2018; Luong et al., 2020). The results of these studies imply that timings of translational activation of dormant mRNAs are regulated by other mechanisms in addition to that depends on CPEB. Indeed, the translation of cyclin B1 mRNA, which is translated in meiosis I, was shown to be regulated by formation and disassembly of RNA granules (Kotani et al., 2013). Pum1 is a sequence-specific RNA-binding protein and belongs to the Pumilio and Fem-3 mRNA-binding factor (PUF) family. Pum1 contains the Q/N-rich region, which is thought to promote self-aggregation (Salazar et al., 2010), in the central region. In chapter II, I showed that cyclin B1 and *Mad2* mRNAs were Pum1-taget mRNAs and formed distinct RNA granules. I also revealed that Pum1 played a key role in regulation of the translation of cyclin B1 and *Mad2* mRNAs through assembly and dissolution of aggregation of Pum1 in early meiosis I. These studies provide a model of translational regulation in meiosis I. However, mechanisms of translational regulation in meiosis II remain unclear.

After resumption of oocyte maturation, the meiosis is arrested again at metaphase of meiosis II by a cytostatic factor (CSF) to await fertilization (Masui and Markert, 1971; Sagata et al., 1989). CSF stabilizes maturation/M-phase-promoting factor (MPF)

activity indirectly by inhibition of anaphase-promoting complex/cyclosome (APC/C), resulting in the prevention of sister chromatid separation at MII (Nixon et al., 2002; Madgwick et al., 2004). EMI2 (early meiotic inhibitor 2) is one of the components of CSF. EMI2 inhibits the activation of APC/C by binding directly and arrests the meiosis at MII (Tunquist and Maller, 2003; Ohe et al., 2010). The expression level of EMI2 protein is low in immature oocytes and is increased in meiosis II. Previous studies reported that the ectopic expression of EMI2 in meiosis I induced MI arrest in *Xenopus* and mouse oocytes (Inoue et al., 2007; Suzuki et al., 2010). In contrast, inhibition of EMI2 synthesis by injection with *Emi2* siRNA or antisense morpholino oligo nucleotide (MO) induced failure in arrest at MII (Shoji et al., 2006; Madgwick et al., 2006). These studies indicate that the timing of EMI2 synthesis as well as EMI2 synthesis itself is critical for the APC/C inhibition at MII.

The 3'UTR of *Emi2* mRNAs contains CPEs and binds to CPEB as in the case of other dormant mRNAs. In *Xenopus* oocytes, removal of the *Emi2* 3'UTR was sufficient to Emi2 expression in immature oocytes, indicating that the 3'UTR of *Emi2* mRNA is essential to control the temporally regulated translation in meiosis II (Tung et al., 2007). CPEB1 is well known to regulate the polyadenylation of many dormant mRNAs during oocyte maturation, however, this protein is degraded during meiosis I (Mendez et al., 2002; Pique ta al., 2008; Setoyama et al., 2007). In meiosis II, polyadenylation of dormant mRNAs is supported by CPEB4 which is one of the vertebrate CPEB family and expressed in meiosis II (Belloc and Mendez, 2008; Igea and Mendez, 2010). However, injection with *Cpeb4* MOs into GV-stage oocytes showed no significant effect on oocyte maturation in mouse (Chen et al., 2011). Therefore, how *Emi2* mRNA translation is regulated remains poorly understood.

In this chapter, I aimed to elucidate the mechanisms of translational regulation of *Emi2* mRNA, which is translated at the timing different from that of cyclin B1 and *Mad2* mRNAs. My results revealed that mouse oocytes deposit dormant *Emi2* mRNA as RNA granules in the cytoplasm as in the case of cyclin B1 RNA granules. However, *Emi2* mRNA localized as granules different from those of cyclin B1 mRNA. Using fluorescence i*n situ* hybridization (FISH) and poly(A) test (PAT) analyses, I revealed that *Emi2* RNA granules disassembled at the timing of translational activation of mRNA. I further found that *Emi2* mRNA did not bind to Pum1, while HuR and HuB, members of Hu family and components of stress granule (Markmiller et al., 2018; Jain et al., 2016), interacted with both *Emi2* and cyclin B1 mRNA. In addition, I showed that *Emi2* mRNA specifically bound to Tudor domain containing protein 3 (TDRD3) by *in vitro* RNA-binding assay and simultaneous detection of TDRD3 and *Emi2* mRNA. The

injection of anti-TDRD3 antibody delayed the timing of Emi2 synthesis but did not affect the translation of cyclin B1 and *Mad2* mRNAs in meiosis I. These results suggest that TDRD3 is a protein to specifically regulate translation of *Emi2* mRNA in meiosis II. From these results, I propose that the components of RNA granules are different between cyclin B1 and *Emi2* mRNAs. I hypothesize that the differences in RNA granule components are a key mechanism to control temporal translation of dormant mRNAs during oocyte maturation.

MATERIALS AND METHODS

Animals

All animal experiments in this study were approved by the Committee on Animal Experimentation, Hokkaido University. ICR mice (CLEA-Japan Inc.) were maintained on a 14 h light/ 10 h dark cycle at 25℃ with free access to food and water.

Recombinant protein

DNA fragment encoding a part of mouse EMI2 (residues 1-366) was amplified by PCR using m*Emi2*-forward primer (5'-CGA ATT CAA GAC TTC CAC CAT TGA AGA TTC C-3') and m*Emi2*-reverse primer (5'-AAG CTT AAA GCC AAG TTC CCA C-3'). The PCR products were inserted into pCRII TOPO-vector (Invitrogen). The resulting plasmids were recombined with pET21c vector to produce a histidine (His)-tagged protein. Recombinant proteins were expressed in *E. coli*, and purified by SDS-PAGE, followed by electroelution in Tris-glycine buffer without SDS. The purified protein was dialyzed against 1 mM HEPES (pH 7.5), lyophilized and used for injection into mice to produce antibody and for immunoblotting.

Production of antibody

Anti-EMI2 antibody was produced using the His-tagged EMI2 (residues 1-366) as an antigen according to the procedure reported previously (Yamashita et al., 1991). The recombinant EMI2-His was injected into two mice. The obtained antisera against EMI2-His were affinity-purified with recombinant EMI2-His protein electroblotted onto an Immobilon membrane.

Preparation of ovaries

Mouse ovaries were dissected from 8- to 12-week-old adult females in PBS (137 mM

NaCl, 2.7 mM KCl, 10 mM Na_2HPO_4, and 2 mM KH_2PO_4, pH 7.2). For *in situ* hybridization, mouse ovaries were fixed with 4% paraformaldehyde in PBS (4% PFA/PBS) overnight at 4℃. For immunoprecipitation analysis, mouse ovaries were homogenized with an equal volume of ice-cold extraction buffer (EB: 100 mM β-glycerophosphate, 20 mM Hepes, 15 mM $MgCl_2$, 5 mM EGTA, 1 mM dithiothreitol, 100 μM (p-amidinophenyl) methanesulfonyl fluoride, and 3 μg/ml leupeptin; pH 7.5) containing 1% Tween 20 and 100 U/ml RNase OUT. After centrifugation at 5,000 rpm for 15 min at 4℃, the supernatant was collected and used for immunoprecipitation. For RNA pull-down assay, the cytoplasmic extract of *Xenopus laevis* ovary was prepared according to the procedure of RiboTrap kit (MBL International). The ovaries were dissected from adult females into small pieces in nuclease-free PBS. *Xenopus* ovaries were homogenized with an equal volume of ice-cold CE Buffer (+) (MBL International) and incubated for 10 min on ice. After then, the extracts were diluted with Detergent Solution (MBL International) and centrifuged at 3,000 g for 3 min at 4℃. The supernatant was transferred to new tubes and diluted with High-Salt Solution (MBL International). After centrifugation at 12,000 g for 3 min at 4℃, the supernatant was collected and used for immunoprecipitation assays to detect RNA-binding proteins using the RiboTrap kit.

PAT assay

Two μg of total RNA extracted from a pool of 200 mouse oocytes was ligated to 0.4 μg of P1 anchor primer (5'-P-GGT CAC CTT GAT CTG AAG C-NH_2-3') in a 10 μl reaction using T4 RNA ligase (New England Biolab) for 30 min at 37℃. The ligase was inactivated for 5 min at 92℃. Eight μl reaction was used in a 20 μl reverse transcription reaction using SuperScript III First Strand Synthesis System with P1' primer (5'-GCT TCA GAT CAA GGT GAC CTT TTT-3'). Aliquots of the cDNA were used for as templates of 1st RCR with primer sets of P1' primer and m*Emi2*-forward primer-1 (5'-ATG TCT GTG CGC TTA TCA CG-3') or P1' primer and mcyclin B1-forward primer-1 (5'-CCA CTC CTG TCT TGT AAT GC-3'). Aliquots of the 1st PCR reactions were used for 2nd PCR with primer sets of P1' primer and m*Emi2*-forward primer-2 (5'-TCC CAT TGA TGA CAG ACG TTG ATT TAC TTC CCA CTT-3') or P1' primer and mcyclin B1-forward primer-2 (5'-CCT GGA AAA GAA TCC TGT CTC-3'). The PCR products were resolved on 3% TAE gel. I confirmed that the increase in PCR product length was due to elongation of the poly(A) tails by cloning the 2nd PCR products and sequencing them.

Polysomal fractionation

Polysomal fractionation was performed according to the procedure described previously (Masek et al., 2020). Briefly, 200 oocytes were treated with 100 µg/ml of cycloheximide (CHX) for 10 min and collected in 350 µl of lysis buffer (10 mM Hepes, pH 7.5; 62.5 mM KCl, 5 mM MgCl2, 2 mM DTT, 1% TritonX-100) containing 100 µg/ml of CHX and 20 U/ml of Ribolock (Thermo Fisher Scientific). After disruption of the zona pellucida with 250 µl of zirconia-silica beads (BioSpec), lysates were centrifuged at 8,000 g for 5 min at 4˚C. Supernatants were loaded onto 10-50% linear sucrose gradients containing 10 mM Hepes, pH 7.5; 100 mM KCl, 5 mM $MgCl_2$, 2 mM DTT, 100 µg/ml of CHX, Complete-EDTA-free Protease Inhibitor (1 tablet/100 ml: Roche) and 5 U/ml of Ribolock. Centrifugation was performed using an Optima L-90 ultracentrifuge (Beckman) at 35,000 g for 65 min at 4˚C. Polysome profiles were recorded using an ISCO UA-5 UV absorbance reader. Ten equal fractions were collected from each sample and subjected to RNA isolation by Trizol reagent (Sigma). Fractions 6 to 10 were taken as for polysome bound RNA. Further the library was prepared using SMART-seq v4 ultra low input RNA kit (Takara Bio). Sequencing was performed by HiSeq 2500 (Illumina) as 150-bp paired-end. Reads were trimmed using Trim Galore v0.4.1 and mapped to the mouse GRCm38 genome assembly using Hisat2 v2.0.5. Gene expression was quantified as fragments per kilobase per million (FPKM) values in Seqmonk v1.40.0.

Morpholino oligonucleotide injection

The sequences of antisense MOs (Gene Tools, LLC) are as follows; *Emi2*-3'UTR-MO, 5'-ATTTATTTCTTAAAAGTCCCAACAA-3', that specifically targets the terminal sequence of the *Emi2* mRNA 3'UTR and *Emi2*-3'UTR 5mm-MO, 5'-ATTCATTACTTAATAGTCACATCAA-3', that contains 5-nts mismatches (underlines) and was used as control. GV-stage oocytes were injected with 10 pl of a solution containing 0.1 mM *Emi2*-3'UTR-MO or *Emi2*-3'UTR 5mm-MO using an IM-9B microinjector (Narishige) under a Dmi8 microscope (Leica) in M2 medium. After being injected, the oocytes were cultured in M16 medium in an atmosphere of 5% CO_2 in air at 37˚C and used for immunoblotting or morphological observation after fixation with 4% PFA for 1 h.

mRNA microinjection

mRNA encoding the GFP and GFP-Emi2 were synthesized using mMESSAGE mMACHINE SP6 kit (Ambion) and dissolved in nuclease-free distilled water. Eight pl

of 1 μg/μl mRNAs were injected into immature oocytes in M2 medium (94.7 mM NaCl, 4.8 mM KCl, 1.2 mM KH_2PO_4, 1.3 mM $MgCl_2$, 5.6 mM Glucose, 23.3 mM sodium lactate, 4.0 mM $NaHCO_3$, 0.3 mM sodium pyruvate, 1.7 mM $CaCl_2$, 21.0 mM HEPES, 0.1 mM gentamicin, 4 mg/ml BSA; pH 7.5) supplemented with 10 μM milrinone (M2+) using IM-9B microinjector under the Dmi8 microscope and washed four times with M2 medium lacking milrinone (M2-) to induce oocyte maturation.

Immunofluorescence

Oocytes were collected at the appropriate time points after incubating M2 medium without milrinone at 37°C. For treatment with nocodazole, the oocytes were transferred into the medium with 5 μM nocodazole before 3 h of the appropriate time points. The oocytes were fixed in 3.7% PFA in PBS for 1 h, permeabilized for 20 min in permeabilization buffer (0.3% BSA, 0.1% Triton-X, 0.02% NaN_3 in PBS), washed three times with blocking solution (0.3% BSA, 0.01% Tween20 in PBS) and incubated in blocking solution for 20 min at room temperature. The oocytes were then incubated with anti-Mad2 (Biolegend) and anti-CREST (Antibodes Incorporated) antibodies for 1 h at room temperature. After washing three times with blocking solution, the oocytes were incubated with secondary antibodies for 1 h at room temperature, washed three times and mounted on slides with VECTASHIELD Mounting Medium containing DAPI (Vector Laboratories, lnc) and observed under an LSM 5 LIVE confocal microscope (Carl Zeiss).

Section *in situ* hybridization

Section *in situ* hybridization with the TSA Plus system (PerkinElmer) was performed according to the procedure described in chapter I. In brief, the fixed ovaries were dehydrated, embedded in paraffin, and cut into 7-μm-thick sections. The digoxigenin (DIG)-labeled sense or antisense RNA probe for full-length *Emi2* were synthesized with a DIG-RNA-labeling kit (Roche Molecular Biochemicals). No signal was detected with sense probes. The sections of mouse ovaries were hybridized with a hybridization mix containing 1 ng/μl of DIG-labeled RNA probe. After hybridization and washing, the sections were incubated with anti-DIG-horseradish peroxidase (HRP) antibody (1:500 dilution; Roche, cat. no. 1 426 346) for 30 min. The reaction with tyramide-DNP, followed by reaction with the anti-DNP–alkaline phosphatase (AP) antibody (PerkinElmer, Inc., cat. no. NEL746A), and the detection of signals were performed according to the manufacturer's instructions. For FISH analysis, the samples were incubated with anti-DNP–Alexa Fluor 488 antibody (1:500 dilution; Molecular Probes,

cat. no. A-11097) for overnight after reaction with tyramide DNP. To detect nuclei, the samples were incubated with 10 μg/ml Hoechst 33258 for 10 min.

Double fluorescence *in situ* hybridization of cyclin B1 and *Emi2* mRNAs was performed as follows. Sections of mouse ovaries were hybridized with fluorescein-labeled cyclin B1 RNA probe and DIG-labeled *Emi2* RNA probe. After hybridization and washing, samples were incubated with anti-DIG-HRP antibody (1:500 dilution; Roche, cat. no. 1 207 733) for 30 min. After reaction with tyramide-DNP, the samples were incubated with anti-DNP–Alexa Fluor 488 antibody (1:500 dilution; Molecular Probes, cat. no. A-11097) for overnight. Before detection of the fluorescein-labeled cyclin B1 RNA probe, the samples were incubated with 1% H_2O_2 in PBS for 15 min for inactivating HRP. The reaction with tyramide-Cy3 (1:50 dilution in 1×Plus Amplification Diluent (PerkinElmer), followed by 1:100 dilution with DW) was performed for 20 min. To detect nuclei, the sections were incubated with 10 μg/ml Hoechst 33258 for 10 min and observed under the LSM 5 LIVE confocal microscope.

In situ hybridization and immunofluorescence

Section *in situ* hybridization with the TSA Plus system (PerkinElmer) was performed as described "section *in situ* hybridization" in this chapter. After reaction with anti-DIG-HRP or anti-FITC-HRP antibody and washing, fluorescein-labeled cyclin B1 RNA probe or DIG-labeled *Emi2* RNA probe was treated with tyramide-FITC (PerkinElmer, Inc.). After washing, samples were microwaved for 10 min in 10 mM sodium acetate buffer pH 6.0. The samples were then incubated with anti-Pum1 (Bethyl; A300-201A) or anti-TDRD3 (Cell Signaling Technology; D302G) antibodies overnight at room temperature. After washing, the samples were incubated with anti-goat IgG-Alexa Flour Plus 647(Invitrogen; cat. no. A32849) or anti-goat IgG-Alexa Flour Plus 555 (Invitrogen; cat. no. A32816) at room temperature for 1 h. After staining with Hoechst 33258, the samples were mounted and observed under N-SIM super-resolution microscope (Nikon).

Collection of oocytes and induction of oocyte maturation

For immunoblotting, microinjection and PAT assay, GV-stage oocytes were collected from puncturing ovaries with a needle in M2+. Oocyte maturation was induced by washing oocytes with M2- four times and cultured at 37℃ in drops of M2- covered with paraffin liquid. At the fit time points after resumption of oocyte maturation, oocytes were collected for immunoblotting and PAT assay. For immunoblot analysis, the collected oocytes were washed with PBS and extracted in 10 μl lithium dodecyl sulfate

(LDS) sample buffer (NOVEX) or SDS sample buffer (50 mM Tris-HCl; pH 6.8, 2% sodium dodecyl sulfate, 6% β-mercaptoethanol, 10% glycerol, 0.1% phenol Red). For PAT analysis, mouse oocytes were extracted with Trizol regent (Life Technologies) according to the manufacture's instruction.

RT-PCR analysis after immunoprecipitation (IP/RT-PCR)

Eighty μl of mouse ovary extracts were incubated with 2 μl of 1.0 mg/ml anti-Pum1 (Bethyl; A300-201A), anti-HuR (SANTA CRUZ; sc-5261) or anti-ELAVL2 (Proteintech; 14008-1-AP) antibodies, and protein G Mag sepharose (GE Healthcare) overnight at 4℃. Same volume of IgG was used as a control. The samples were washed five times with EB containing 1% Tween20. An aliquot of the samples was used for RT-PCR with primer sets specific to cyclin B1, mcyclin B1- forward primer-2 (5'-CCT GGA AAA GAA TCC TGT CTC-3') and mcyclin B1- reverse primer-1, to *Emi2*, m*Emi2*-forward primer-2 (5'-TCC CAT TGA TGA CAG ACG TTG ATT TAC TTC CCA CTT-3') and *Emi2*-reverse primer (5'-GGG GAT ATG ACA TAG TAA AA-3'), and to *α-tubulin*, m*α-tubulin*-forward primer (5'-CTT TGT GCA CTG GTA TGT GGG T-3') and m*α-tubulin*-reverse primer (5'-ATA AGT GAA ATG GGC AGC TTG GGT-3').

RNA pull-down assay and mass spectrometry

The RNA-binding assay was performed according to the manufacture's instruction of RiboTrap Kit (MBL International). In brief, bromouridine (BrU)-labeled RNAs of 3' UTR of mouse *Emi2*, *Xenopus Emi2*, and mouse cyclin B1 were generated using Riboprobe *in vitro* Transcription Systems kit according to the manufacture's protocol (Promega). Anti-BrdU antibodies were conjugated with protein A-Sepharose beads for overnight at 4℃ (GE Healthcare). Then, the RNAs were bound to the beads. The cytoplasmic extract of *Xenopus* ovaries was transferred to tubes containing the BrU-labbeled RNAs conjugated with the beads for 2 h at 4℃. The samples were washed with Wash BufferII, eluted with elution buffer (4% BrdU/DMSO solution in nuclease-free PBS; MBL International), and subjected to SDS-PAGE. The SDS-PAGE gels were stained by silver staining with Silver Stain MS kit (Wako Pure Chemical Industries, ltd) to visualize the proteins associated with BrU-labeled RNAs. The bands were excised from the gel and subjected to a mass spectrometric analysis with Orbitrap Velos Pro (Thermo Fisher Scientific). For protein identification, MASCOT 2.5.1 were used for database searching against NCBInr_*Xenopus laevis* (update on 05/09/2015, 17,456 sequences). The results from each run were filtered with the peptide confidence value,

in which peptides showing the false discovery rate (FDR) less than 1% were selected. In addition, proteins identical to the sequenced peptides with the rank1 values were selected. The number of peptides identical to the proteins was more than one.

Immunoblotting

The crude extracts from mouse ovary and rabbit reticulocyte lysate were separated by SDS-PAGE, blotted onto an immobilon membrane, and probed with anti-EMI2 (this study), anti-FLAG M2 (Sigma; F1804-1MG), anti-TDRD3 (Cell Signaling Technology; D302G) and anti-DIG-AP (Roche) antibodies. Pum1, HuR and HuB were detected by immunoblotting from the ovary extracts and the immunoprecipitates with anti-Pum1 (Bethyl; A300-201A), anti-HuR (SANTA CRUZ; sc-5261) or anti-ELAVL2 (Proteintech; 14008-1-AP) antibodies. Mouse oocyte extracts were separated by SDS-PAGE with Bolt Bis-Tris Plus Gels (Novex), blotted onto an immobilon membrane using a Bolt Mini Blot Module (Novex), and probed with anti-EMI2 (this study), anti-γ-tubulin (Sigma; T6557) and anti-Mad2 (Bethyl; A300-301A) antibodies. The intensity of signals was quantified using ImageJ software.

Protein syntheses in rabbit reticulocyte lysate

The full length of *Tdrd3* was amplified by PCR using *Tdrd3*-f1 (5'-TGG ATC CTA TGG CCG AGG TGT CCG-3') and *Tdrd3*-r1(5'-ATC GAT GTT CCG AGC TCG AGG-3'). N-terminal region of *Tdrd3* (1-473 aa) was amplified by PCR using *Tdrd3*-f1 and *Tdrd3*-r2(5'-ATC GAT TGG CCT GTC ACA CTT-3'). C-terminal region of *Tdrd3* (246-744 aa) was amplified by PCR using *Tdrd3*-f2 (5'-GGA TCC TAT GGG TGG TGC CAG AAG TAA-3') and *Tdrd3*-r1. The PCR products were inserted into pGEM-T Easy vector (Promega). Sequences encoding the full length and part of *Tdrd3* (1-473 aa and 246-744 aa) were cloned into pCS2-FLAG-N or pCS2-FLAG-C to produce TDRD3 fused with FLAG at the N-terminus or C-terminus of TDRD3. Sequences encoding the full length *Tdrd3* was cloned into pCS2-GFP-N to produce TDRD3 fused with GFP at N-terminus of TDRD3. mRNAs encoding FLAG-tagged TDRD3, GFP-tagged TDRD3, FLAG-tagged TDRD3 (1-473 aa) and FLAG-tagged TDRD3 (246-744 aa) were synthesized with an mMESSAGE mMACHINE SP6 kit (Ambion), and the resulting mRNAs (2000 ng) were translated in 50-μl of rabbit reticulocyte lysate (Promega).

UV-cross linking assay

FLAG-tagged proteins were purified by immunoprecipitation with anti-FLAG M2 antibody (Sigma) and Protein G Mag Sepharose (GE healthcare). DIG-labeled 3'UTR

of *Emi2* and cyclin B1 RNA probes were synthesized with a DIG-RNA-labeling kit (Roche Molecular Biochemicals). Two μg of probes was incubated with purified FLAG-tagged proteins for 15 min. the reaction mix were irradiated in a UV cross-linker (XL-1000, Funakoshi) at an energy setting of 86 mJ/cm^2 twice.

RESULTS

Expression of EMI2 during oocyte maturation

To investigate protein expression of EMI2 in mouse oocytes, a polyclonal antibody against mouse EMI2 was raised in mouse, affinity purified and used for immunoblotting. The anti-EMI2 antibody specifically recognized recombinant EMI2-His (Fig. 18A). This antibody recognized GFP-EMI2 expressed in mouse oocytes by injection with GFP-Emi2 mRNA (Fig. 18B), indicating specificity of the signal. To test whether the anti-EMI2 antibody recognized endogenous EMI2, I performed immunoblot analysis using the extracts of immature and mature oocytes. In mature oocyte extracts, anti-EMI2 antibody recognized an approximately 85 kDa protein (Fig. 18C). The apparent molecular mass of this protein corresponds to the values estimated from the cDNA sequence of EMI2 in mouse and to the size of EMI2 shown in previous study (Madgwick et al., 2006). Furthermore, this signal was attenuated after incubation with recombinant EMI2-His (Fig. 18D), confirming that the anti-EMI2 antibody specifically recognizes endogenous EMI2.

Next the timing of EMI2 expression during oocyte maturation was examined by immunoblotting. The amount of cyclin B1 was gradually increased in metaphase I (MI) and metaphase II (MII)-stage oocytes. In contrast, EMI2 was not detected in GV- and MI-stage oocytes and the amount of EMI2 was significantly increased in MII-stage oocytes (Fig. 19A).

The results of immunoblot analyses suggested the translational activation of *Emi2* mRNA after the MI. Translational activation of maternal mRNAs has been shown to be driven by cytoplasmic elongation of the poly(A) tail in oocytes (McGrew et al., 1989; Vassalli et al., 1989; Sheets rt al., 1994; Stutz et al., 1998). To examine the timing of poly(A) tail elongation of *Emi2* mRNA, PAT assay was performed. Poly(A) tails of *Emi2* mRNA were elongated slightly in prometaphase I (PMI) and significantly in MII at the time when the amount of Emi2 was increased (Fig. 19B). In contrast, poly(A) tails of cyclin B1 mRNA were significantly elongated in PMI-stage oocytes. I then analyzed the amount of *Emi2* mRNA in polysomal fractionation. The amount of *Emi2*

mRNA in polysomal fraction was low in GV-stage oocytes but was significantly increased in MII-stage oocytes (Fig. 19C). The amount of EMI2 mRNA in MII-stage was 4.5-fold higher than in GV-stage oocytes. These results indicate that the translation of *Emi2* mRNA is repressed in GV-stage oocytes and activated possibly by poly(A) tail elongation in meiosis II.

Biological importance of temporal control of *Emi2* mRNA translation.

To assess the importance of poly(A) elongation of *Emi2* mRNA during oocyte maturation, I injected the antisense *Emi2* MOs into mouse oocytes. A previous study demonstrated that antisense MOs targeting the 3'-end sequences of mRNA prevent poly(A) tail elongation (Wada et al., 2012). I injected *Emi2* MO that targets the terminal sequence of *Emi2* mRNA 3'UTR (*Emi2*-3'UTR-MO) and *Emi2* MO that contains 5-nts mismatches (*Emi2*-5mm-MO) as a control (Fig. 20A) into GV-stage oocytes. Oocytes were then incubated for 2 h in M2+ medium and were released in M2- medium to induce oocyte maturation for 24-26 h. Immunoblot analysis showed that the synthesis of EMI2 was significantly inhibited by *Emi2*-3'UTR-MO, but not *Emi2*-5mm-MO. (Fig. 20B).

In oocytes injected with control MO, the first polar body was extruded and meiosis II spindle was observed with aligned chromosomes at 28 h after resumption of meiosis, indicating that the meiosis was arrested at MII as in the case of uninjected oocytes (Fig. 20C). In contrast, in oocytes injected with *Emi2*-3'UTR-MO, I observed a pronucleus like structure and decondensed chromatin with the first polar body (Fig. 20C). Subsequently, *Emi2*-3'UTR-MO-injected oocytes entered into the two-cell stage at 48 h after resumption of meiosis. These phenotypes of *Emi2*-3'UTR-MO injected oocytes were consistent with that of Emi2-knockdowned oocytes using RNAi or *Emi2*-MO which targets the translational start site of the *Emi2* mRNA (Shoji et al., 2006; Madgwick et al., 2006). These results suggested that EMI2 depletion through preventing poly(A) elongation of *Emi2* mRNA induced parthenogenetic activation.

Next, to assess the effects of presence of EMI2 in meiosis I, I injected mRNA encoding GFP or GFP-Emi2 into GV-stage oocytes and cultured them for 18 h in M2 medium to induce oocyte maturation. In oocytes expressing GFP, 81.1% of oocytes underwent normal meiotic progression and were arrested at MII (Fig. 21A and C). In contrast, 83.5% of the oocytes expressing GFP-EMI2 were arrested at MI (Fig. 21B and C). In these oocytes, GFP-EMI2 was localized at metaphase I spindle (Fig. 21B). These results were consistent with previous studies (Madgwick et al., 2006; Suzuki et al., 2010). However, it remained unresolved whether that the MI arrest in the GFP-EMI2-

expressing oocytes was induced by the spindle assembly checkpoint (SAC), which is a safeguard mechanism to ensure accurate chromosome segregation by delaying cell division until the all chromosomes are aligned. Mad2 is a key component of the SAC and monitors the microtubule attachment on kinetochores (Musacchio and Salmon., 2007). The SAC activity is maintained by the localization of Mad2 on kinetochores. To address the possibility that SAC activity was maintained in oocytes arrested at MI, I examined the distribution of Mad2 in meiosis I. Immunofluorescence analysis showed that Mad2 was not localized on kinetochores in oocytes expressing GFP-EMI2 and non-injected oocytes at 8 h after resumption of meiosis (Fig 21D). In contrast, Mad2 remained localized on kinetochores in oocytes treated with nocodazole, an inhibitor of microtubule polymerization. These results suggested that SAC was inactivated in GFP-EMI2-expressing oocytes. Thereby, MI arrest was caused by other factors; for instance, GFP-EMI2 might directly inhibit the APC/C activity by binding to a component of APC/C as observed in the arrest at MII in *Xenopus* oocytes (Inoue et al., 2007). Taken together, my results indicate that temporal control of translation of *Emi2* mRNA is important for correct progression of meiosis and embryonic development.

Emi2 mRNA forms granules distinct from cyclin B1 RNA granules

Dormant cyclin B1 and *Mad2* mRNAs were distributed as granules in immature oocytes and the granule formation is important to regulate the temporal translation of these mRNAs (Kotani et al., 2013; chapter II). I then assessed the mechanisms by which the translation of *Emi2* mRNA is temporally regulated. To detect *Emi2* mRNA in immature oocytes, I performed highly sensitive *in situ* hybridization with the tyramide signal amplification (TSA) system (chapter I). Using this methods, *Emi2* mRNA was detected in immature oocytes in mouse ovaries (Fig. 22A). To further investigate the distribution of dormant *Emi2* mRNA, I performed fluorescent *in situ* hybridization (FISH) with the TSA system. *Emi2* mRNA was detected as RNA granules in the cytoplasm of immature oocytes (Fig. 22B). Interestingly, double FISH analysis showed that *Emi2* and cyclin B1 mRNAs formed distinct granules (Fig. 22C).

The changes in RNA granules were further analyzed by time course of oocyte maturation. The number of cyclin B1 RNA granules was decreased in PMI and had almost completely disappeared in MII (Fig. 22D and E) (Kotani et al., 2013). In contrast, the number of *Emi2* RNA granules was decreased slightly in PMI, and the granules were almost completely disappeared in MII (Fig. 22D and E). The timing of *Emi2* RNA granule disassembly was coincident with that of poly (A) tail elongation of *Emi2* mRNA (Fig. 19B). These results suggest that translation of *Emi2* mRNA is

regulated through formation and disassembly of RNA granules as well as the translational regulation of cyclin B1 and *Mad2* mRNA (Kotani et al., 2013; chapter II). However, the timings of RNA granule disassembly were different between *Emi2* and cyclin B1 RNA granules, suggesting that there are some differences in the regulation of these granules.

The components of *Emi2* RNA granules are different from those of cyclin B1 RNA granules

To further assess the mechanism of *Emi2* mRNA translation, I investigated the RNA-binding proteins which interact with *Emi2* mRNA. Translational activation of cyclin B1 and *Mad2* mRNA was related to aggregation-dissolution of Pum1 aggregates (chapter II). Since *Emi2* mRNA formed RNA granules similar to these mRNAs (Fig. 22B), Pum1 was predicted to bind *Emi2* mRNA and regulate the translation of *Emi2* mRNA. I then investigated whether Pum1 binds to *Emi2* mRNA by IP/RT-PCR. cyclin B1 mRNA were detected in precipitation with an anti-Pum1 antibody, while not detected in precipitation with control IgG (Fig. 23A). In contrast, neither *Emi2* nor *α-tubulin* were detected in precipitation with anti-Pum1 antibody and control IgG. These results indicated that Pum1 binds to cyclin B1 mRNA but not *Emi2* mRNA even though these two mRNAs form granules in mouse immature oocytes.

Next, I investigated components common to both *Emi2* and cyclin B1 RNA granules by IP/RT-PCR. Several proteins that localize to stress granules have also been identified as components of other RNA granules, e.g. P bodies and neuronal granules (Buchan and Parker, 2009). HuR and HuB, members of ELAVL RNA-binding family, are known to be components of stress granules and to contribute mRNA stabilization (Gowrishankar et al., 2006; Snee and Macdonald, 2004). HuR is expressed in various cells and tissues (Hinman and Lou, 2008), and cyclin B1 RNA granules are co-localized with HuR in zebrafish oocytes (Kotani et a., 2013). HuB is expressed in brain and gonads (Colombrita et al., 2013). *Emi2* and cyclin B1 mRNAs, but not *α-tubulin* mRNAs, were detected in precipitations with anti-HuR or anti-HuB antibodies, while neither of them were detected in precipitation with control IgG (Fig. 23B and C), indicating that HuR and HuB bound to both *Emi2* and cyclin B1 mRNAs. These results suggest that HuR and HuB are components common to *Emi2* and cyclin B1 RNA granules, whereas Pum1 is specific to cyclin B1 RNA granule.

Identification of *Emi2*-specific RNA-binding proteins

Above results suggest that RNA granules in oocytes contain RNA-binding proteins

specific to each RNA granule. To isolate RNA-binding proteins consisting of *Emi2* RNA granules, I performed RNA pull-down assay by using *in vitro*-synthesized RNAs of *Xenopus Emi2* (x*Emi2*), mouse *Emi2* (m*Emi2*) and mouse cyclin B1 (mcyclin B1) 3' UTRs with extracts of *Xenopus* oocytes. Proteins bound to each RNAs were separated by SDS-PAGE and visualized by silver staining. Mass spectrometry analysis of individual gel bands identified 867 proteins in total, in which keratin and ribosomal proteins were excluded (Fig. 24). The 71 overlapping proteins were identified as proteins interacting with 3'UTR of x*Emi2* and m*Emi2* mRNA and 162 overlapping proteins were identified as proteins interacting with 3'UTR of x*Emi2*, m*Emi2* and mcyclin B1. In these proteins, 12 proteins were identified as candidates of RNA-binding proteins which interact with *Emi2* mRNA specifically (Table. 3). These candidate proteins have been shown to function in translational control or in mRNA stability, and the number of detected peptides was low (0 to 4 peptides) by mass spectrometry analysis in the extracts incubated with 3'UTR of mcyclin B1. I confirmed the expression of 5 out of 12 genes, which encode High density lipoprotein binding protein (Hdlbp), Tudor domain-containing protein3 (Tdrd3), Heterogenous nuclear ribonucleoprotein M (Hnrnpm), Elavl2 (HuB), and ATP-dependent RNA helicase DDX4 (Ddx4), in mouse ovaries by RT-PCR (Fig. 25A). The expression of remaining 7 genes remains to be analyzed. Although HuB was isolated as one of the proteins interacting with *Emi2* mRNA, immunoprecipitation analysis showed that it interacted with both *Emi2* and cyclin B1 mRNAs (Fig. 23C).

Tdrd3 is a modular protein identified based on its Tudor domain, and known to be a component of stress granules (Goulet et al., 2008). The N-terminal region contains DUF and OB-fold domains, thought to mediate interaction with nucleic acid, sugar and/or other proteins (Fig. 25 C). At the central region, an ubiquitin binding domain (UBA) is located. A domain responsible for the interaction with Fragile X mental retardation protein (FMRP) is located next to the Tudor domain. An exon junction complex binding motif (EBM) is located at the C-terminal end. The expression of *Tdrd3* mRNAs and TDRD3 protein ware confirmed in oocytes isolated from ovaries by RT-PCR and immunoblotting (Fig. 25B).

To examine whether TDRD3 binds to *Emi2* mRNA, I performed UV cross-linking assay. 3'UTR of *Emi2* and cyclin B1 RNA probes were incubated with FLAG-tagged TDRD3 and CPEB1. Both RNA probes were associated with CPEB1 (Fig. 26A), consistent with results of previous studies in *Xenopus* oocytes (Tung et al., 2007; Igea and Mendez, 2010). TDRD3 seemed to bind 3'UTR of *Emi2* RNA probe strongly and 3'UTR of cyclin B1 RNA probe weekly (Fig. 26A and B). However, in this assay, a

large fraction of TDRD3 was destructed (Fig. 25E), and thereby the amount of TDRD3-FLAG precipitated with anti-FLAG antibody was significantly small, resulting in very week specific signals and high background signals of UV cross-linking assay. To clearly demonstrate the interaction between TDRD3 and *Emi2* and cyclin B1 RNAs, I prepared FLAG-tagged TDRD3 deletion constructs, which consist of N-terminus (1-473 aa) and C-terminus (246-744 aa) of TDRD3 (Fig. 25C). Immunoblot analysis showed that TDRD3 (246-744 aa) was divided into many fragments when it was translated using rabbit reticulocyte lysate system regardless of the position of FLAG-tag, while TDRD3 (1-473 aa) was not destructed (Fig. 25D). Therefore, I used FLAG-tagged TDRD3 (1-473 aa) for UV cross-linking assay. 3'UTR of *Emi2* and cyclin B1 RNA probes were incubated with FLAG-tagged TDRD3 (1-473 aa). The 3'UTR of *Emi2* RNA probe was associated with FLAG-tagged TDRD3 (1-473 aa), whereas the cyclin B1 RNA probe was not (Fig. 26C), indicating that TDRD3 (1-473 aa) specifically interacts with *Emi2* mRNA.

TDRD3 overlapped with *Emi2* mRNA but not cyclin B1 mRNA in oocyte cytoplasm

To further assess the specificity of interaction between TDRD3 and *Emi2* mRNA, I analyzed the distribution of TDRD3 in the oocyte cytoplasm by a super resolution microscope. Immunofluorescence analysis showed that TDRD3 was distributed in the cytoplasm of immature oocytes as many particles (Fig. 27A). In addition, double immunofluorescence using anti-TDRD3 and anti-Pum1 antibodies showed that signals of TDRD3 were smaller than those of Pum1, and that these proteins were not co-localized (Fig. 27B). To visualize the localization of mRNAs, I performed FISH of *Emi2* and cyclin B1 mRNAs, combined with immunostaining of TDRD3 and Pum1 (Fig. 27C and D). In most case, TDRD3 was partially overlapped with the periphery of the granules (Fig. 27C, indicated by arrows), while Pum1 was not overlapped with *Emi2* RNA granules. Pum1 surrounded and overlapped with cyclin B1 RNA granules (Fig. 27D, indicated by arrows), while TDRD3 did not. These observations were consistent with the results of IP/RT-PCR (Fig. 23A) and UV cross-linking assay (Fig. 26C). Taken together, these results demonstrate that *Emi2* RNA granules contain TDRD3 but not Pum1, and cyclin B1 RNA granules contain Pum1 but not TDRD3.

TDRD3 functions in the temporal regulation of *Emi2* mRNA translation in meiosis II.

UV cross-linking assay and FISH analysis combined with immunofluorescence

indicated that TDRD3 interacted with *Emi2* mRNA, however, the function of TDRD3 in mouse oocytes was unclear. I finally assessed whether TDRD3 plays a role in the translational regulation of *Emi2* mRNA. To examine the effects of TDRD3 inhibition on the progression of oocyte maturation, immature oocytes were injected with anti-TDRD3 antibody or IgG and incubated in M2 medium. After resumption of meiosis, oocytes injected with IgG or anti-TDRD3 antibody underwent meiosis and were arrested at metaphase II (MII). The MII arrest was maintained for more than 48 hours. In addition, morphological difference was not observed between anti-TDRD3 antibody- and IgG-injected oocytes (data not shown). Next, I analyzed the timing of expression of EMI2 protein during oocyte maturation in injected oocytes. Anti-TDRD3 antibody- or IgG-injected oocytes were collected at 0, 8, 12, and 18 h after resumption of meiosis for immunoblotting. Immunoblot analysis showed that the amount of EMI2 in anti-TDRD3 antibody-injected oocytes was smaller than that in IgG-injected oocytes at 12 h, while there is no difference at 18 h (Fig. 28A and B). The amount of cyclin B1 was not affected in meiosis I; however, synthesis of cyclin B1 was attenuated at MII in anti-TDRD3 antibody-injected oocytes. In contrast, the amount of Mad2 was not changed between the oocytes injected with anti-TDRD3 antibody and IgG. Analysis of the timing of first polar body (PB1) extrusion showed that the timing of PB1 extrusion was almost the same between two samples, indicating that TDRD3 inhibition by injection of anti-TDRD3 antibody did not affect the progression of meiosis till PB1 extrusion (Fig. 28C). These results suggest that TDRD3 regulates the timing of *Emi2* mRNA translation in meiosis II.

DISCUSSION

Translational regulation by assembling RNA granules during oocyte maturation

In zebrafish oocytes, the temporal translation of cyclin B1 mRNA was shown to be regulated by formation and disassembly of RNA granules (Kotani et al., 2013). In addition, zebrafish *mos* mRNA was identified as RNA granules in immature oocytes (Horie and Kotani, 2016). In mouse oocytes, the temporal translation of cyclin B1 and *Mad2* mRNA was shown to be regulated by Pum1-mediated RNA granules (Kotani et al., 2013; chapter II). These mRNAs are translated in meiosis I. Therefore, the translation of dormant mRNAs that translated in meiosis I seems to be regulated by granule formation in zebrafish and mouse. In this study, the temporal translation of *Emi2* mRNA was shown to be regulated by formation and disassembly of RNA granules

(Fig. 22). My results showed for the first time that a dormant mRNA, which is translated in meiosis II, forms granules and suggested that temporal translation of dormant mRNAs is regulated through formation and disassembly of RNA granules in both meiosis I and meiosis II.

Interestingly, although Pum1 is a key protein to form granules and regulate the translation of cyclin B1 and *Mad2* mRNA in mouse oocytes, IP/RT-PCR revealed that *Emi2* mRNA did not interact with Pum1 (Fig. 23A). This result suggests that the components of these RNA granules in oocytes are different in distinct mRNAs, and the specific proteins would contribute to the regulation of temporal translation. In contrast to the specific proteins such as Pum1, HuR and HuB proteins bound to both cyclin B1 and *Emi2* mRNAs (Fig. 23C). HuR is widely expressed in various cells and tissues, and has been shown to be a component of stress granules (Gallouzi et al., 2000). In HuR-knockdown HeLa cells, the size of stress granules became generally much smaller, and the number of granules decreased, indicating that HuR is a key component to assemble granules (Fujimura et al., 2009). HuB is expressed specifically in neurons, ovary, testis and oocytes. HuB is a component of neuronal stress granules (Markmiller et al., 2018) and has been shown to function in translational regulation in mouse oocytes (Chalupnikova et al., 2014). Therefore, my results suggest that HuR and HuB may function in assembling cyclin B1 and *Emi2* RNA granules in mouse oocytes. In contrast to Pum1 and TDRD3, HuR and HuB would be a basic component of RNA granules in mouse oocytes regardless of the timing of translational activation of assembled mRNAs.

Function of TDRD3 in *Emi2* RNA granules

The *tudor* gene was identified in *Drosophila* in 1985 as one of the maternal factors that regulate embryonic development and fertility (Boswell and Mahowald, 1985). More than 200 Tudor-domain containing proteins have been identified from many eukaryotes. The functions of Tudor-domain containing proteins have reported widely in histone modification, DNA damage response, pi-RNA-mediated transposon silencing, RNA metabolism including RNA splicing and small RNA pathway, and so on (Ponting, 1997; reviewed by Siomi et al., 2010). Consistent with these functions, Tudor domains have been found together in the same polypeptide as various RNA-binding motifs (DEAD-box or KH-domain), chromatin-binding domain, DNA-binding domains, and several others. Previous studies indicated that TDRD3 has some domains, such as DUF, OB-fold, UBA, Tudor, FMRP and EBM (Fig. 25C) (Morettin et al., 2017). However, a domain which directly interact with mRNA has not been reported.

In my study, FLAG-tagged TDRD3 (1-473 aa) bound to 3'UTR of *Emi2* mRNA in

UV cross-linking analysis (Fig. 26C), indicating that this region has a potential for binding to mRNA directly. In addition, this region may bind to a specific mRNA because FLAG-tagged TDRD3 (1-473 aa) did not bind to 3'UTR of cyclin B1 mRNA (Fig. 26C). In breast cancer cells, TDRD3 has been shown that it can selectively promote translation of specific mRNAs using TDRD3-knockdown cells and polyribosome fraction analysis (Morettin et al., 2017). Taken together, my results suggest that TDRD3 binds to specific mRNAs and regulates the translation of the mRNAs in mouse oocytes. Identification of a domain, which directly interact with specific mRNA, will be an interesting issue to be explored.

My results showed that TDRD3 signals of immunofluorescence in immature oocytes were smaller than Pum1 signals (Fig. 27B). As mentioned in chapter II, Pum1 has a prion-like domain which is thought to promote highly ordered aggregation of proteins. Therefore, signals of Pum1 were comparatively large because the number of Pum1 molecules would be larger than that of TDRD3 molecules in each signal. Simultaneous detection of TDRD3 and *Emi2* mRNA showed that TDRD3 was partially overlapped with the periphery of the *Emi2* RNA granules (Fig. 27C). TDRD3 has been shown to be a component of stress granules and to engage in protein-protein interactions, but does not significantly induce stress granule formation on its own (Goulet et al., 2008). Therefore, TDRD3 may not nucleate *Emi2* RNA granule assembly but interact with other component proteins of granules and with *Emi2* mRNA directly. Therefore, TDRD3 may participate in *Emi2* RNA granules assembly "after assembly of core granules", and distributed at the periphery of the granules. However, my experiments were insufficient to support the structure of *Emi2* RNA granules. Further experiments will be needed to reveal the structure of *Emi2* RNA granules in detail.

In the anti-TDRD3 antibody-injected oocytes, the synthesis of EMI2 was attenuated at 12 h after resumption of meiosis even though the progression of meiosis I and the timing of PB1 extrusion were not delayed (Fig. 28). This antibody would prevent the function of TDRD3 in the translational activation of *Emi2* mRNA in early meiosis II. However, the amount of EMI2 was recovered until 18 h after resumption of meiosis and no morphological affects were observed in anti-TDRD3 antibody injected oocytes. Injection with anti-TDRD3 antibody might not sufficiently prevent translational activation of *Emi2* mRNA and the amount of EMI2 achieved enough to inhibit APC/C activity until metaphase II. In contrast to the recovery of EMI2, the synthesis of cyclin B1 was attenuated in meiosis II. This result would be induced by indirect effects because cyclin B1 mRNA is not interact with TDRD3. These results suggest that 1) TDRD3 is not involved in translational control in meiosis I and 2) TDRD3 functions in

the temporal regulation of *Emi2* mRNA translation in meiosis II. Further studies are needed to clearly indicate the functions of TDRD3 in meiosis II.

My study revealed a novel specific component of *Emi2* RNA granules which functions in the translational control in meiosis II. In addition, *Emi2* mRNA does not interact with Pum1, which plays important roles in the regulation of cyclin B1 and *Mad2* mRNAs translation in meiosis I. This difference in the RNA-binding proteins might contribute to control highly ordered temporal translation of mRNAs. These results will be important in future studies to explore the mechanisms of temporal regulation that are mediated by RNA granules.

GENERAL DISCUSSION

Extensive biochemical studies have shown that the translational regulation of dormant mRNAs in oocytes rely on *cis*-acting elements of the mRNAs. CPEB is a *trans*-acting factor that binds to a *cis*-acting element, CPE located in the 3'UTR of mRNAs. After induction of oocyte maturation, CPEB directs polyadenylation of CPE-containing mRNAs and activates the translation of the mRNAs (McGrew et al., 1989; Vassalli et al., 1989; Sheets rt al., 1994; Stutz et al., 1998). In addition to *cis*-acting element-mediated cytoplasmic polyadenylation, our laboratory showed that formation and disassembly of cyclin B1 RNA granules regulate the timing of translation of cyclin B1 mRNA (Kotani et al., 2013). In Chapter II, I revealed that the translation of *Mad2* mRNA is temporally regulated through formation and disassembly of RNA granules in meiosis I (Fig. 8). I also showed that *Emi2* mRNA, which is translated in meiosis II, formed granules in immature oocytes and the granules were disassembled at the timing of translational activation of *Emi2* mRNA (Fig. 22), in Chapter III. Interestingly, cyclin B1, *Mad2* and *Emi2* mRNAs formed distinct granules (Fig.8 and 22). In neurons, distinct neuronal RNA granules are independently disassembled by different neuronal stimuli, suggesting that translational activation of the mRNAs is regulated by the formation and disassembly of distinct granules (Baez et al., 2011; Luchelli et al., 2015; Mikl et al., 2011). My results suggested that distinct granules of dormant mRNAs could be independently regulated for achieving translational regulation of distinct mRNAs in temporal order. Indeed, my results provided that an aggregation of Pum1 ensures translational repression of cyclin B1 and *Mad2* mRNA by stably maintaining their granular structures, and the dissolution of aggregates possibly by phosphorylation permits the disassembly of granules and translational activation of mRNAs (Fig. 14, 15 and 16). In contrast to these mRNAs, *Emi2* mRNA was not a Pum1-target mRNA (Fig. 23), so the other mechanisms might regulate the translation of *Emi2* mRNAs. Instead of Pum1, TDRD3 was revealed as a novel protein which bound to *Emi2* mRNA, but not to cyclin B1 mRNA. My results suggested that TDRD3 regulates the timing of translation of *Emi2* mRNA in meiosis II (Fig. 26, 27 and 28). In contrast to Pum1 and TDRD3, HuR and HuB, which are components of stress granules and neuronal granules, were bound to both cyclin B1 and *Emi2* mRNAs (Fig. 23). Taken together, my results provide a model for the temporal and spatial regulation of dormant mRNAs during oocyte maturation as follows.

(1) The dormant mRNAs assemble into granules in immature oocytes by RNA-binding proteins, which function in assembling the other types of RNA granules such as

stress granules.

(2) The translation of dormant mRNAs is regulated through formation and disassembly of RNA granules during oocyte maturation regardless of the different timings of the translation.

(3) The changes in property of RNA-binding proteins are involved in the translational regulation of target mRNAs during oocyte maturation.

(4) The components of RNA granules are different in distinct mRNAs, and this difference in the RNA-binding proteins contribute to the regulation of temporal translation.

In addition to the translational activation by *cis*-acting element-mediated polyadenylation, my results propose the new mechanisms by which the timings of translation of various dormant mRNAs are regulated.

This model will contribute to an understanding of the translational mechanisms during oocyte maturation not only in mouse but also in other species. In zebrafish oocytes, the translation of *cyclin B1* and *mos* mRNAs has been shown to be regulated by formation and disassembly of RNA granules (Kotani et al., 2013; Horie and Kotani, 2016). In addition, *cyclin B1* mRNA has been shown to be a Pum1-targeted mRNA in *Xenopus* and zebrafish oocytes (Nakahata et al., 2001; Pique et al., 2008; Ota et al., 2011; Kotani et al., 2013) and Pum1 is phosphorylated during oocyte maturation (Oha et al., 2011; Saitoh et al., 2018).

Especially, Pum1 phosphorylation is a key step to promote the disassembly of *cyclin B1* RNA granules and activate the translation of *cyclin B1* mRNA in zebrafish oocytes (Saitoh et al., 2018). These results imply that the mechanisms of translational regulation are, at least, partially common in these specie's oocytes. Therefore, I expect that the model described here for mouse oocytes contribute to an understanding of the molecular mechanisms of translational regulation during oocyte maturation in wide range of species.

SUMMARY

Chapter I. Subcellular localization of mRNAs has emerged as major regulatory mechanisms of gene expression in various cell types and many organisms. However, techniques that enable detection of the subcellular distribution of mRNAs with high sensitivity and high resolution remain limited, particularly in vertebrate adult tissues and organs. In this study, I examined the expression and localization of mRNAs encoding Pou5f1/Oct4, Mos, Cyclin B1 and Deleted in Azoospermia-like (Dazl) in zebrafish and mouse ovaries by combining tyramide signal amplification (TSA)-based *in situ* hybridization with paraffin sections which can preserve cell morphology of tissues and organs at subcellular levels. The mRNAs encoding Mos, Cyclin B1 and Dazl were found to assemble into distinct granules that were distributed in different subcellular regions of zebrafish and mouse oocytes, suggesting conserved and specific regulations of these mRNAs. Therefore, the *in situ* hybridization method demonstrated in this study achieved the detection and comparison of precise distribution patterns of mRNAs at subcellular levels in single cells of adult tissues and organs. This high-sensitivity and high-resolution *in situ* hybridization is applicable to many vertebrate species and to various tissues and organs and will be useful for studies on the subcellular regulation of gene expression at the level of RNA localization.

Chapter II. Temporal and spatial control of mRNA translation has emerged as a major mechanism for promoting diverse biological processes. However, the molecular nature of temporal and spatial control of translation remains unclear. In oocytes, many mRNAs are deposited as a translationally repressed form and are translated at appropriate timings to promote the progression of meiosis and development. Here, I show that changes in subcellular structures and states of the RNA-binding protein Pumilio1 regulate the translation of target mRNAs and progression of oocyte maturation. Pumilio1 was shown to bind to *Mad2* and cyclin B*1* mRNAs, assemble highly clustered aggregates, and surround *Mad2* and cyclin B1 RNA granules in mouse oocytes. These Pumilio1 aggregates were dissolved prior to the translational activation of target mRNAs possibly by phosphorylation. Stabilization of Pumilio1 aggregates prevented the translational activation of target mRNAs and progression of oocyte maturation. Together, my results provide an aggregation-dissolution model for the temporal and spatial control of translation.

Chapter III. Many translationally repressed mRNAs are accumulated in the oocyte cytoplasm and translated in periods specific to distinct mRNAs. *Emi2* mRNA is translated in meiosis II and encodes proteins to arrest the meiosis at metaphase II. The timing of translation of *Emi2* mRNA is strictly regulated for normal progression of meiosis and development. However, the mechanisms by which the temporal translation of *Emi2* mRNA is regulated remain unclear. I demonstrated that Pumilio1 (Pum1)-mediated RNA granules of cyclin B1 and *Mad2* mRNAs regulate the temporal translation of these mRNAs in meiosis I in mouse oocytes in chapter II. In chapter III, I found that *Emi2* mRNA forms granules distinct from cyclin B1 RNA granules in the mouse oocyte cytoplasm. Interestingly, immunoprecipitation analysis followed by RT-PCR showed that Pum1 did not interact with *Emi2* mRNA, while stress granule components, HuR and HuB, interacted with both *Emi2* and cyclin B1 mRNAs. In addition, RNA-binding proteins specifically interacting with *Emi2* mRNA were detected by RNA pull-down assay, and of these proteins, Tudor domain-containing protein 3 (TDRD3) was identified by UV cross-linking assay and simultaneous detection of mRNAs and proteins using a super-resolution microscope. Injection of anti-TDRD3 antibody induced the delay of the translational timing of *Emi2* mRNA, but not affected the translation and meiotic progression in meiosis I. These results suggest that TDRD3 regulates the temporal translation of *Emi2* mRNA and that specific RNA-binding proteins are a key factor to control the timing of translation during oocyte maturation.

REFERENCES

Asaoka-Taguchi, M., M. Yamada, A. Nakamura, K. Hanyu, and S. Kobayashi. (1999). Maternal Pumilio acts together with Nanos in germline development in Drosophila embryos. *Nat. Cell Biol*. 1:431-437.

Arthur, K.P., M. Claussen, S. Koch, K. Tarbashevich, O. Jahn, and T. Pieler. (2009). Participation of Xenopus Elr-type proteins in vegetal mRNA localization during oogenesis. *J. Biol. Chem.* 284:19982-19992.

Barkoff, A.F., K.S. Dickson, N.K. Gray, and M. Wickens. (2000). Translational control of cyclin B1 mRNA during meiotic maturation: coordinated repression and cytoplasmic polyadenylation. *Dev. Biol*. 220:97-109.

Barnard, D.C., K. Ryan, J.L. Manley, and J.D. Richter. (2004). Symplekin and xGLD-2 are required for CPEB-mediated cytoplasmic polyadenylation. *Cell.* 119:641–651.

Belloc, E., and R. Méndez. (2008). A deadenylation negative feedback mechanism governs meiotic metaphase arrest. *Nature*. 456:1017-1022.

Blower, M.D., E. Feric, K. Weis, and R. Heald. (2007) Genome-wide analysis demonstrates conserved localization of messenger RNAs to mitotic microtubules. *The J. cell biol*. 179:1365-1373.

Boag, P.R., A. Atalay, S. Robida, V. Reinke, and T.K. Blackwell. (2008). Protection of specific maternal messenger RNAs by the P body protein CGH-1 (Dhh1/RCK) during *Caenorhabditis elegans* oogenesis. *J. Cell Biol.* 182:543–557.

Boswell, R.E., and A.P. Mahowald. (1985). tudor, a gene required for assembly of the germ plasm in Drosophila melanogaster. *Cell*. 43:97-104

Brangwynne, C.P., C.R. Eckmann, D.S. Courson, A. Rybarska, C. Hoege, J. Gharakhani, F. Julicher, and A.A. Hyman. (2009). Germline P granules are liquid droplets that localize by controlled dissolution/condensation. *Science*. 324:1729-1732.

Buchan, J.R., and R. Parker. (2009). Eukaryotic stress granules: the ins and outs of translation. *Mol. Cell*. 36: 932-41

Bury, L., P.A. Coelho, A. Simeone, S. Ferries, C.E. Eyers, P.A. Eyers, M. Zernicka-Goetz, and D.M. Glover. (2017). Plk4 and Aurora A cooperate in the initiation of acentriolar spindle assembly in mammalian oocytes. *J. Cell Biol*. 216:3571-3590.

Buxbaum, A.R., G. Haimovich, and R.H. Singer. (2015). In the right place at the right time: visualizing and understanding mRNA localization. *Nat. Rev. Mol. Cell*

Biol. 16:95-109.

Buxbaum, A.R., B. Wu, and R.H. Singer. (2014). Single β-actin mRNA detection in neurons reveals a mechanism for regulating its translatability. *Science*. 343:419-422.

Chalupnikova, K., P. Solc, V. Sulimenko, R. Sedlacek, and P. Svoboda. (2014). An oocyte-specific ELAVL2 isoform is a translational repressor ablated from meiotically competent antral oocytes. *Cell Cycle*. 13:1187-1200.

Chandrakesan, P., R. May, D. Qu, N. Weygant, V.E. Taylor, J.D. Li, N. Ali, S.M. Sureban, M. Qante, and T.C. Wang. (2015) Dclk1+ small intestinal epithelial tuft cells display the hallmarks of quiescence and self-renewal. *Oncotarget*. 6:30876-30886.

Chen, D., W. Zheng, A. Lin, K. Uyhazi, H. Zhao, and H. Lin. (2012). Pumilio 1 suppresses multiple activators of p53 to safeguard spermatogenesis. *Curr. Biol.* 22:420-425.

Chen, J., C. Melton, N. Suh, J.S. Oh, K. Horner, F. Xie, C. Sette, R. Blelloch, and M. Conti. (2011). Genome-wide analysis of translation reveals a critical role for deleted in azoospermia-like (Dazl) at the oocyte-to-zygote transition. *Genes Dev*. 25:755-766.

Colombrita, C., V. Silani, and A. Ratti. (2013). ELAV proteins along evolution: back to the nucleus? *Mol. Cell. Neurosci.* 56:447–455.

Conti,M. and Franciosi,F. (2018). Acquisition of oocyte competence to develop as an embryo: integrated nuclear and cytoplasmic events. *Hum. Reprod*. 24:245–266.

Cox, K.H., D.V. DeLeon, L.M. Angerer, and R.C. Angerer. (1984). Detection of mRNAs in sea urchin embryos by in situ hybridization using asymmetric RNA probes. *Dev. Biol*. 101:485-502.

Davydenko, O., R.M. Schultz, and M.A. Lampson. (2013). Increased CDK1 activity determines the timing of kinetochore-microtubule attachments in meiosis I. *J. Cell Biol*. 202:221-229.

Daldello, E.M., X.G. Luong, C.R. Yang, J. Kuhn, and M. Conti. (2019). Cyclin B2 is required for progression through meiosis in mouse oocytes. *Development*. 146.

de Moor, C.H., and J.D. Richter. (1999). Cytoplasmic polyadenylation elements mediate masking and unmasking of cyclin B1 mRNA. *EMBO J*. 18:2294-2303.

de Moor, C.H., H. Meijer, and S. Lissenden. (2005). Mechanisms of translational control by the 3' UTR in development and differentiation. Semin. *Cell Dev. Biol*. 16:49–58.

Decker, C.J., D. Teixeira, and R. Parker. (2007). Edc3p and a glutamine/asparagine-rich

domain of Lsm4p function in processing body assembly in Saccharomyces cerevisiae. *J. Cell Biol*. 179:437-449.

Elbaum-Garfinkle, S., Y. Kim, K. Szczepaniak, C.C. Chen, C.R. Eckmann, S. Myong, and C.P. Brangwynne. (2015). The disordered P granule protein LAF-1 drives phase separation into droplets with tunable viscosity and dynamics. *Proc. Natl. Acad. Sci.* 112:7189-7194.

Fujimura, K., J. Katahira, F. Kano, Y. Yoneda, and M. Murata. (2009). Microscopic dissection of the process of stress granule assembly. BBM Mol. Cell Res. 1793:1728-1737.

Furuno, N., M. Nishizawa, K. Okazaki, H. Tanaka, J. Iwashita, N. Nakajo, Y. Ogawa, and N. Sagata. (1994). Suppression of DNA replication via Mos function during meiotic divisions in Xenopus oocytes. *EMBO J*. 13: 2399–2410.

Gaffré, M., A. Martoriati, N. Belhachemi, J.P. Chambon, E. Houliston, C. Jessus, and A. Karaiskou. 2011. A critical balance between Cyclin B synthesis and Myt1 activity controls meiosis entry in Xenopus oocytes. *Development*. 138:3735–3744.

Gallo, C.M., J.T. Wang, F. Motegi, and G. Seydoux. (2010). Cytoplasmic partitioning of P granule components is not required to specify the germline in C. elegans. *Science*. 330:1685-1689.

Gallouzi, I.E., C.M. Brennan, M.G. Stenberg, M.S. Swanson, A. Eversole, N. Maizels, and J.A. Steitz. (2000). HuR binding to cytoplasmic mRNA is perturbed by heat shock. *PNAS.* 97:3073–3078.

Gebauer, F., W. Xu, G.M. Cooper, and J.D. Richter. (1994). Translational control by cytoplasmic polyadenylation of c-mos mRNA is necessary for oocyte maturation in the mouse. *EMBO J*. 13:5712-5720.

Gennarino, V.A., R.K. Singh, J.J. White, A. De Maio, K. Han, J.Y. Kim, P. Jafar-Nejad, A. di Ronza, H. Kang, L.S. Sayegh, T.A. Cooper, H.T. Orr, R.V. Sillitoe, and H.Y. Zoghbi. (2015). Pumilio1 haploinsufficiency leads to SCA1-like neurodegeneration by increasing wild-type Ataxin1 levels. *Cell*. 160:1087-1098.

Gilks, N., N. Kedersha, M. Ayodele, L. Shen, G. Stoecklin, L.M. Dember, and P. Anderson. (2004). Stress granule assembly is mediated by prion-like aggregation of TIA-1. *Mol. Biol. Cell*. 15:5383-5398.

Goulet, I., S. Boisvenue, S. Mokas, R. Mazroui, J. Côté. (2008). TDRD3, a novel Tudor domain-containing protein, localizes to cytoplasmic stress granules. *Hum. Mol. Genet*. 17:3055-74.

Gowrishankar, G., R. Winzen, O. Dittrich-Breiholz, N. Redich, M. Kracht, H. H.

Holtmann. (2006). Inhibition of mRNA deadenylation and degradation by different types of cell stress. *Biol. Chem*. 387:323-7.

Gupta, T., F.L. Marlow, D. Ferriola, K. Mackiewicz, J. Dapprich, D. Monos, and M.C. Mullins. (2010). Microtubule actin crosslinking factor 1 regulates the Balbiani body and animal-vegetal polarity of the zebrafish oocyte. *PLoS Genet*. 6:e1001073.

Hampl, A. and J.J. Eppig. (1995). Translational regulation of the gradual increase in histone H1 kinase activity in maturing mouse oocytes. *Mol. Reprod. Dev*. 40:9-15.

Harrison, P.R., Conkie, D., Paul, J. and Jones, K. (1973) Localisation of cellular globin messenger RNA by in situ hybridisation to complementary DNA. *FEBS Letters*. 32, 109-112.

Hashimoto, Y., S. Maegawa, T. Nagai, E. Yamaha, H. Suzuki, K. Yasuda, and K. Inoue. (2004). Localized maternal factors are required for zebrafish germ cell formation. *Dev. Biol*. 268:152-161.

Hayden, A.H., A. McdDougall, M. Levasseur, K. Yallop, A.P. Murdoch, and M. Herbert. (2005). Mad2 prevents aneuploidy and premature proteolysis of cyclin B and securing during meiosis I in mouse oocytes. *Gene Dev*. 19:202-207.

Heim, A.E., O. Hartung, S. Rothhamel, E. Ferreira, A. Jenny, and E.F. Marlow, (2014). Oocyte polarity requires a Bucky ball-dependent feedback amplification loop. *Development*. 141:842-854.

Hinman, M.N., and H. Lou. (2008). Diverse molecular functions of Hu proteins. *Cell Mol. Life Sci*. 65:3168 –3181.

Hochegger, H., A. Klotzbücher, J. Kirk, M. Howell, K. le Guellec, K. Fletcher, T. Duncan, M. Sohail, and T. Hunt. (2001). New B-type cyclin synthesis is required between meiosis I and II during Xenopus oocyte maturation. *Development*. 128:3795–3807.

Homer, H.A., A. McDougall, M. Levasseur, K. Yallop, A.P. Murdoch, and M. Herbert. (2005). Mad2 prevents aneuploidy and premature proteolysis of cyclin B and securin during meiosis I in mouse oocytes. *Genes Dev*. 19:202-207.

Horie, M. and T. Kotani. (2016). Formation of mos RNA granules in the zebrafish oocyte that differ from cyclin B1 RNA granules in distribution, density and regulation. *Eur. J. Cell. Biol*. 95:563-573.

Houston, D.W. and M.L. King. (2000). A critical role for Xdazl, a germ plasm-localized RNA, in the differentiation of primordial germ cells in Xenopus. *Development*. 127:447-456.

Igea, A., and R. Méndez. (2010). Meiosis requires a translational positive loop where CPEB1 ensues its replacemrnt by CPEB4. *EMBO J*. 29:2182-2193.

Inoue, D., M. Ohe, Y. Kanemori, T. Nobui, and N. Sagata. (2007). A direct link of the Mos-MAPK pathway to Erp/Emi2 in meiotic arrest of Xenopus laevis eggs. Nature. 26:1100-1104

Itzkovitz, S., A. Lyubimova, I.C. Blat, M. Maynard, J. van Es, J. Lees, T. Jacks, H. Clevers, and A. van Oudenaarden. (2011). Single-molecule transcript counting of stem-cell markers in the mouse intestine. *Nat. Cell Biol*. 14:106-114.

Jaenisch, R. and R. Young. (2008). Stem cells, the molecular circuitry of pluripotency and nuclear reprogramming. *Cell*. 132:567-582.

Jain, S., J.R. Wheeler, R.W. Walters, A. Agrawal, A. Barsic, and R. Parker. (2016). ATPase-modulated stress granules contain a diverse proteome and substructure. *Cell*. 164:487-498.

Kimura, H., and P.R. Cook. (2001). Kinetics of core histones in living human cells: little exchange of H3 and H4 and some rapid exchange of H2B. *J. Cell Biol*. 153:1341-1353.

Kloc, M., M.T. Dougherty, S. Bilinski, A.P. Chan, E. Brey, M.L. King, C.W. Patrick Jr., and L.D. Etkin. (2002). Three-dimensional ultrastructural analysis of RNA distribution within germinal granules of Xenopus. *Dev. Biol*. 241:79–93.

Kloc, M., N.R. Zearfoss, and L.D. Etkin. (2002). Mechanisms of subcellular mRNA localization. *Cell*. 108:533-544.

Kloc, M., I. Jedrzejowska, W. Tworzydlo, and S.M. Bilinski. (2014). Balbiani body, nuage and sponge bodies--term plasm pathway players. *Arthropod struct Dev*. 43:341-348.

Kondo, T., T. Yanagawa, N. Yoshida, and M. Yamashita. (1997). Introduction of cyclin B induces activation of the maturation-promoting factor and breakdown of germinal vesicle in growing zebrafish oocytes unresponsive to the maturation-inducing hormone. *Dev. Biol*.190:142-152.

Kondo, T., T. Kotani, and M. Yamashita. (2001). Dispersion of cyclin B mRNA aggregation is coupled with translational activation of the mRNA during zebrafish oocyte maturation. *Dev. Biol*. 229:421-431.

Kosaka, K., K. Kawakami, H. Sakamoto, and K. Inoue. (2007). Spatiotemporal localization of germ plasm RNAs during zebrafish oogenesis. *Mech. Dev*. 124:279-289.

Kotani, T., K. Maehata, and N. Takei. (2017). Regulation of translationally repressed mRNAs in zebrafish and mouse oocytes. *Results Probl. Cell Differ*. 63:297-324.

Kotani, T., and M. Yamashita. (2002). Discrimination of the roles of MPF and MAP kinase in morphological changes that occur during oocyte maturation. *Dev. Biol*. 252:271-286.

Kotani, T., K. Yasuda, R. Ota, and M. Yamashita. (2013). Cyclin B1 mRNA translation is temporally controlled through formation and disassembly of RNA granules. *J. Cell Biol*. 202:1041-1055.

Kuersten, S., and E.B. Goodwin. (2003). The power of the 3' UTR: translational control and development. *Nat. Rev*. *Genet*. 4:626–637.

Lancaster, A.K., A. Nutter-Upham, S. Lindquist, and O.D. King. (2014). PLAAC: a web and command-line application to identify proteins with prion-like amino acid composition. *Bioinformatics*. 30:2501-2502.

Lecuyer, E., H. Yoshida, N. Parthasarathy, C. Alm, T. Babak, T. Cerovina, T.R. Hughes, P. Tomancak, and H.M. Krause. (2007). Global analysis of mRNA localization reveals a prominent role in organizing cellular architecture and function. *Cell*. 131:174-187.

Ledan, E., Z. Polanski, M.E. Terret, and B. Maro. (2001). Meiotic maturation of the mouse oocyte requires an equilibrium between cyclin B synthesis and degradation. *Dev. Biol*. 232:400-413.

Lee, C.D., and B.P. Tu. (2015). Glucose-regulated phosphorylation of the PUF protein Puf3 regulates the translational fate of its bound mRNAs and association with RNA granules. *Cell Rep*. 11:1638-1650.

Lehmann, R., and C. Nussleinvolhard. (1987). Involvement of the Pumilio gene in the transport of an abdominal signal in the Drosophila embryo. *Nature*. 329:167-170.

Li, Y.R., O.D. King, J. Shorter, and A.D. Gitler. (2013). Stress granules as crucibles of ALS pathogenesis. *J. Cell Biol*. 201:361-372.

Lin, Y., D.S.W. Protter, M.K. Rosen, and R. Parker. (2015). Formation and maturation of phase-separated liquid droplets by RNA-binding proteins. *Mol. Cell*. 60:208-219.

Luong, X.G., E.M. Daldello, G. Rajkovic, C.R. Yang, and M. Conti. (2020). Genome-wide analysis reveals a switch in the translational program upon oocyte meiotic resumption. *Nucleic Acids Res*. 48:3257-3276.

Madgwick, S., V.L. Nixon, H.-Y. Chang, M. Herbert, M. Levasseur, and K.T. Jones. 2004. Maintenance of sister chromatid attachment in mouse eggs through maturation-promoting factor activity. *Dev. Biol*. 275:68–81.

Madgwick, S., D.V. Hansen, M. Leavasseur, P.K. Jackson, and K.T. Jones. (2006).

Mouse Emi2 is required to enter meiosis II by reestablished cyclin B1 during interkinesis. *J Cell Biol*. 174:791-801.

Maegawa, S., K. Yasuda, and K. Inoue. (1999). Maternal mRNA localization of zebrafish DAZ-like gene. *Mech. Dev*. 81:223-226.

Maharana, S., J. Wang, D.K. Papadopoulos, D. Richter, A. Pozniakovsky, I. Poser, M. Bickle, S. Rizk, J. Guillen-Boixet, T.M. Franzmann, M. Jahnel, L. Marrone, Y.T. Chang, J. Sterneckert, P. Tomancak, A.A. Hyman, and S. Alberti. (2018). RNA buffers the phase separation behavior of prion-like RNA binding proteins. *Science*. 360:918-921.

Mak, W., C. Fang, T. Holden, M.B. Dratver, and H. Lin. (2016). An important role of Pumilio 1 in regulating the development of the mammalian female germline. *Biol. Reprod*. 94:134.

Markmiller, S., S. Soltanieh, K.L. Server, R. Mak, W. Jin, M.Y. Fang, E. Luo, F. Krach, D. Yang, A. Sen, A. Fulzele, J.M. Wozniak, D.J. Gonzalez, M.W. Kankel, F. Gao, E.J. Bennett, E. Lecuyer, and G.W. Yeo. (2018). Context-dependent and disease-specific diversity in protein interactions within stress granules. *Cell*. 17:590-604

Marlow, F.L. and Mullins, M.C. (2008) Bucky ball functions in Balbiani body assembly and animal-vegetal polarity in the oocyte and follicle cell layer in zebrafish. *Dev. Biol.* 321:40-50.

Martin, K.C. (2004). Local protein synthesis during axon guidance and synaptic plasticity. *Curr. Opin. Neurobiol.* 14:305–310.

Martin, K.C., and A. Ephrussi. (2009). mRNA localization: gene expression in the spatial dimension. *Cell*. 136:719-730.

Masek, T., E. Llana, L. Gahurova, M. Kubelka, A. Susor, K. Roucova, C. Lin, A.W. Bruce, and M. Pospisek. (2020). Identifying the translatome of mouse NEBD-stage oocytes via SSP-profiling; a novel polysome fractionation method. *Int. Mol. Sci.* 12:1254

Masui, Y., and C.L. Markert. (1971). Cytoplasmic control of nuclear behavior during meiotic maturation of frog oocytes. *J. Exp. Zool*. 177:129–145.

Masui, Y., and H.J. Clarke. (1979). Oocyte maturation. *Int. Rev. Cytol*. 57:185-282.

McGrew, L.L., E. Dworkin-Rastl, M.B. Dworkin, and J.D. Richter. (1989). Poly(A) elongation during Xenopus oocyte maturation is required for translational recruitment and is mediated by a short sequence element. *Genes Dev*. 3:803-815.

Mendez, R., D. Barnard, and J.D. Richter. (2002). Differential mRNA translation and meiotic progression require Cdc2- mediated CPEB destruction. *EMBO J.*

21:1833–1844.

Mendez, R., and J.D. Richter. (2001). Translational control by CPEB: a means to the end. *Nat. Rev. Mol. Cell Biol*. 2:521-529.

Mikl, M., G. Vendra, and M.A. Kiebler. (2011). Independent localization of MAP2, CaMKIIalpha and b-actin RNAs in low copy numbers. *EMBO Rep.* 12:1077-1084.

Mili, S., K. Moissoglu, and I.G. Macara. (2008) Genome-wide screen reveals APC-associated RNAs enriched in cell protrusions. *Nature*. 453, 115-119.

Mili, S., and I.G. Macara. (2009). RNA localization and polarity: from A(PC) to Z(BP). *Trends Cell Biol*. 19:156-164.

Mingle, L.A., N.N. Okuhama, J. Shi, R.H. Singer, J. Condeelis, and G. Liu. (2005). Localization of all seven messenger RNAs for the actin-polymerization nucleator Arp2/3 complex in the protrusions of fibroblasts. *J. Cell Sci*. 118:2425-2433.

Moissoglu, K., K. Yasuda, T. Wang, G. Chrisafis, and S. Mili. (2019). Translational regulation of protrusion-localized RNAs involves silencing and clustering after transport. *eLife*. 8.

Molliex, A., J. Temirov, J. Lee, M. Coughlin, A.P. Kanagaraj, H.J. Kim, T. Mittag, and J.P. Taylor. (2015). Phase separation by low complexity domains promotes stress granule assembly and drives pathological fibrillization. *Cell*. 163:123-133.

Morettin, A., G. Paris, Y. Bouzid, R. M. Baldwin, T.J. Falls, J.C. Bell, and J. Cote. (2017). Tudor domain containing protein 3 promotes tumorigenesis and invasive capacity of breast cancer cells. *Sci. Rep*. 7:5153

Murata, Y., and R.P. Wharton. (1995). Binding of pumilio to maternal hunchback mRNA is required for posterior patterning in Drosophila embryos. *Cell*. 80:747-756.

Mussacchio, A and E.D. Salmon. (2007). The spindle-assembly checkpoint in space and time. *Nat. Rev. Mol. Cell Biol.* 8:379-393

Nakahata, S., T. Kotani, K. Mita, T. Kawasaki, Y. Katsu, Y. Nagahama, and M. Yamashita. (2003). Involvement of Xenopus Pumilio in the translational regulation that is specific to cyclin B1 mRNA during oocyte maturation. *Mech. Dev*. 120:865-880.

Nabti, I. P. Marangos, J. Bormann, N.R. Kudo, and J. Carroll. (2014). Dual-mode regulation of the APC/C by CDK1 and MAPK controls meiosis I progression and fidelity. *J. Cell Biol.* 204:891-900.

Nakahata, S., Y. Katsu, K. Mita, K. Inoue, Y. Nagahama, and M. Yamashita. (2001).

Biochemical identification of Xenopus Pumilio as a sequence-specific cyclin B1 mRNA-binding protein that physically interacts with a Nanos homolog, Xcat-2, and a cytoplasmic polyadenylation element-binding protein. *J. Biol. Chem*. 276:20945–20953.

Nakahata, S., T. Kotani, K. Mita, T. Kawasaki, Y. Katsu, Y. Nagahama, and M. Yamashita. (2003). Involvement of Xenopus Pumilio in the translational regulation that is specific to cyclin B1 mRNA during oocyte maturation. *Mech. Dev.* 120:865-880.

Nakajo, N., S. Yoshitome, J. Iwashita, M. Iida, K. Uto, S. Ueno, K. Okamoto, and N. Sagata. (2000). Absence of Wee1 ensures the meiotic cell cycle in Xenopus oocytes. *Genes Dev*. 14:328–338.

Nichols, J., B. Zevnik, K. Anastassiadis, H. Niwa, D. Klewe-Nebenius, I. Chambers, H. Scholer, and A. Smith. (1998). Formation of pluripotent stem cells in the mammalian embryo depends on the POU transcription factor Oct4. *Cell*. 95:379-391.

Nixon, V.L., M. Levasseur, A. McDougall, and K.T. Jones. (2002). Ca2+ oscillations promote APC/C-dependent cyclin B1 degradation during metaphase arrest and completion of meiosis in fertilizing mouse eggs. *Curr. Biol.* 12:746–750.

Noble, S.L., B.L. Allen, L.K. Goh, K. Nordick, and T.C. Evans. 2008. Maternal mRNAs are regulated by diverse P body–related mRNP granules during early Caenorhabditis elegans development. *J. Cell Biol*. 182:559–572.

Nott, T.J., E. Petsalaki, P. Farber, D. Jervis, E. Fussner, A. Plochowietz, T.D. Craggs, D.P. Bazett-Jones, T. Pawson, J.D. Forman-Kay, and A.J. Baldwin. (2015). Phase transition of a disordered nuage protein generates environmentally responsive membraneless organelles. *Mol. Cell*. 57:936-947.

Nukada, Y., Horie, M., Fukui, A., Kotani, T. and Yamashita, M. (2015) Real-time imaging of actin filaments in the zebrafish oocyte and embryo. *Cytoskeleton (Hoboken)*. 72:491-501.

Nurse, P. (1990) Universal control mechanism regulating onset of M-phase. *Nature*. 344:503-508.

Ohe, M., Y. Kawamura, H. Ueno, D. Inoue, Y. Kanemori, C. Senoo, M. Isoda, N. Nakajp, and N. Sagata. (2010). Emi2 inhibition of the anaphase-promoting complex/cyclosome absolutely requires Emi2 Binding via the C-terminal RL tail. *Mol. Biol. Cell*. 21, 905-913.

Ota, R., T. Kotani, and M. Yamashita. (2011a). Biochemical characterization of Pumilio1 and Pumilio2 in Xenopus oocytes. *J. Biol. Chem*. 286:2853-2863.

Ota, R., T. Kotani, and M. Yamashita. (2011b). Possible involvement of Nemo-like kinase 1 in Xenopus oocyte maturation as a kinase responsible for Pumilio1, Pumilio2, and CPEB phosphorylation. *Biochemistry*. 50:5648-5659.

Pahlavan, G., Z. Polanski, P. Kalab, R. Golsteyn, E.A. Nigg, and B. Maro. (2000). Characterization of polo-like kinase 1 during meiotic maturation of the mouse oocyte. *Dev. Biol*. 220:392-400.

Pique, M., J.M. Lopez, S. Foissac, R. Guigo, and R. Mendez. (2008). A combinatorial code for CPE-mediated translational control. *Cell*. 132:434-448.

Polanski, Z., E. Ledan, S. Brunet, S. Louvet, M.H. Verlhac, J.Z. Kubiak, and B. Maro. (1998). Cyclin synthesis controls the progression of meiotic maturation in mouse oocytes. *Development*. 125:4989-4997.

Ponding, C.P. (1997). Evidence for PDZ domains in bacteria, yast, and plants. *Protein Sci.* 6:464-468.

Raap, A.K., M.P. van de Corput, R.A. Vervenne, R.P. van Gijlswijk, H.J. Tanke, and J. Wiegant. (1995). Ultra-sensitive FISH using peroxidase-mediated deposition of biotin- or fluorochrome tyramides. *Human Mol. Genet*. 4:529-534.

Radford, H.E., H.A. Meijer, and C.H. de Moor. (2008). Translational control by cytoplasmic polyadenylation in Xenopus oocytes. *Biochim. Biophys. Acta*. 1779:217-229.

Raj, A., van den Bogaard, P., Rifkin, S.A., van Oudenaarden, A. and Tyagi, S. (2008) Imaging individual mRNA molecules using multiple singly labeled probes. *Nat. Methods.* 5, 877-879.

Reijns, M.A., R.D. Alexander, M.P. Spiller, and J.D. Beggs. (2008). A role for Q/N-rich aggregation-prone regions in P-body localization. *J Cell Sci*. 121:2463-2472.

Reijo, R.,T.Y. Lee, P. Salo, R. Alagappan, L.G. Brown, M. Rosenberg, S. Rozen, T. Jaffe, D. Straus, and O. Hovatta. (1995). Diverse spermatogenic defects in humans caused by Y chromosome deletions encompassing a novel RNA-binding protein gene. *Nat. Genet*. 10:383-393.

Richter, J.D. (2007). CPEB: a life in translation. *Trends Biochem Sci*. 32:279-285.

Ruggiu, M., R. Speed, M. Taggart, S.J. McKay, F. Kilanowski, P. Saunders, J. Dorin, and H.J. Cooke. (1997). The mouse Dazla gene encodes a cytoplasmic protein essential for gametogenesis. *Nature*. 389:73-77.

Russo, A., C. Cirulli, A. Amoresano, P. Pucci, C. Pietropaolo, and G. Russo. (2008). cis-acting sequences and trans-acting factors in the localization of mRNA for mitochondrial ribosomal proteins. *Biochim. Biophys. Acta*. 1779:820-829.

Sagata, N., I. Daar, M. Oskarsson, S.D. Showalter, and G.F. Vande Woude. (1989). The

product of the mos proto-oncogene as a candidate "initiator" for oocyte maturation. *Science*. 245:643-646.

Sagata, N. (1996). Meiotic metaphase arrest in animal oocytes: its mechanisms and biological significance. Trends *Cell. Biol*. 6:22–28.

Saitoh, A., Y. Takada, M. Horie, and T. Kotani. (2018). Pumilio1 phosphorylation precedes translational activation of its target mRNA in zebrafish oocytes. *Zygote*. 26:372-380.

Satoh, Y., N. Takei, S. Kawamura, N. Takahashi, T. Kotani, and A.P. Kimura. (2018). A novel testis-specific long noncoding RNA, *Tesra*, activates the *Prss42/Tessp-2* gene during mouse spermatogenesis. *Biol. Reprod*. 100:833-848

Salazar, A.M., E.J. Silverman, K.P. Menon, and K. Zinn. (2010). Regulation of synaptic Pumilio function by an aggregation-prone domain. *J. Neurosci.* 30:515-522.

Schisa, J.A., J.N. Pitt, and J.R. Priess. (2001). Analysis of RNA associated with P granules n germ cells of *C elegans* adults. *Development.* 128:1287-1298.

Scholer, H.R., A.K. Hatzopoulos, R. Balling, N. Suzuki, and P. Gruss. (1989). A family of octamer-specific proteins present during mouse embryogenesis: evidence for germline-specific expression of an Oct factor. *EMBO J*. 8:2543-2550.

Setoyama D, M. Yamashita, and N. Sagata. (2007). Mechanism of degradation of CPEB during Xenopus oocyte maturation. *PNAS.* 104:18001–18006.

Sheets, M.D., C.A. Fox, T. Hunt, G. Vande Woude, and M. Wickens. (1994). The 3'-untranslated regions of c-mos and cyclin mRNAs stimulate translation by regulating cytoplasmic polyadenylation. *Genes Dev*. 8:926-938.

Shiina, N. (2019). Liquid- and solid-like RNA granules form through specific scaffold proteins and combine into biphasic granules. *J. Biol. Chem*. 294:3532-3548.

Shoji, S., N. Yoshida, M. Amanai, M. Ohgishi, T Fukui, S. Fujimoto, Y. Nakano, E. Kajikawa, and A.C. Perry. (2006). Mammalian Emi2 mediates cytostatic arrest and transduces the signal for meiotic exit via Cdc20. *EMBO J*. 25:834-845.

Siomi, A.C., T. Mannen, and H. Siomi. (2010). How does the Royal Family of Tudor rule the PIWI-interacting RNA pathway? *Genes Dev*. 24:636-646.

Smith, G.D., A. Sadhu, S. Mathies, and D.P. Wolf. (1998). Characterization of protein phosphatases in mouse oocytes. *Dev. Biol*. 204:537-549.

Snee, M.J., and P.M. Macdonald. (2004). Live imaging of nuage and polar granules: evidence against a precursor-product relationship and a novel role for Oskar in stabilization of polar granule components. *J Cell Sci*. 117:2109-20.

Souquere, S., G. Beauclair, F. Harper, A. Fox, and G. Pierron. (2010). Highly ordered spatial organization of the structural long noncoding NEAT1 RNAs within

paraspeckle nuclear bodies. *Mol. Biol. Cell*. 21:4020-4027.

Spassov, D.S., and R. Jurecic. (2003). The PUF family of RNA-binding proteins: does evolutionarily conserved structure equal conserved function? *IUBMB Life*. 55:359-366.

St Johnston, D. (2005) Moving messages: the intracellular localization of mRNAs. *Nat. Rev. Mol. Cell. Biol*. 6:363-375.

Stutz, A., B. Conne, J. Huarte, P. Gubler, V. Völkel, P. Flandin, and J.D. Vassalli. (1998). Masking, unmasking, and regulated polyadenylation cooperate in the translational control of a dormant mRNA in mouse oocytes. *Genes Dev*. 12:2535–2548.

Susor, A., D. Jansova, R. Cerna, A. Danylevska, M. Anger, T. Toralova, R. Malik, J. Supolikova, M.S. Cook, J.S. Oh, and M. Kubelka. (2015). Temporal and spatial regulation of translation in the mammalian oocyte via the mTOR-eIF4F pathway. *Nat. Commun*. 6:6078.

Suzuki, H., T. Tsukahara, and K. Inoue. (2009) Localization of c-mos mRNA around the animal pole in the zebrafish oocyte with Zor-1/Zorba. *Bioscience Trends*. 3:96-104.

Suzuki, T., E. Suzuki, N. Yoshida, A. Kubo, H. Li, E. Okuda, M. Amanai and A.C.F. Perry. (2010). Mouse Emi2 as a distinctive regulatory hub in second meiotic metaphase. *Development*. 137:3281-3291.

Tay, J., R. Hodgman, and J.D. Richter. (2000). The control of cyclin B1 mRNA translation during mouse oocyte maturation. *Dev. Biol*. 221:1-9.

Thomson, T., and P. Lasko. (2004). Drosophila tudor is essential for polar granule assembly and pole cell specification, but not for posterior patterning. *Genesis*. 40:16470

Trcek, T., M. Grosch, A. York, H. Shroff, T. Lionnet, and R. Lehmann. (2015). Drosophila germ granules are structured and contain homotypic mRNA clusters. *Nat. Commun*. 6:7962.

Tsutsumi, M., H. Muto, S. Myoba, M. Kimoto, A. Kitamura, M. Kamiya, T. Kikukawa, S. Takiya, M. Demura, K. Kawano, M. Kinjo, and T. Aizawa. (2016). In vivo fluorescence correlation spectroscopy analyses of FMBP-1, a silkworm transcription factor. *FEBS Open Bio*. 6:106-125.

Tung, J.J., K. Padmanabhan, D.V. Hansen, J.D. Richter and P.K. Jackson. (2007). Translational unmasking of Emi2 directs cytostatic factor arrest in meiosis II. *Cell Cycle*. 6:725-731.

Tunquist, B.J., and J.L. Maller. (2003). Under arrest: cytostatic (CSF)-mediated

metaphase arrest in vertebrate eggs. *Genes Dev.* 17:683-710.

Vassalli, D.J., J. Huarte, D. Belin, P. Gubler, A. Vassalli, L.M. O'Connell, A.L. Parton, J.R. Rickles, and S. Strickland. (1989). Regulated polyadenylation controls mRNA translation during meiotic maturation of mouse oocytes. *Genes Dev.* 3:2163-2171.

Vogler, T.O., J.R. Wheeler, E.D. Nguyen, M.P. Hughes, K.A. Britson, E. Lester, B. Rao, N.D. Betta, O.N. Whitney, T.E. Ewachiw, E. Gomes, J. Shorter, T.E. Lloyd, D.S. Eisenberg, J.P. Taylor, A.M. Johnson, B.B. Olwin, and R. Parker. (2018). TDP-43 and RNA form amyloid-like myo-granules in regenerating muscle. *Nature*. 563:508-513.

Wada, T., M. Hara, T. Taneda, C. Qingfu, R. Takata, K. Moro, K. Takeda, T. Kishimoto, and H. Haneda. (2012). Antisense morpholino targeting just upstream from a poly(A) tail junction of maternal mRNA removes the tail and inhibits translation. *Nucleic Acids Res*. 40:e173

Wang, F., Flanagan, J., Su, N., Wang, L.C., Bui, S., Nielson, A., Wu, X., Vo, H.T., Ma, X.J. and Luo, Y. (2012) RNAscope: a novel in situ RNA analysis platform for formalin-fixed, paraffin-embedded tissues. *J. Mol. Diagn.* 4:22-29.

Wang, J.T., J. Smith, B.C. Chen, H. Schmidt, D. Rasoloson, A. Paix, B.G. Lambrus, D. Calidas, E. Betzig, and G. Seydoux. (2014). Regulation of RNA granule dynamics by phosphorylation of serine-rich, intrinsically disordered proteins in C. elegans. *eLife*. 3:e04591.

Weber, S.C., and C.P. Brangwynne. (2012). Getting RNA and protein in phase. *Cell*. 149:1188-1191.

West, J.A., M. Mito, S. Kurosaka, T. Takumi, C. Tanegashima, T. Chujo, K. Yanaka, R.E. Kingston, T. Hirose, C. Bond, A. Fox, and S. Nakagawa. (2016). Structural, super-resolution microscopy analysis of paraspeckle nuclear body organization. *J. Cell Biol*. 214:817-830.

Wickens, M., D.S. Bernstein, J. Kimble, and R. Parker. (2002). A PUF family portrait: 3'UTR regulation as a way of life. *Trends Genet*. 18:150-157.

Wilk, R., J. Hu, D. Blotsky, and H.M. Krause. (2016). Diverse and pervasive subcellular distributions for both coding and long noncoding RNAs. *Genes Dev.* 30:594-609.

Winata, C.L., and V. Korzh. (2018). The translational regulation of maternal mRNAs in time and space. *FEBS Letters*. 592:3007-3023.

Wu, G., D. Han, Y. Gong, V. Sebastiano, L. Gentile, N. Singhal, K. Adachi, G. Fischedick, C. Ortmeier, and M. Sinn. (2013). Establishment of totipotency does

not depend on Oct4A. *Nat. Cell Biol*. 15:1089-1097.

Yamashita, M., M. Yoshikuni, T. Hirai, S. Fukada, Y. Nagahama. (1991). A monoclonal antibody against the PSTAIR sequence of p34cdc2, catalytic subunit of maturation-promoting factor and key regulator of the cell cycle. *Dev.Growth Differ.* 33:617-624.

Yang, Y., Y. Lu, A. Espejo, J. Wu, W. Xu, S. Liang, and M.T. Bedfor. (2010). TDRD3 is an effector molecule for arginine methylated histone marks. *Mol. Cell*. 40:1016-1023.

Yasuda, K., T. Kotani, R. Ota, and M. Yamashita. (2010). Transgenic zebrafish reveals novel mechanisms of translational control of cyclin B1 mRNA in oocytes. *Dev. Biol*. 348:76-86.

Yasuda, K., H. Zhang, D. Loiselle, T. Haystead, L.G. Macara and S. Mili. (2013). The RNA-binding protein Fus directs translation of localized mRNAs in APC-RNP granules. *J. Cell Biol*. 203:737-746

Yasuda, K., T. Kotani, and M. Yamashita. (2013). A cis-acting element in the coding region of cyclin B1 mRNA couples subcellular localization to translational timing. *Dev. Biol*. 382:517-529.

Zhang, B., M. Gallegos, A. Puoti, E. Durkin, S. Fields, J. Kimble, and M.P. Wickens. (1997). A conserved RNA-binding protein that regulates sexual fates in the C. elegans hermaphrodite germ line. *Nature*. 390:477-484.

Zhang, M., D. Chen, J. Xia, W. Han, X. Cui, N. Neuenkirchen, G. Hermes, N. Sestan, and H. Lin. (2017). Post-transcriptional regulation of mouse neurogenesis by Pumilio proteins. *Genes Dev*. 31:1-16.

COPYRIGHT STATEMENT

TABLES

TABLE 1. Reagents used in chapter I.

Slide coating
- Gelatin powder (Wako Pure Chemical Industries, Ltd., cat.no. 077-03155)
Paraffin sections
- Isoamyl acetate (Wako Pure Chemical Industries, Ltd., cat.no. 016-03646)
- Lemosol (Wako Pure Chemical Industries, Ltd., cat.no. 128-03993)
- Paraffin (Fisher Scientific; melting point, 56-57˚C, cat.no. T-565-1)
Stock solutions
- Torula RNA (Sigma, cat.no. R6625)
Probe preparation - SP6 RNA polymerase (Roche, cat.no. 810 274)
- T7 RNA polymerase (Roche, cat.no. 881 767)
- T3 RNA polymerase (Roche, cat.no. 1 031 163)
- DIG RNA Labeling Mix (Roche, cat.no. 1 277 073)
- Fluorescein RNA Labeling Mix (Roche, cat.no. 1 685 619)
Proteinase K stimulation
- Proteinase K (Sigma, cat.no. P2308)
Hybridization
- RNase A (Sigma, cat.no. R4875)
Detection of DIG- and fluorescein-labeled RNA probes
- Blocking reagent (PerkinElmer, Inc., cat.no. FP1020)
- Anti-DIG-HRP antibody (Roche, cat.no. 1 207 733)
- Anti-Fluorescein-HRP antibody (Roche, cat.no. 1 426 346)
- Anti-DNP-AP antibody (PerkinElmer, Inc., cat.no. NEL746A)
- Anti-DNP-Alexa 488 antibody (Molecular Probes, cat.no. A-11097)
- Tyramide-DNP (PerkinElmer, Inc., cat.no. NEL746A)
- Tyramide-Cy3 (PerkinElmer, Inc., cat.no. NEL744)
- Tyramide-Fluorescein (PerkinElmer, Inc., cat.no. NEL741)
Mounting
- Prolong Antifade Kit (Molecular probes, cat.no. P7184)
- Fluoro-KEEPER Antifade Reagent (Nacalai Tesque, cat.no. 12593-64)

TABLE 2. RNA probes used for detection of target mRNAs.

Species	Transcripts	Labeling	Strands
Mouse	*Pou5f1/Oct4*	DIG	Antisense/Sense
Zebrafish	*mos*	Fluorescein	Antisense/Sense
Zebrafish	*cyclin B1*	DIG, Fluorescein	Antisense/Sense
Zebrafish	*dazl*	DIG	Antisense/Sense
Mouse	*Cyclin B1*	Fluorescein	Antisense/Sense
Mouse	*Dazl*	DIG	Antisense/Sense

TABLE 3. Candidate proteins to interact with *Emi2* mRNA. Peptide count indicates the number of detected peptides by mass spectrometry analysis

Symbol	Name	Peptide count		
		x*Emi2*	m*Emi2*	m*Cyclin B1*
Eif2s1	Eukaryotic translation initiation factor 2 subunit 1	1	2	0
Eif2b2	eukaryotic translation initiation factor 2B, subunit 2 beta	2	3	0
Dhx29	DEAH (Asp-Glu-Ala-His) box polypeptide 29	1	3	0
Hnrnpdl	heterogeneous nuclear ribonucleoprotein D-like	1	1	0
Hdlbp	high density lipoprotein (HDL) binding protein	1	4	0
Tdrd3	tudor domain-containing protein 3	1	1	0
Drg	developmentally regulated GTP binging protein	2	6	1
Hnrnpm	heterogeneous nuclear ribonucleoprotein M	2	16	1
Elavl2	ELAV like RNA binding protein 1	11	9	4
Ddx4	DEAD box helicase 4	13	9	4
Tarbp2	TARBP2, RISC loading complex RNA binding subunit	16	5	4
Srp	signal recognition particle	5	9	4

FIGURES

Fig. 1. Photographs of zebrafish and mouse ovaries. (A) A zebrafish ovary after being dissected into several pieces, followed by fixing with 4% PFA/PBS and washing with PBS. (B) A mouse ovary after being fixed with 4% PFA/PBS and washed with PBS. Bars: 2 mm.

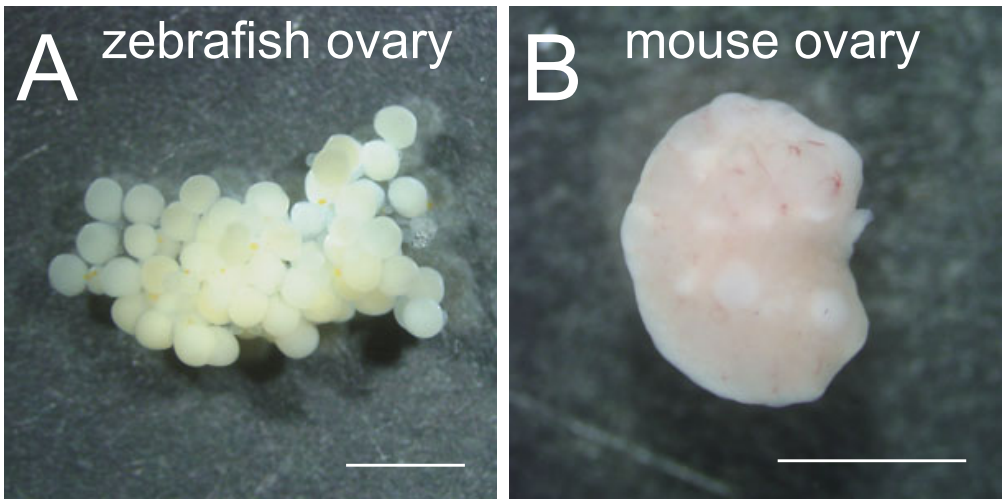
A
zebrafish ovary
B
mouse ovary

Fig. 2. Single *in situ* hybridization of *Pou5f1/Oct4* mRNA (purple) in mouse ovaries. (A-B) Mouse ovary sections hybridized with the antisense (A) or sense (B) *Pou5f1/Oct4* RNA probe without amplification of signals using the TSA system (-TSA). No signal was detected in this conventional *in situ* hybridization method. (C-D) Mouse ovary sections hybridized with the antisense (C) or sense (D) *Pou5f1/Oct4* RNA probe with amplification of signals using the TSA system (+TSA). The signals were detected in oocytes of sections hybridized with the antisense RNA probe (C) but not in those hybridized with the sense RNA probe (D). Arrows indicate oocytes observed in the sections. Bars: 100 μm.

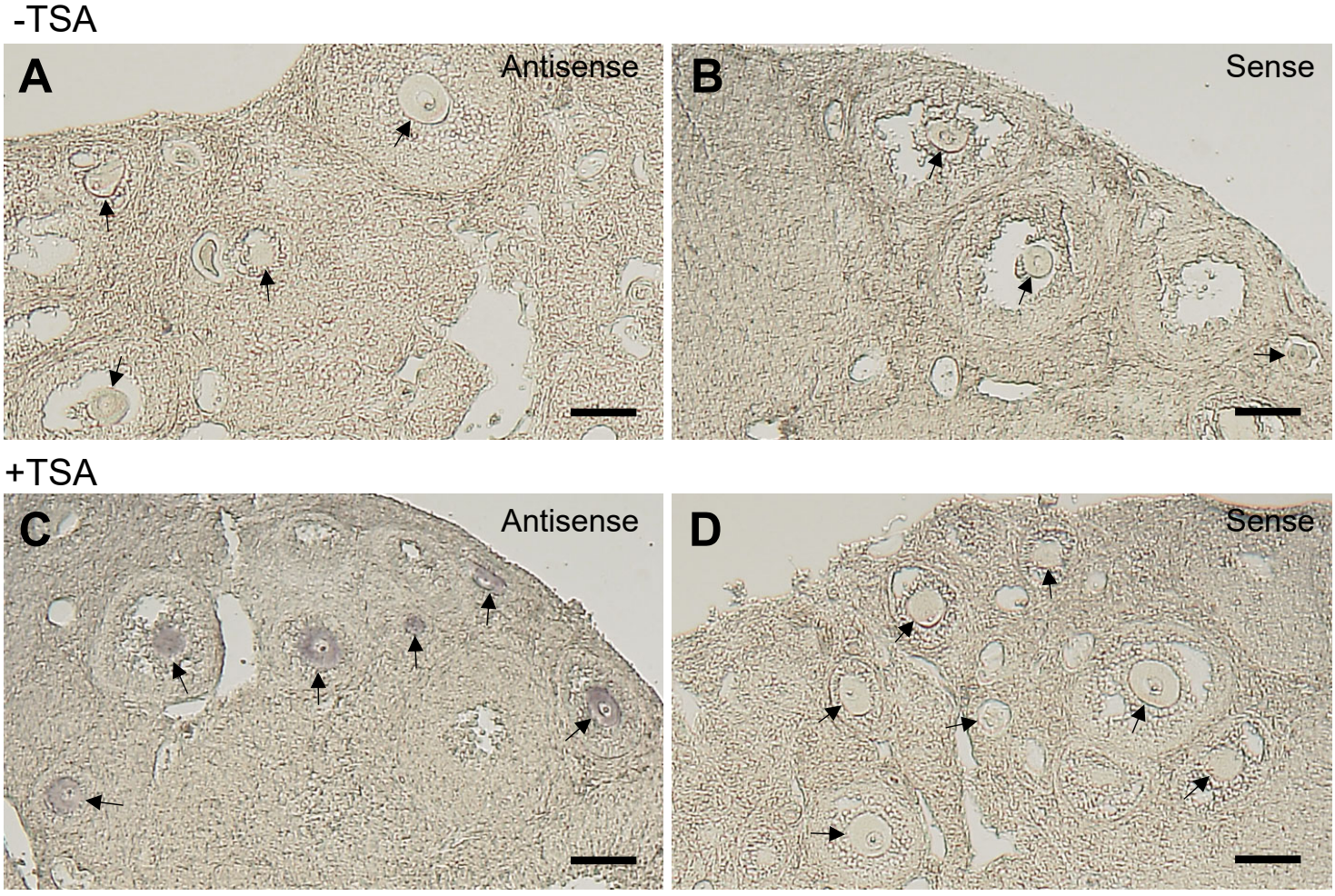
-TSA
A
Antisense
B
Sense
+TSA
C
Antisense
D
Sense

Fig. 3. The tissue and cell morphology of mouse and zebrafish ovaries. (A) A section of mouse ovary stained with hematoxylin and eosin (HE). A follicle consisting of fully grown oocyte is shown.. (B-D) Sections of zebrafish ovary stained with HE. Follicles consisting of stage I oocytes (B), stage II and III oocytes (C), and stage IV oocyte (D). a, antrum; Bb, Balbiani body; c, chorion; fc, follicle cells; GV, germinal vesicle; m, micropyle; oc, oocyte cytoplasm; y, yolk. Bars: 50 μm in A-D.

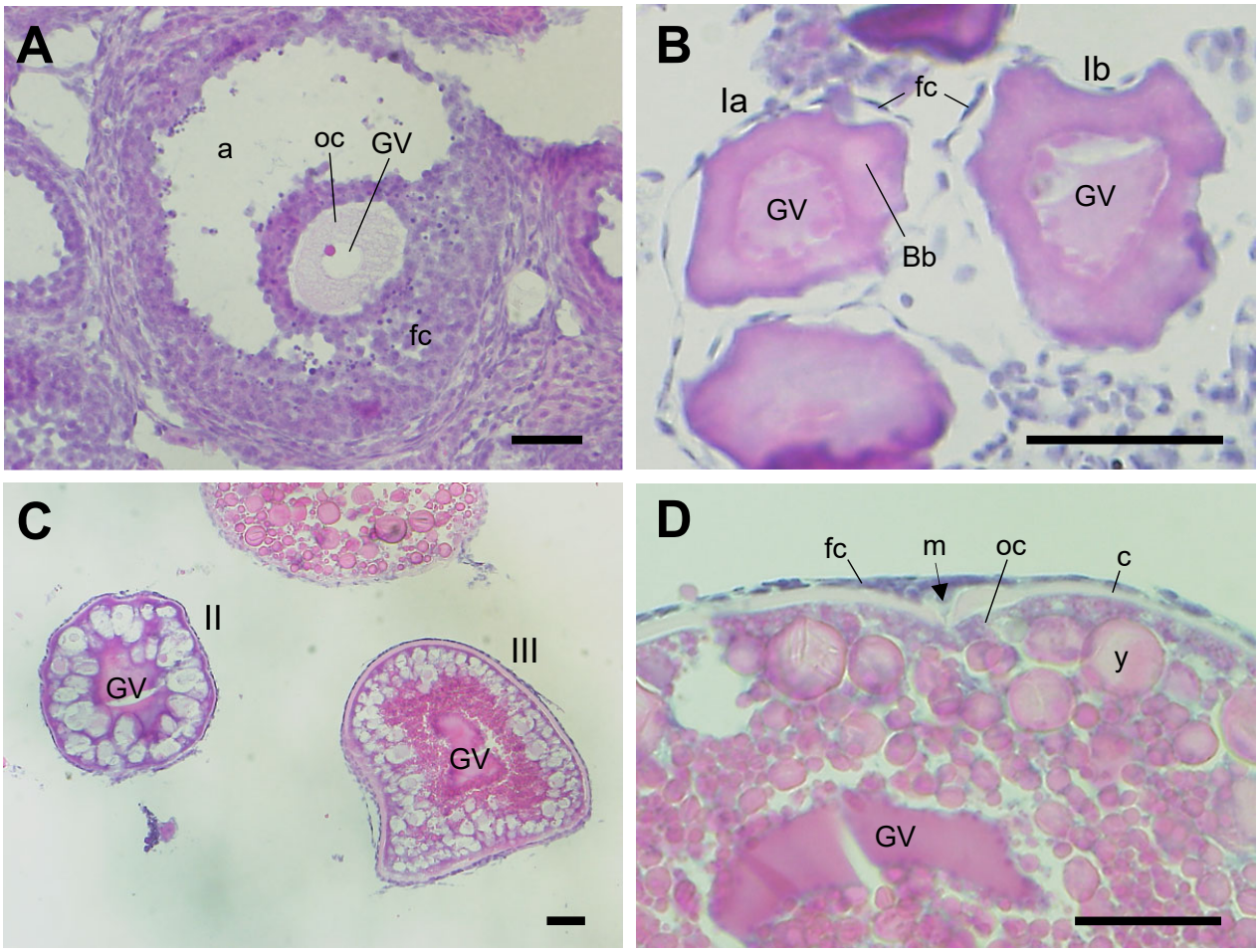
A
a
oc
GV
fc
B
Ia
fc
Ib
GV
GV
Bb
C
II
GV
III
GV
D
fc
m
oc
c
y
GV

Fig. 4. Double fluorescence *in situ* hybridization of *mos* (red) and *cyclin B1* (green) mRNAs in zebrafish ovaries. DNA is shown in blue. (A-C) A zebrafish ovary section showing localization of *mos* (A) and *cyclin B1* (B) mRNAs in a fully grown oocyte. A merged image is shown in (C). The *mos* and *cyclin B1* mRNAs were localized at the animal polar cytoplasm beneath the micropyle (m). fc, follicle cells; c, chorion. (D-F) High resolution imaging of the oocyte shown in A-C. The insets are enlarged views of the boxed regions. The *mos* and *cyclin B1* mRNAs were distributed in the animal polar cytoplasm of oocyte as different granules. Bars: 50 μm in A-C, 10 μm in D-F.

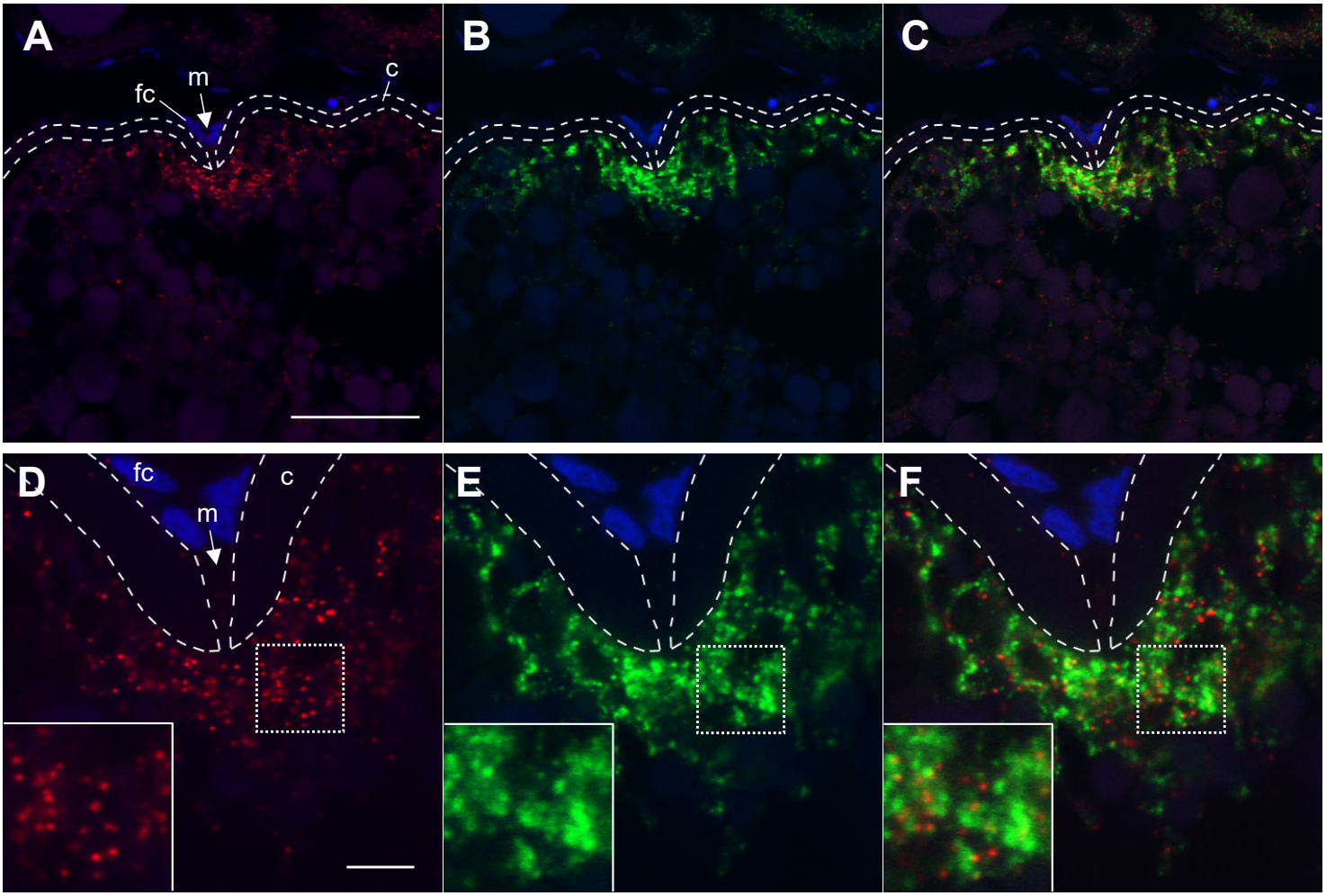

mos mRNA - *cyclin B1* mRNA - Hoechst

Fig. 5. Double fluorescence *in situ* hybridization of *cyclin B1* (red) and *dazl* (green) mRNAs in zebrafish ovaries. DNA is shown in blue. (A) A follicle consisting of stage Ia oocyte. Insets are enlarged views of the boxed region showing *cyclin B1* mRNA (upper), *dazl* mRNA (middle) and a merged image (lower). (B) A follicle consisting of stage Ib oocyte. Insets are enlarged views of the boxed region showing *cyclin B1* mRNA (upper), *dazl* mRNA (middle) and a merged image (lower). (C) A follicle consisting of stage II oocyte. The inset is an enlarged view of the boxed region. (D) A follicle consisting of stage III oocyte. The inset is an enlarged view of the boxed region. Arrowheads indicate *cyclin B1* RNA granules localized at the animal polar cytoplasm of oocytes. Arrows indicate *dazl* RNA granules distributed in the vegetal polar cytoplasm of oocytes. Bb, Balbiani body; fc, follicle cells; GV, germinal vesicle. Bars: 20 μm in A and B, 50 μm in C and D.

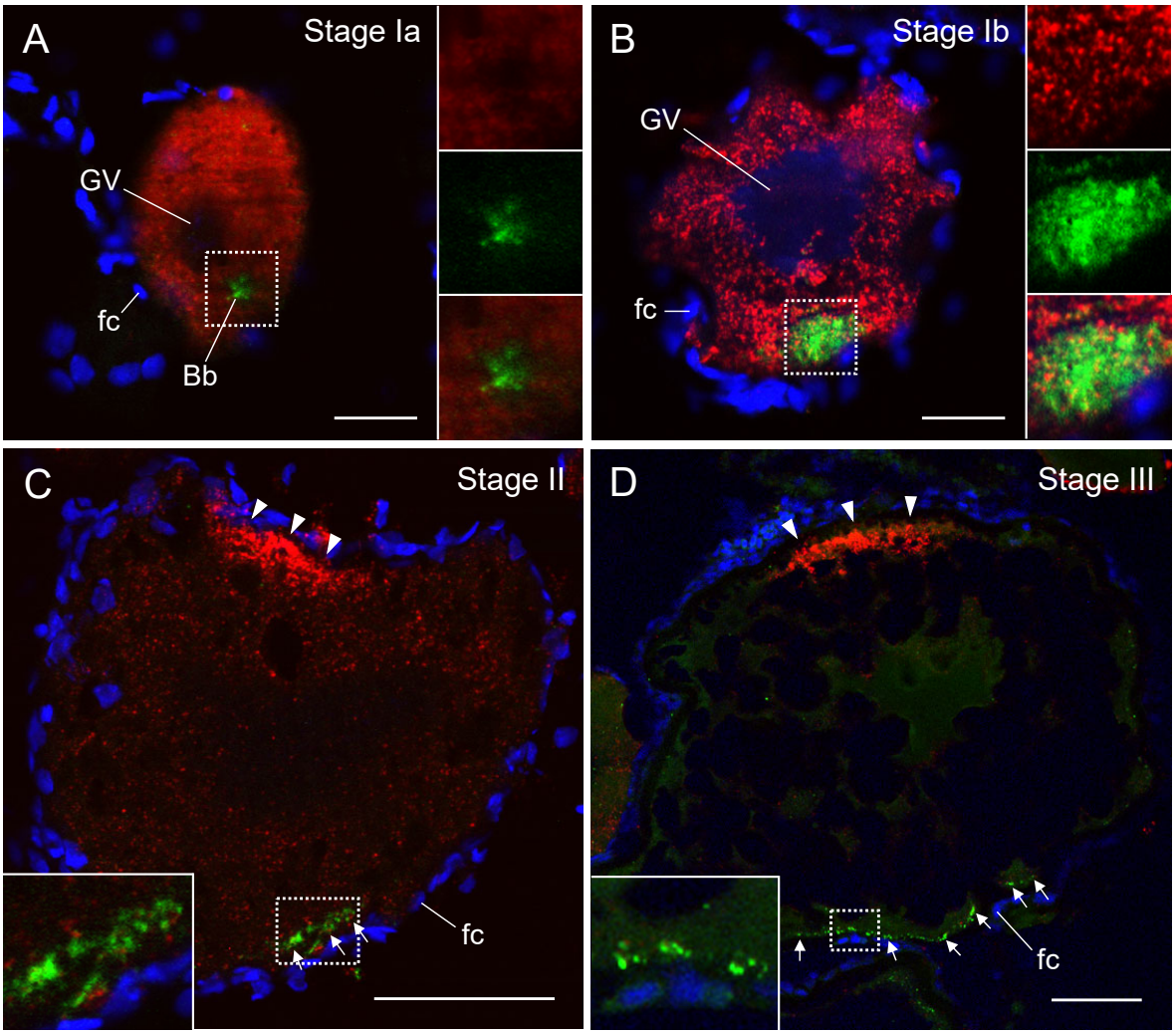

cyclin B1 mRNA - *dazl* mRNA - Hoechst

Fig. 6. Double fluorescence *in situ* hybridization of *Cyclin B1* (red) and *Dazl* (green) mRNAs in mouse ovaries. DNA is shown in blue. Insets are enlarged views of the boxed region showing *cyclin B1* mRNA (upper), *dazl* mRNA (middle) and a merged image (lower). fc, follicle cells; GV, germinal vesicle. Bar: 20 μm.

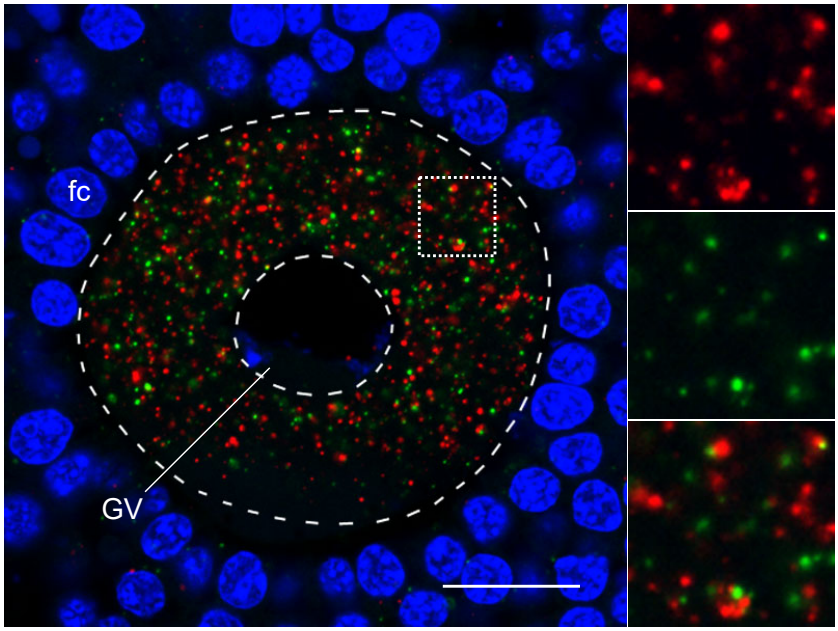

Cyclin B1 mRNA - *Dazl* mRNA - Hoechst

Fig. 7. Expression and translational regulation of *Mad2* mRNA in mouse oocytes. (A, top) RT-PCR amplification for *Mad2* mRNA in the mouse ovary and oocyte. Similar results were obtained from three independent experiments. (bottom) Schematic views of long and short *Mad2* mRNAs (GenBank number: BC089012.1 and NM_001355624.1, respectively). (B) Quantitative PCR for the two types of *Mad2* mRNA (mean ± SD; n = 3). (C) Detection of *Mad2* mRNA in oocytes by *in situ* hybridization with the TSA system. Similar results were obtained from three independent experiments. (D) FISH analysis of *Mad2* mRNA (green). DNA is shown in blue. Similar results were obtained from three independent experiments. (E) Pum1, cyclin B1 and Mad2 in oocytes at 0, 10, and 18 h after resumption of meiosis. (left) Immunoblotting. (right) Quantitative analysis (mean ± SD; n = 3). *t*-test: $*P < 0.05$, $**P < 0.01$. (F) Poly(A) tail analysis of cyclin B1 and *Mad2* mRNAs in oocytes at 0, 4, and 18 h after resumption of meiosis. Similar results were obtained from three independent experiments. (G) Effect of puromycin on Mad2 protein accumulation. (left) Immunoblotting of Pum1, Mad2 and γ-tubulin in oocytes incubated with puromycin at 0, 10, and 18 h after resumption of meiosis. (right) Quantitative analysis of Mad2 protein (mean ± SD; n = 2). The intensities of Mad2 were normalized by that of γ-tubulin. (H) Time course analysis of GFP-Mad2 fluorescence after treated with puromycin (mean ± SD; n = 3). GV, germinal vesicle; fc, follicle cells. Bars: 20 μm.

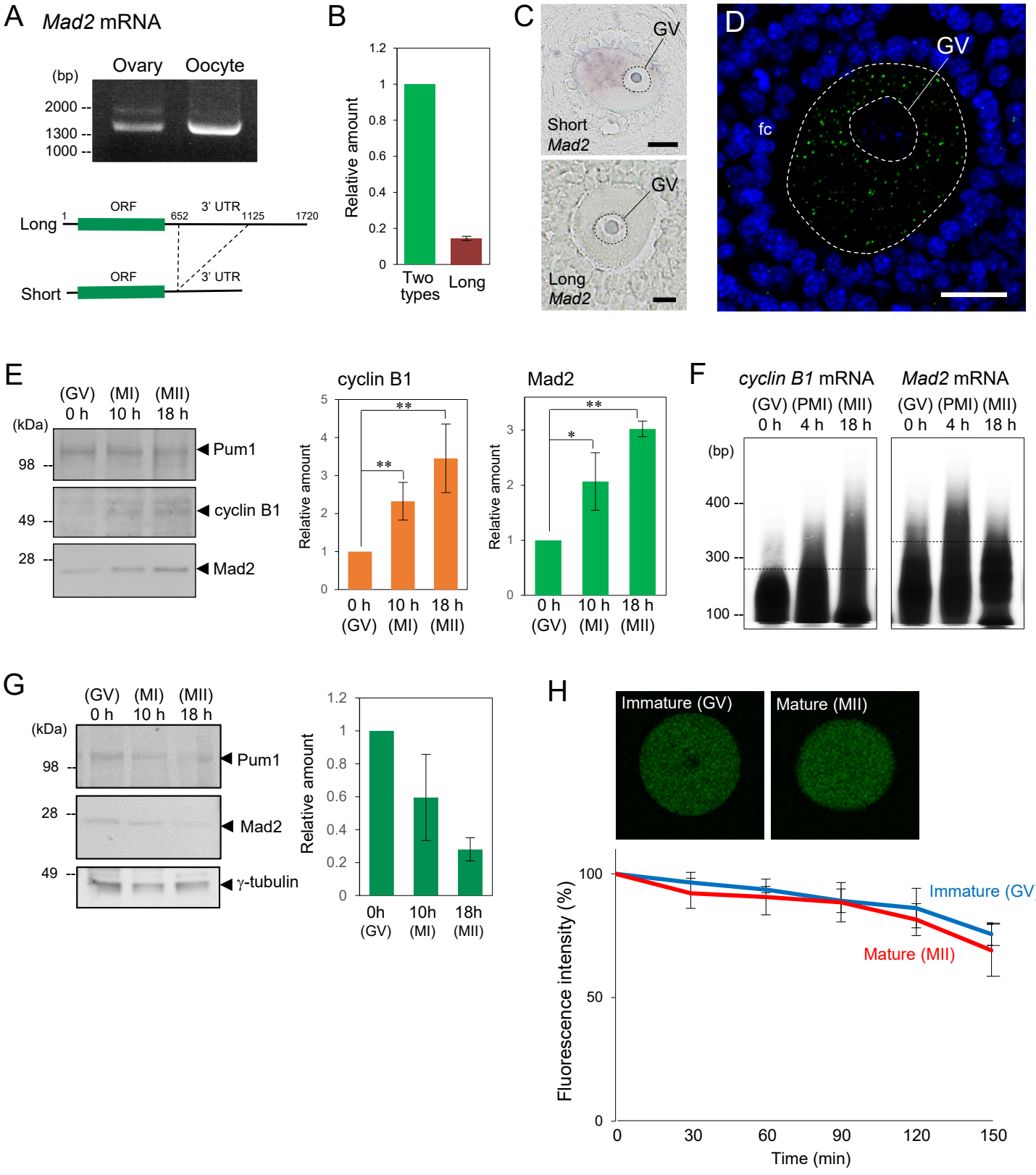
A
Mad2 mRNA
(bp)
Ovary
Oocyte
2000
1300
1000
Long
ORF
3' UTR
1
652
1125
1720
Short
ORF
3' UTR
B
Relative amount
1.2
1
0.8
0.6
0.4
0.2
0
Two types
Long
C
GV
Short Mad2
GV
Long Mad2
D
GV
fc
E
(GV) 0 h
(MI) 10 h
(MII) 18 h
(kDa)
98
49
28
Pum1
cyclin B1
Mad2
cyclin B1
Mad2
Relative amount
0 h (GV)
10 h (MI)
18 h (MII)
F
cyclin B1 mRNA
Mad2 mRNA
(GV) (PMI) (MII)
0 h 4 h 18 h
(bp)
400
300
100
G
(GV) 0 h
(MI) 10 h
(MII) 18 h
(kDa)
98
28
49
Pum1
Mad2
γ-tubulin
Relative amount
0h (GV)
10h (MI)
18h (MII)
H
Immature (GV)
Mature (MII)
Fluorescence intensity (%)
100
50
0
Immature (GV)
Mature (MII)
0
30
60
90
120
150
Time (min)

Fig. 8. Interaction with Pum1 and cytoplasmic regulation of *Mad2* mRNA in mouse oocytes. (A) Schematic diagrams of mouse cyclin B1 and *Mad2* 3'UTRs. Green rectangles indicate putative Pumilio-binding elements (PBEs), and red rectangles indicate the poly(A) signal. (B, top) Immunoblotting of Pum1 and semi-quantitative RT-PCR for cyclin B1, *Mad2*, *α-tubulin*, and *β-actin* transcripts of ovary extracts before IP (Initial) and IP with goat IgG (IgG) or anti-Pum1 goat antibody (α-Pum1). (bottom) Quantitative analysis (mean ± SD; n = 3). *t*-test: $^{**}P < 0.01$. (C) FISH analysis of *Mad2* (green) and cyclin B1 (red) mRNAs in a mouse oocyte. DNA is shown in blue. (insets) Enlarged views of the boxed region. Similar results were obtained from three independent experiments. (D) FISH analysis of oocytes at 0, 4, and 18 h after resumption of meiosis. (E) The numbers of RNA granules per 100 μm^2 in individual oocytes at 0, 4, and 18 h were counted (mean ± SD). The numbers in parentheses indicate the total numbers of oocytes analyzed. *t*-test: $^{**}P < 0.01$. (F) Quantitative PCR for *Mad2* mRNA in oocytes at 0 and 18 h after resumption of meiosis (mean ± SD; n = 3). GV, germinal vesicle; fc, follicle cells; PB, polar body. Bars: 20 μm.

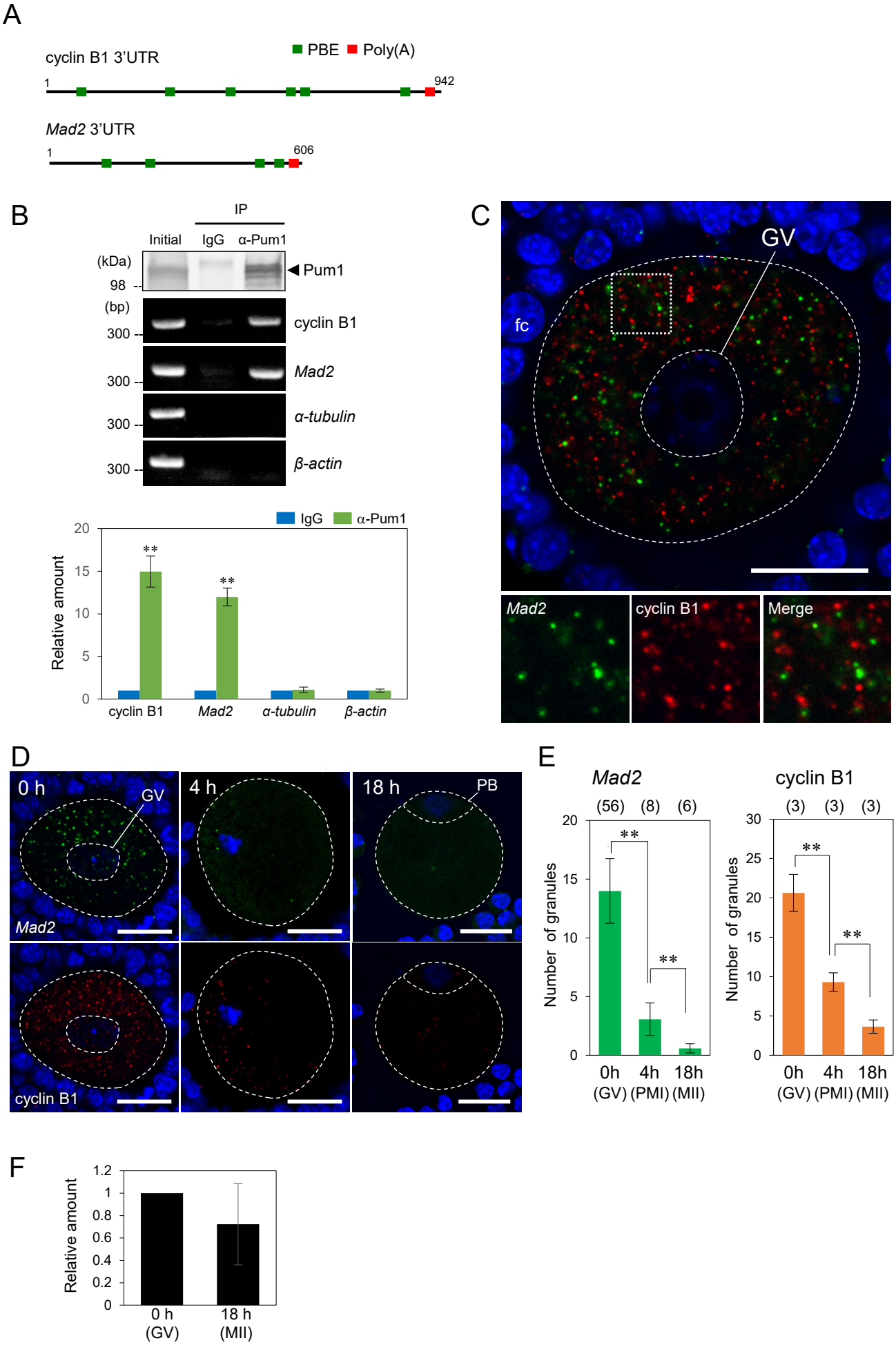
A
cyclin B1 3'UTR
PBE
Poly(A)
1
942
Mad2 3'UTR
1
606
B
IP
Initial
IgG
α-Pum1
(kDa)
98
Pum1
(bp)
300
cyclin B1
Mad2
α-tubulin
β-actin
IgG
α-Pum1
Relative amount
cyclin B1
Mad2
α-tubulin
β-actin
C
GV
fc
Mad2
cyclin B1
Merge
D
0 h
GV
4 h
18 h
PB
Mad2
cyclin B1
E
Mad2
cyclin B1
(56)
(8)
(6)
(3)
(3)
(3)
Number of granules
0h
4h
18h
(GV)
(PMI)
(MII)
F
Relative amount
0 h
(GV)
18 h
(MII)

Fig. 9. Distribution of endogenous Pum1 that surrounds *c*yclin B1 and *Mad2* RNA granules. (A, left) Immunofluorescence of Pum1 (magenta) in immature oocytes. DNA is shown in blue. (right) An enlarged view of the boxed region. Similar results were obtained from three independent experiments. (B) FISH analysis of cyclin B1 (blue) and *Mad2* (green) mRNAs and immunostaining of Pum1 (magenta) in immature oocytes. Arrows indicate Pum1 aggregates surrounding cyclin B1 and *Mad2* RNA granules. Similar results were obtained from three independent experiments. (C) Representative images of the distribution of Pum1 (magenta) and cyclin B1 (blue) and *Mad2* (green) mRNAs. Line graphs display intensity profiles along the dotted lines. (D) FISH analysis of *α-tubulin* mRNA (green) and immunostaining of Pum1 (magenta) in immature oocytes. GV, germinal vesicle. Bars: 20 μm in A (left), 2 μm in A (right), B and D, 0.5 μm in C.

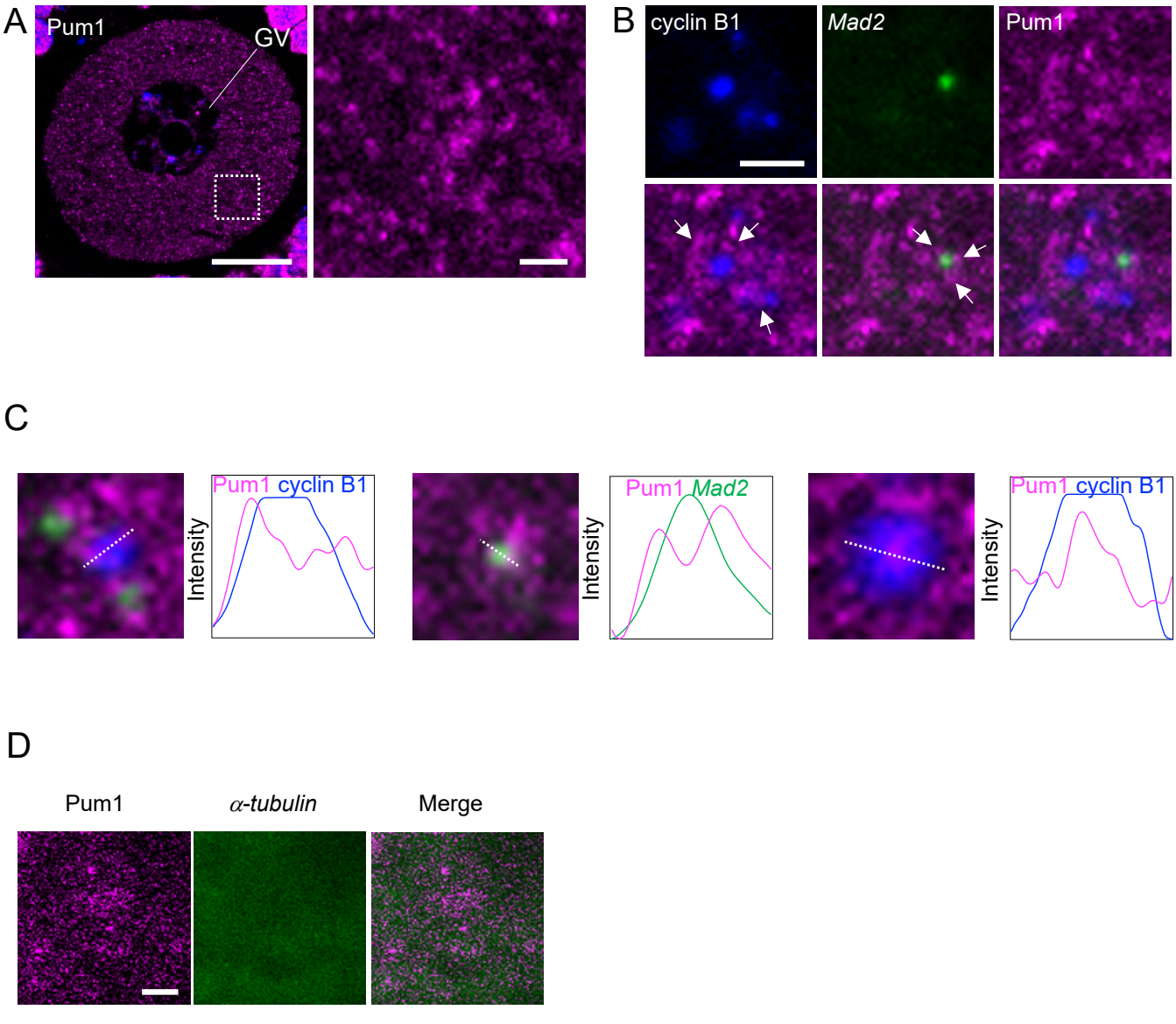
A
Pum1
GV
B
cyclin B1
Mad2
Pum1
C
Pum1 cyclin B1
Intensity
Pum1 Mad2
Intensity
Pum1 cyclin B1
Intensity
D
Pum1
α-tubulin
Merge

Fig. 10. Formation of Pum1 aggregates that surround cyclin B1 and *Mad2* RNA granules. (A) Distributions of GFP-Pum1 (top) and GFP-Pum1ΔQN (bottom). Images in a bright field are shown on the right. (B, left) A high-resolution image of GFP-Pum1. (right) An enlarged view of the boxed region. Similar results were obtained from six independent experiments. (C) FISH analysis of cyclin B1 (top) and *Mad2* mRNA (bottom) and immunostaining of GFP in oocytes expressing GFP-Pum1. Arrows indicate aggregates of GFP-Pum1 surrounding cyclin B1 or *Mad2* RNA granules. Similar results were obtained from two independent experiments. (D) Schematic diagrams of Pum1, Pum1ΔQN, Pum1ΔN, and Pum1ΔC. (E) Identification of prion-like domains by using the PLAAC web application (http://plaac.wi.mit.edu/.). (F) Distribution of GFP-Pum1ΔN and GFP-Pum1ΔC in immature oocytes. Similar results were obtained from six independent experiments. GV, germinal vesicle. Bars: 20 μm in A (left) and F, 2 μm in B and C.

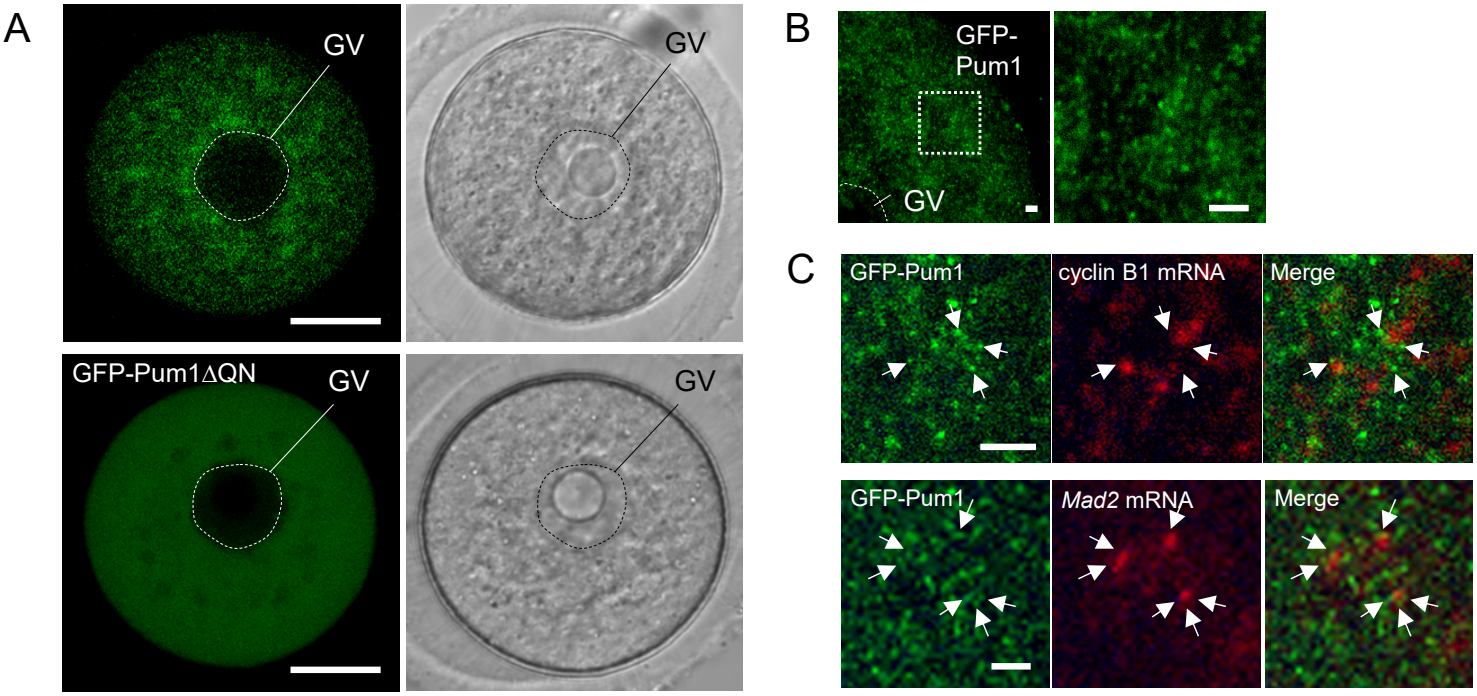
A
GV
GV
GFP-Pum1ΔQN
GV
GV
B
GFP-
Pum1
GV
C
GFP-Pum1
cyclin B1 mRNA
Merge
GFP-Pum1
Mad2 mRNA
Merge

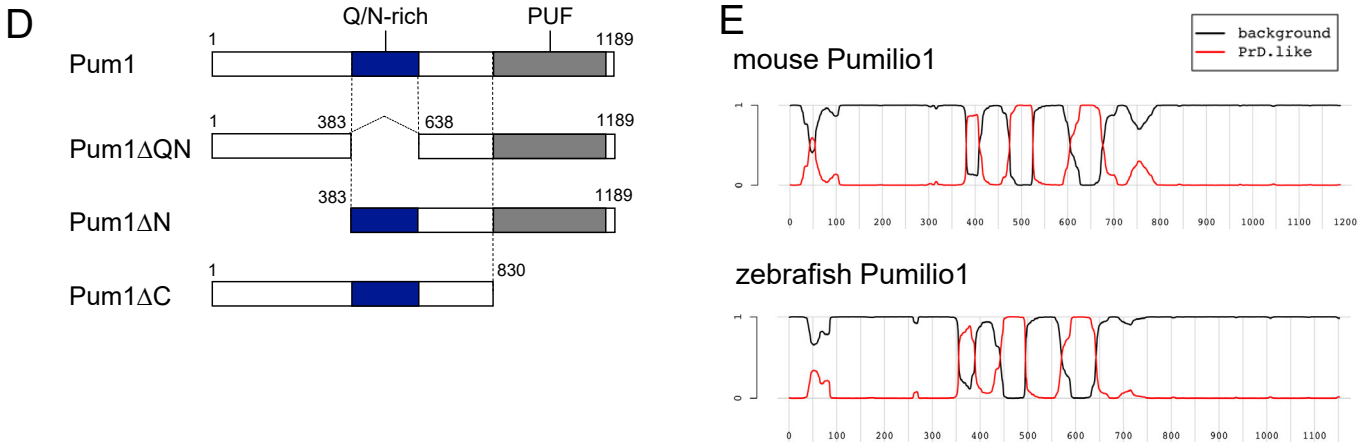
D
Q/N-rich
PUF
Pum1
1
1189
Pum1ΔQN
1
383
638
1189
Pum1ΔN
383
1189
Pum1ΔC
1
830
E
mouse Pumilio1
background
PrD.like
0
100
200
300
400
500
600
700
800
900
1000
1100
1200
zebrafish Pumilio1
0
100
200
300
400
500
600
700
800
900
1000
1100

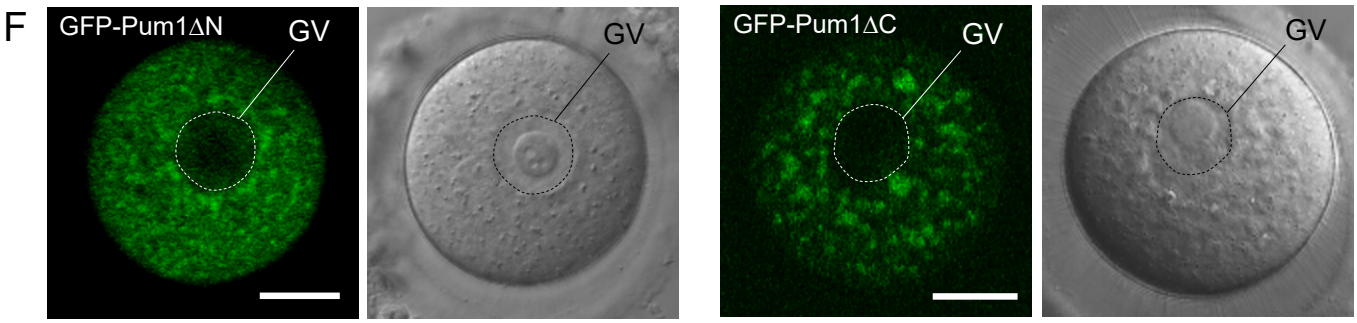
F
GFP-Pum1ΔN
GV
GV
GFP-Pum1ΔC
GV
GV

Fig. 11. Insoluble and immobile properties of Pum1 in immature oocytes. (A, left) Ultracentrifugation analysis of Pum1. Immature (Im) and mature (M) zebrafish oocytes were centrifuged, and the supernatant (S) and pellet (P) equivalent to one oocyte were analyzed by immunoblotting. GM130 is a Golgi matrix protein. **(**right**)** Quantitative analysis of Pum1 and GM130 (means ± SD; n = 3). *t*-test: ***P* < 0.01. (B) FRAP analysis of GFP-Pum1 (Pum1) and GFP-Pum1ΔQN (ΔQN) in immature mouse oocytes. Fluorescence recovery curves for GFP-Pum1 (n = 12) and GFP-Pum1ΔQN (n = 14) are shown (mean ± SD). (C) Values of $t_{1/2}$ (left) and percentages of immobile fractions of GFP-Pum1 and GFP-Pum1ΔQN (right). *t*-test: ***P* < 0.01. (D) Time course of GFP-Pum1 after photobleaching (yellow circle) using a high-resolution microscope. (E) Time course of GFP and GFP-Pum1 after permeabilization with digitonin. Similar results were obtained in 11 oocytes from two independent experiments. (F) Quantitative analysis of fluorescence intensity in E (mean ± SD; n = 3). *t*-test relative to GFP: ***P* < 0.01. Bars: 10 μm in B, 5 μm in D, and 20 μm in E.

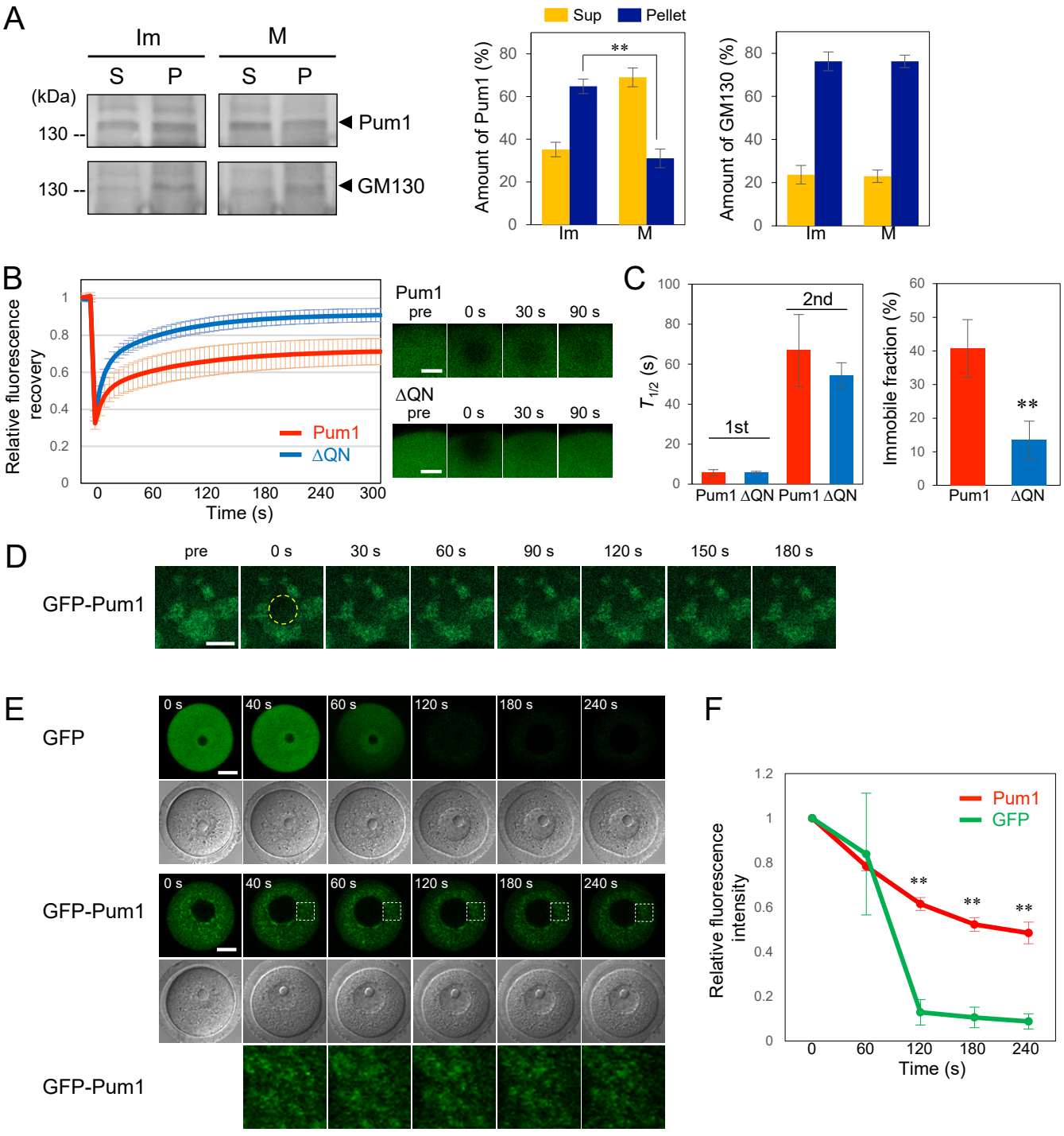
A
Im
M
S
P
S
P
(kDa)
130 --
130 --
Pum1
GM130
Sup
Pellet
Amount of Pum1 (%)
Amount of GM130 (%)
**
Im
M
B
Relative fluorescence recovery
Time (s)
Pum1
ΔQN
pre
0 s
30 s
90 s
C
$T_{1/2}$ (s)
1st
2nd
Pum1 ΔQN Pum1 ΔQN
Immobile fraction (%)
D
GFP-Pum1
pre
0 s
30 s
60 s
90 s
120 s
150 s
180 s
E
GFP
GFP-Pum1
GFP-Pum1
0 s
40 s
60 s
120 s
180 s
240 s
F
Relative fluorescence intensity
Pum1
GFP
Time (s)

Fig. 12. Insoluble and immobile properties of Pum1 are changed during oocyte maturation. (A) Time course of GFP-Pum1 at 0, 2, 4 and 18 h after resumption of meiosis. Similar results were obtained from six independent experiments. GV, germinal vesicle. (B) FRAP analysis of GFP-Pum1 in immature and mature mouse oocytes. Fluorescence recovery curves in immature (n = 12) and mature (n = 6) oocytes are shown (mean ± SD). (C) Values of half time of recovery (t_{half}) (left) and percentages of immobile fractions of GFP-Pum1 (right) in immature (Im) and mature (M) oocytes. *t*-test: $^{**}P < 0.01$. Bars: 20 μm in A, 10 μm in B.

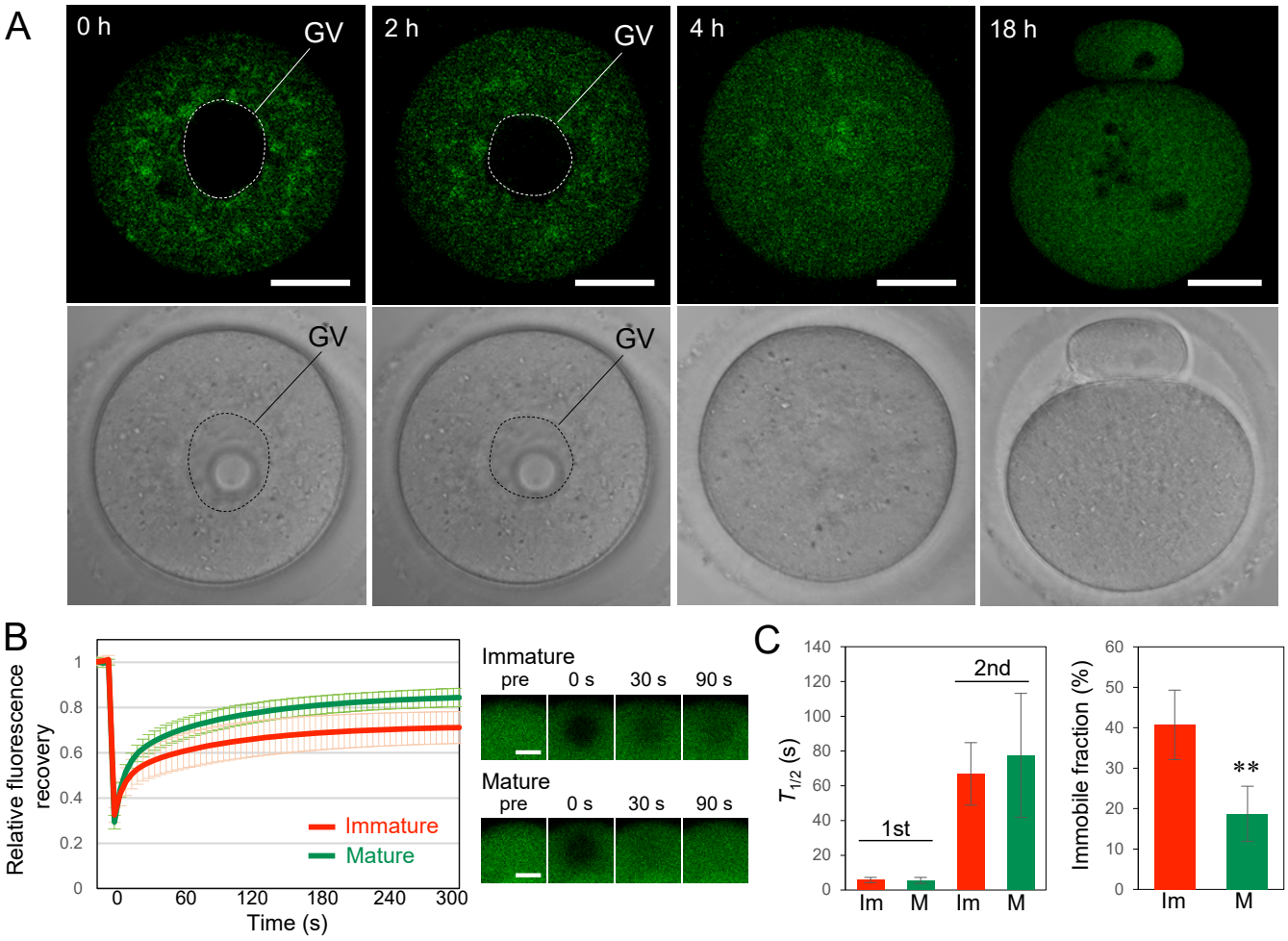
A
0 h
GV
2 h
GV
4 h
18 h
GV
GV
B
Relative fluorescence recovery
Time (s)
Immature
Mature
Immature
pre
0 s
30 s
90 s
Mature
pre
0 s
30 s
90 s
C
$T_{1/2}$ (s)
1st
2nd
Im
M
Im
M
Immobile fraction (%)
**
Im
M

Fig. 13. Distribution and time course of GFP-Pum1ΔC, GFP-Pum1ΔQN and GFP-Pum1ΔN during oocyte maturation. (A) Distributions of GFP and GFP-Pum1ΔC at 0 and 18 h after resumption of meiosis. (B) Time course of GFP-Pum1ΔQN at 0, 2, 4 and 18 h after resumption of meiosis. (C) Time course of GFP-Pum1ΔN at 0, 2, 4 and 18 h after resumption of meiosis. Similar results were obtained from two independent experiments. GV, germinal vesicle; PB, polar body. Bars: 20 μm in A, B and C.

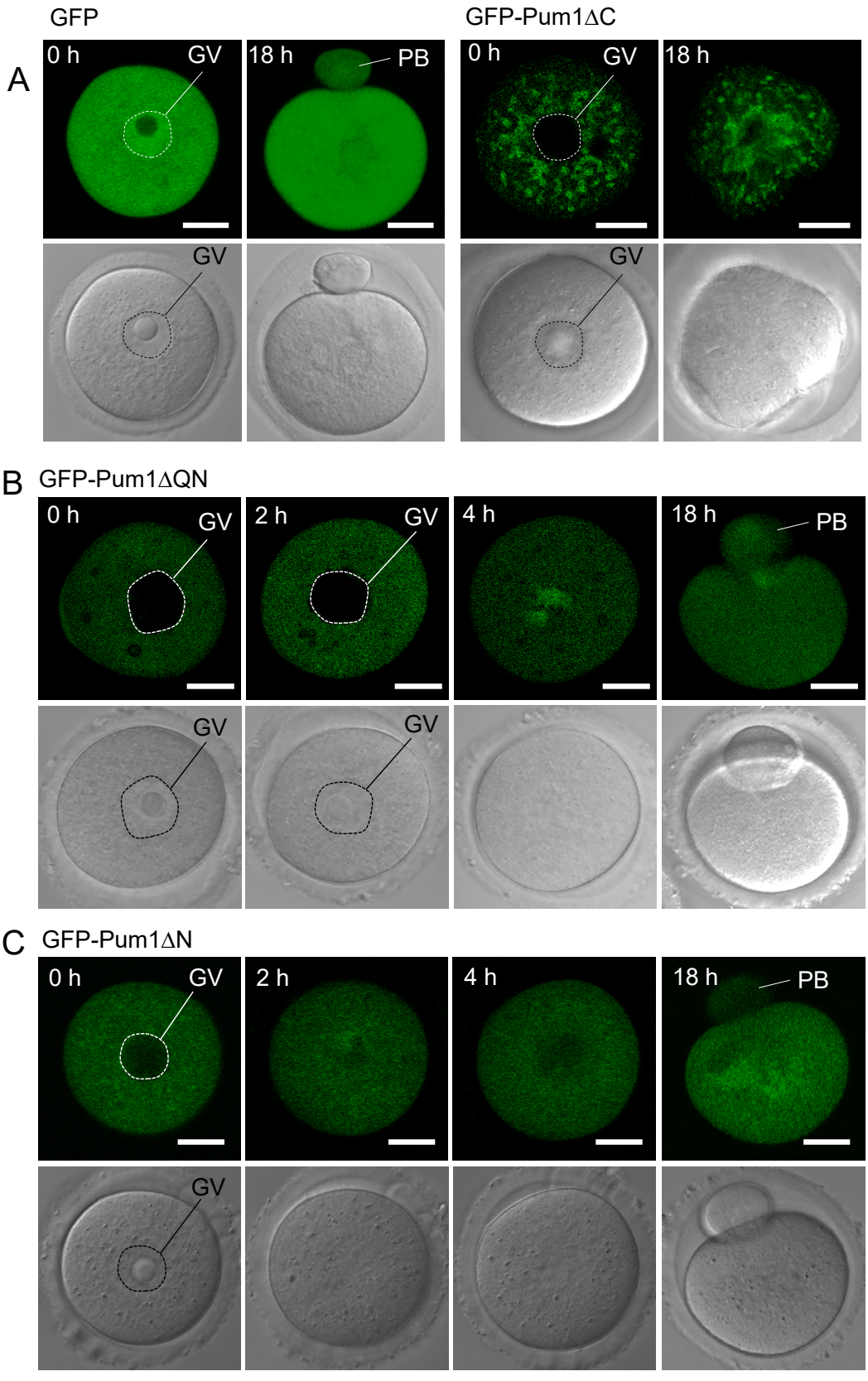
A
GFP
GFP-Pum1ΔC
0 h
GV
18 h
PB
0 h
GV
18 h
GV
GV
GV
B
GFP-Pum1ΔQN
0 h
GV
2 h
GV
4 h
18 h
PB
GV
GV
C
GFP-Pum1ΔN
0 h
GV
2 h
4 h
18 h
PB
GV

Fig. 14. Stabilization of Pum1 aggregates by expression of Pum1ΔC prevents the translation of target mRNA. (A) Percentages of oocytes not injected (-) and injected with GFP, GFP-Pum1 (Pum1), GFP-Pum1ΔQN (ΔQN), GFP-Pum1ΔN (ΔN), and GFP-Pum1ΔC (ΔC) that extruded a polar body (means ± SD; n = 3). The numbers in parentheses indicate the total numbers of oocytes analyzed. *t*-test relative to the oocytes injected with GFP: $^{**}P < 0.01$. (B) Immunofluorescence of β-tubulin (red) in oocytes injected with GFP or GFP-Pum1ΔC (Pum1ΔC) at 18h after resumption of meiosis. DNA is shown in blue. Arrows indicate multiple poles. Similar results were obtained from three independent experiments. (C) FISH analysis of *Mad2* (green) and cyclin B1 (red) mRNAs in oocytes expressing GFP, GFP-Pum1ΔQN (Pum1ΔQN), GFP-Pum1ΔN (Pum1ΔN), and GFP-Pum1ΔC (Pum1ΔC) at 0 and 4 h after resumption of meiosis. (D) The numbers of RNA granules per 100 μm^2 in individual oocytes in C were counted (mean ± SD). The numbers in parentheses indicate the total numbers of oocytes analyzed. *t*-test: $^{**}P < 0.01$, $^{***}P < 0.001$. (E) FISH analysis of cyclin B1 (red) mRNA and immunostaining of GFP-Pum1ΔC or GFP (green) in immature oocytes. (F) Immunoblotting of Pum1 in oocytes not injected (-) and injected with GFP-Pum1 (Pum1), GFP-Pum1ΔC (ΔC) and GFP-Pum1ΔQN (ΔQN). GFP-Pum1ΔN is unable to be detected since the anti-Pum1 antibody recognizes the region deleted in this mutant Pum1. (G) Immunoblotting of cyclin B1, Mad2 and γ-tubulin in oocytes not injected (-) and injected with GFP, GFP-Pum1 (Pum1), GFP-Pum1ΔQN (ΔQN), GFP-Pum1ΔN (ΔN), and GFP-Pum1ΔC (ΔC) 4 h after resumption of meiosis. Similar results were obtained from three independent experiments. (H) Quantitative analysis of cyclin B1 and Mad2 in oocytes not injected (-) and injected with GFP, GFP-Pum1 (Pum1), GFP-Pum1ΔQN (ΔQN), GFP-Pum1ΔN (ΔN), and GFP-Pum1ΔC (ΔC) (mean ± SD; n = 3). *t*-test: $^{**}P < 0.01$, $^{***}P < 0.001$. (I) Immunofluorescence of β-tubulin (red) in oocytes not injected (Control) and injected with GFP, GFP-Pum1ΔC (Pum1ΔC) or GFP-Pum1ΔC followed by the injection with cyclin B1 mRNA (Pum1ΔC + cyclin B1) at 9 h after resumption of meiosis. DNA is shown in blue. GV, germinal vesicle; PB, polar body. Bars: 20 μm in B and I, 5 μm in C and E.

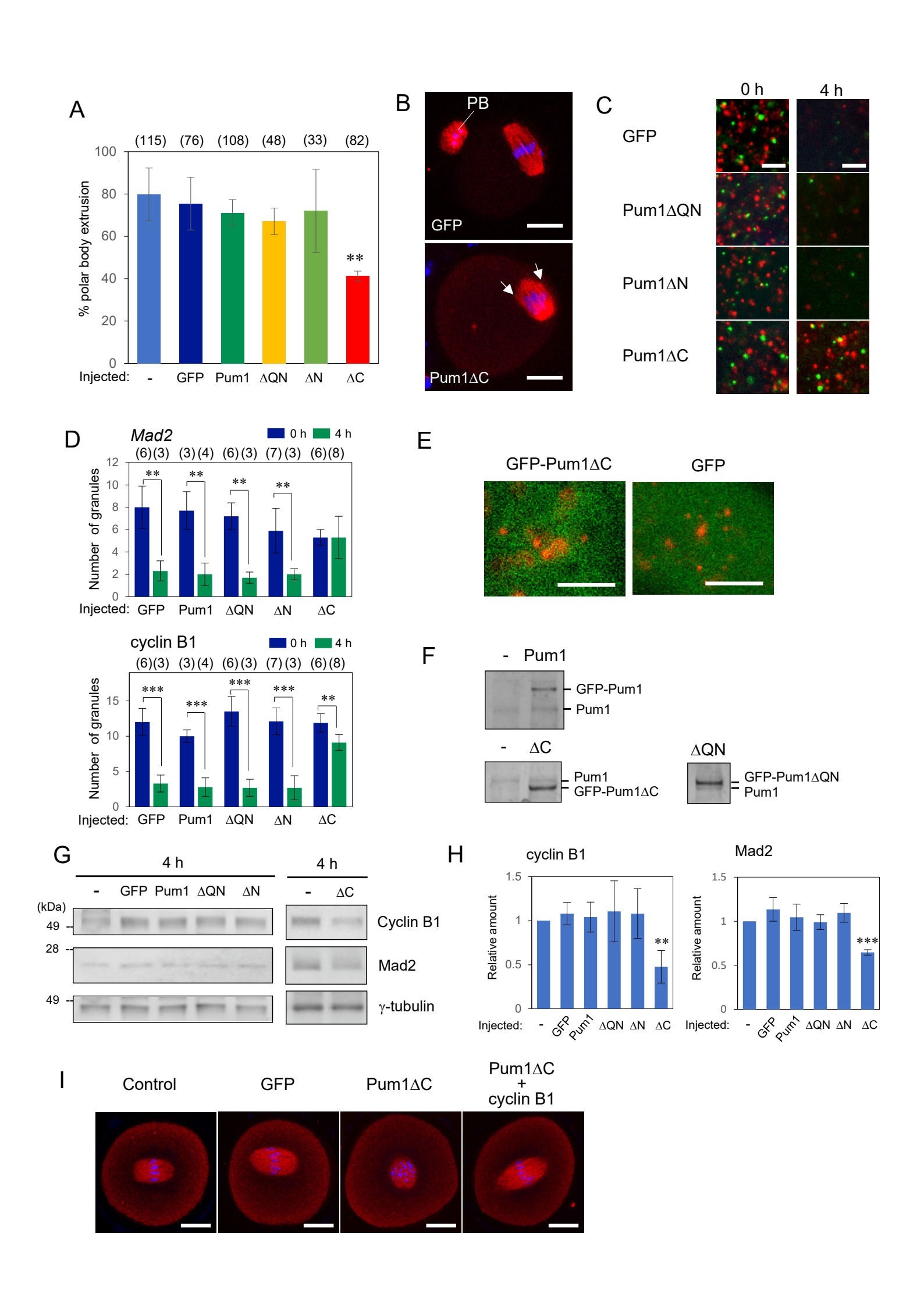
A
(115) (76) (108) (48) (33) (82)
% polar body extrusion
Injected: - GFP Pum1 ΔQN ΔN ΔC
B
PB
GFP
Pum1ΔC
C
0 h
4 h
GFP
Pum1ΔQN
Pum1ΔN
Pum1ΔC
D
Mad2
0 h
4 h
Number of granules
Injected: GFP Pum1 ΔQN ΔN ΔC
cyclin B1
E
GFP-Pum1ΔC
GFP
F
- Pum1
GFP-Pum1
Pum1
- ΔC
Pum1
GFP-Pum1ΔC
ΔQN
GFP-Pum1ΔQN
Pum1
G
4 h
- GFP Pum1 ΔQN ΔN
4 h
- ΔC
(kDa)
49
28
49
Cyclin B1
Mad2
γ-tubulin
H
cyclin B1
Mad2
Relative amount
Injected: - GFP Pum1 ΔQN ΔN ΔC
I
Control
GFP
Pum1ΔC
Pum1ΔC + cyclin B1

Fig. 15. Stabilization of Pum1 aggregates by anti-Pum1 antibody prevents the translation of target mRNA. (A) Percentages of oocytes incubated with (+) and without (-) puromycin (Puro) that induced GVBD (mean ± SD; n = 3). *t*-test: $^{**}P < 0.01$. (B) Percentages of oocytes not injected (-) and injected with anti-Pum1 antibody (α-Pum1) or control IgG (IgG) that induced GVBD (means ± SD; n = 5). *t*-test: $^{*}P < 0.05$. (C) Distribution of GFP-Pum1 in oocytes injected with anti-Pum1 antibody (α-Pum1) or control IgG (IgG). (D) Immunoblotting of cyclin B1, Mad2 and γ-tubulin in oocytes not injected (-) and injected with anti-Pum1 antibody (α-Pum1) or control IgG (IgG) at 0 and 18 h after resumption of meiosis. Similar results were obtained from two independent experiments. (E) Quantitative analysis of cyclin B1 and Mad2 in oocytes not injected (-) and injected with anti-Pum1 antibody (α-Pum1) or control IgG (IgG) (mean ± SD; n = 2). (F) Distribution of the injected anti-Pum1 antibody (magenta). DNA is shown in blue. (G) Immunoblotting of Pum1 in oocytes not injected (-) and injected with anti-Pum1 antibody (α-Pum1) or control IgG (IgG) at 0 and 18 h after resumption of meiosis. Similar results were obtained from two independent experiments. GV, germinal vesicle; PB, polar body. Bars: 20 μm.

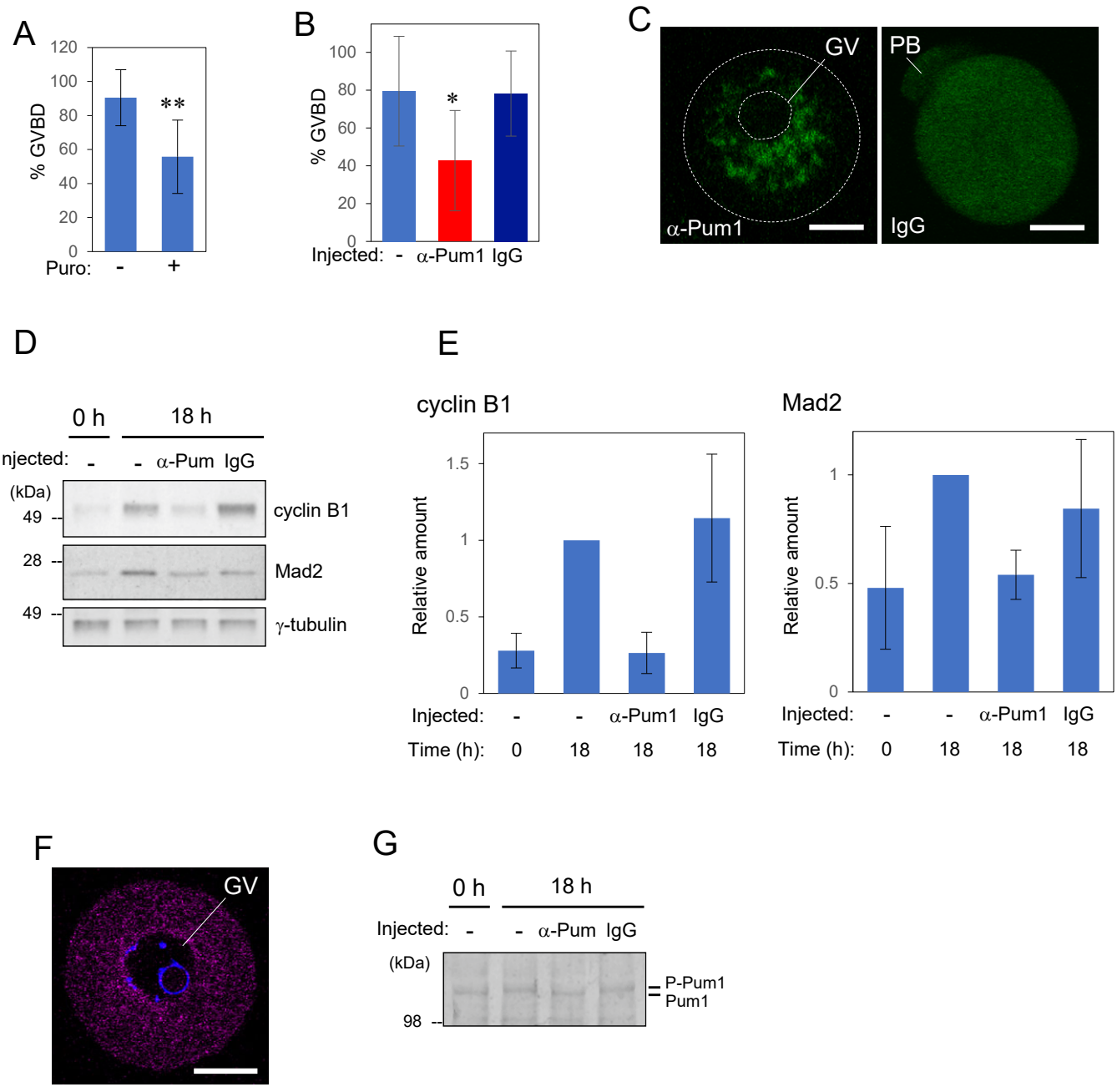
A
% GVBD
120
100
80
60
40
20
0
**
Puro: - +
B
% GVBD
100
80
60
40
20
0
*
Injected: - α-Pum1 IgG
C
GV
α-Pum1
PB
IgG
D
0 h
18 h
Injected: - - α-Pum IgG
(kDa)
49
cyclin B1
28
Mad2
49
γ-tubulin
E
cyclin B1
Relative amount
1.5
1
0.5
0
Injected: - - α-Pum1 IgG
Time (h): 0 18 18 18
Mad2
Relative amount
1
0.5
0
Injected: - - α-Pum1 IgG
Time (h): 0 18 18 18
F
GV
G
0 h
18 h
Injected: - - α-Pum IgG
(kDa)
98
P-Pum1
Pum1

Fig. 16. Phosphorylation of Pum1 is coupled with the dissolution of aggregates, disassembly of RNA granules and translational activation of target mRNAs. (A) Phosphorylation of Pum1 (P-Pum1). (left) Immature (Im) and mature (M) oocytes were analyzed by immunoblotting. (right) Treatment with (+) and without (-) alkaline phosphatase (AP). Similar results were obtained from two independent experiments. (B) (top) Pum1 phosphorylation in oocytes treated with OA (+) or DMSO (-). Similar results were obtained from four independent experiments. (bottom) Pum1 phosphorylation in oocytes at 60 min after treatment with (+) and without (-) OA or Plk4 inhibitor. (C) Time course of GFP-Pum1 in oocytes treated with DMSO, OA, or OA and Plk4 inhibitor 0-120 min after treatment. Similar results were obtained from three independent experiments. (D) Quantitative analysis of Pum1 aggregates in oocytes treated with (+) and without (-) OA or Plk4 inhibitor at 0 min and 90 min after treatment. The numbers in parentheses indicate the total numbers of oocytes analyzed. *t*-test: $^{**}P < 0.01$. (E) FISH analysis of *Mad2* (green) and cyclin B1 (red) mRNAs in oocytes treated with DMSO, OA or OA and Plk4 inhibitor (OA + Plk4 inhibitor) at 120 min after treatment. (F) The numbers of RNA granules per 100 μm^2 in individual oocytes in E were counted (mean $\pm$ SD). The numbers in parentheses indicate the total numbers of oocytes analyzed. *t*-test: $^{**}P < 0.01$. (G) Immunoblotting of Mad2, cyclin B1 and γ-tubulin in oocytes treated with (+) and without (-) OA or Plk4 inhibitor 120 min after resumption of meiosis. Similar results were obtained from three independent experiments. GV, germinal vesicle. Bars: 20 μm.

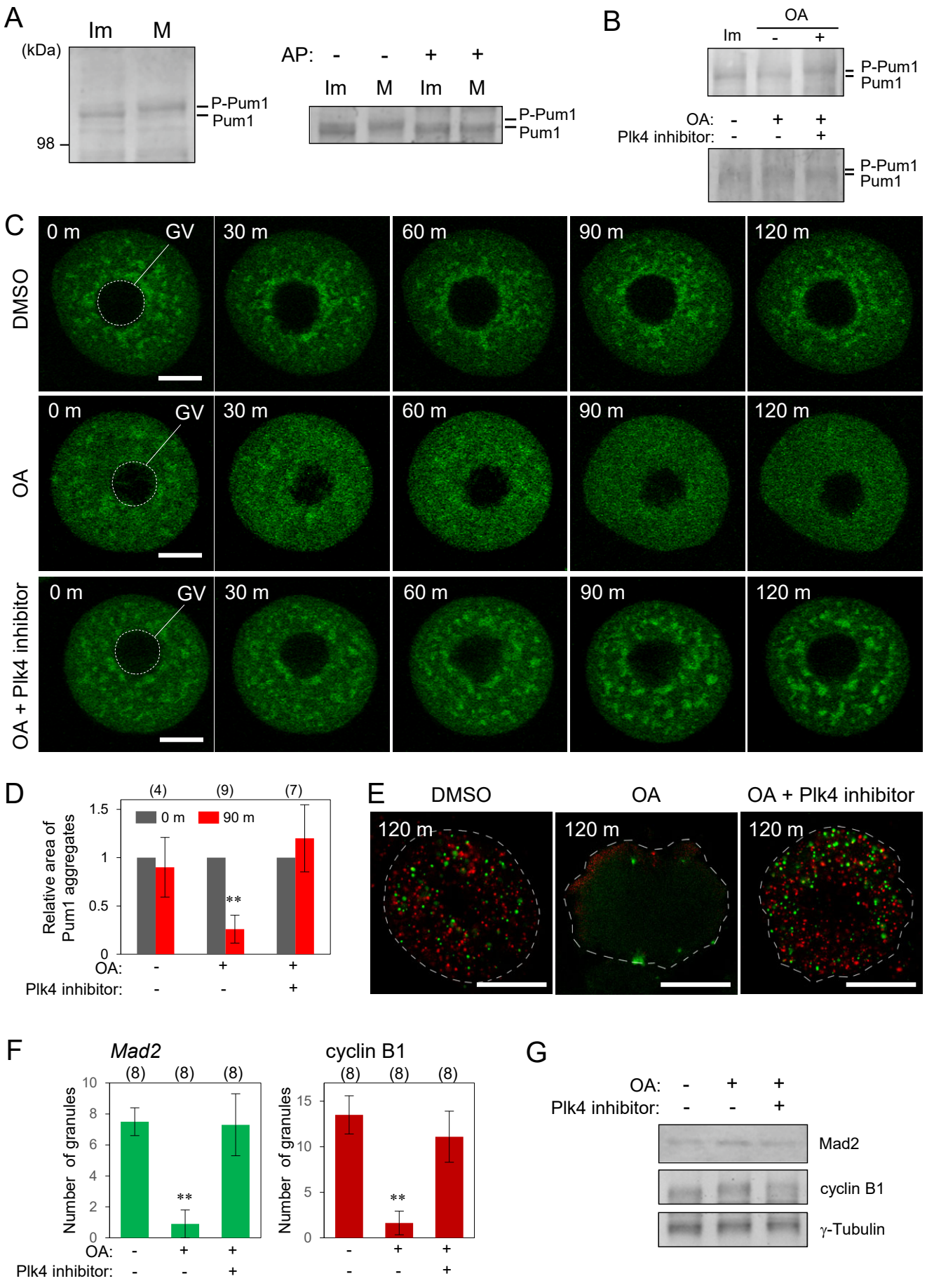
A
Im
M
(kDa)
98
P-Pum1
Pum1
AP: - - + +
Im M Im M
P-Pum1
Pum1
B
OA
Im - +
P-Pum1
Pum1
OA: - + +
Plk4 inhibitor: - - +
P-Pum1
Pum1
C
DMSO
OA
OA + Plk4 inhibitor
0 m
GV
30 m
60 m
90 m
120 m
D
(4) (9) (7)
Relative area of Pum1 aggregates
1.5
1
0.5
0
0 m
90 m
**
OA: - + +
Plk4 inhibitor: - - +
E
DMSO
OA
OA + Plk4 inhibitor
120 m
F
Mad2
cyclin B1
(8) (8) (8)
Number of granules
10
8
6
4
2
0
15
10
5
**
OA: - + +
Plk4 inhibitor: - - +
G
OA: - + +
Plk4 inhibitor: - - +
Mad2
cyclin B1
γ-Tubulin

Fig. 17. Time course of GFP-Pum1 after OA treatment. (A) Time course of GFP-Pum1 in oocytes treated with OA, OA and Plk1 inhibitor, OA and MAPK inhibitor, or OA and MPF inhibitor 0-120 min after treatment. Similar results were obtained in 6 oocytes from two independent experiments. GV, germinal vesicle. Bars: 20 μm. (B) Quantitative analysis of Mad2 and cyclin B1 in oocytes treated with (+) and without (-) OA or Plk4 inhibitor 120 min after resumption of meiosis (mean ± SD; n = 3). *t*-test: $*P < 0.05$, $**P < 0.01$.

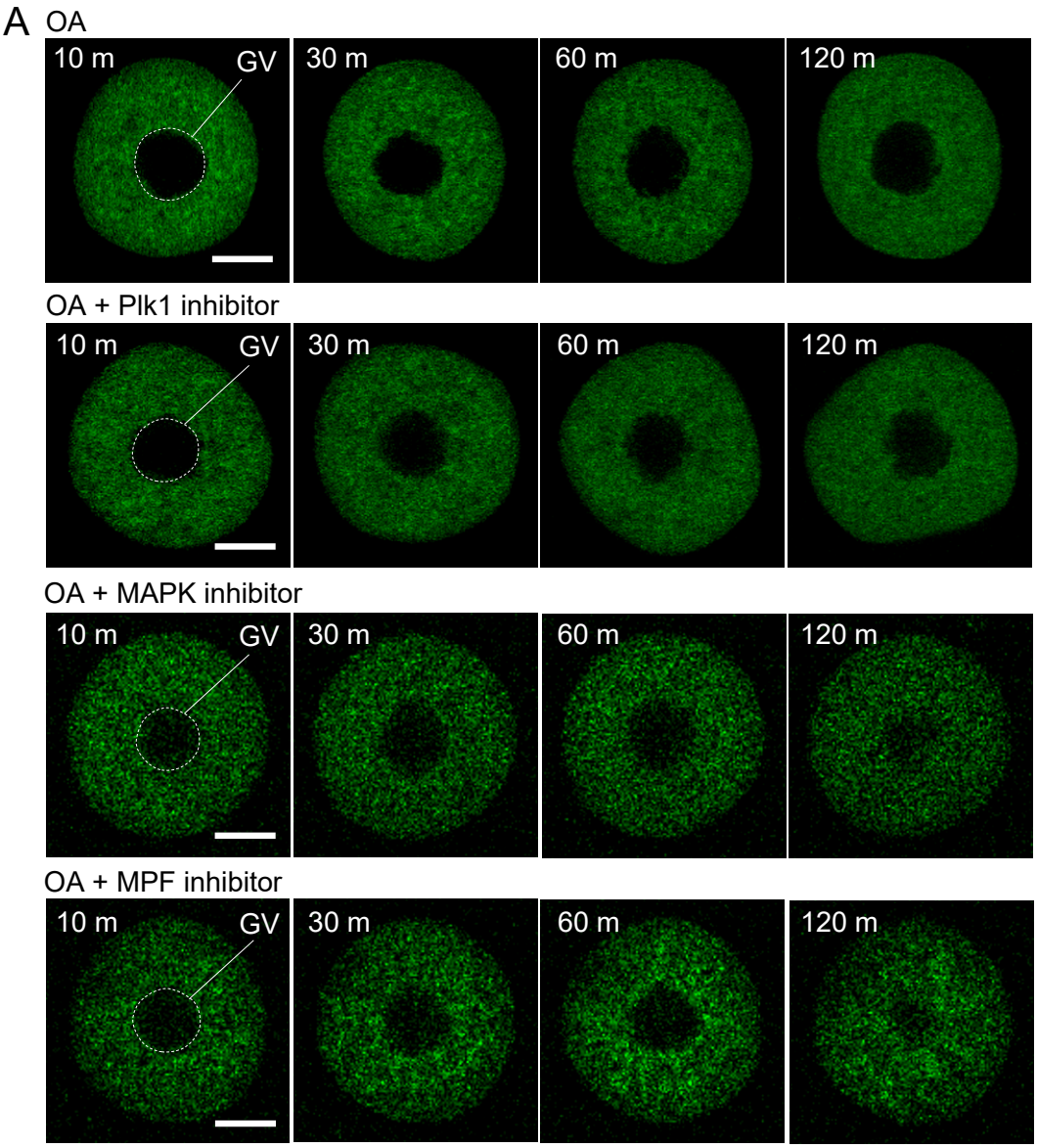
A
OA
10 m
GV
30 m
60 m
120 m
OA + Plk1 inhibitor
OA + MAPK inhibitor
OA + MPF inhibitor
B
Mad2
cyclin B1
Relative amount
2
1.5
1
0.5
0
**
*
OA:
Plk4 inhibitor:
-
+

Fig. 18. **Characterization of anti-EMI2 antibody by immunoblotting**. (A) EMI2-His recombinant protein (1 ng) was probed with (+) or without (-) anti-EMI2 antibody (α-EMI2). (B) The extracts of *GFP-Emi2*-mRNA-injected oocytes were probed with anti-GFP (α-GFP) and anti-EMI2 (α-EMI2) antibodies. (C) The extracts of immature (IM) or mature (M) oocytes were probed with anti-EMI2 antibody. (D) Immunoblotting was performed with anti-EMI2 antibody reacted with EMI2-His recombinant proteins.

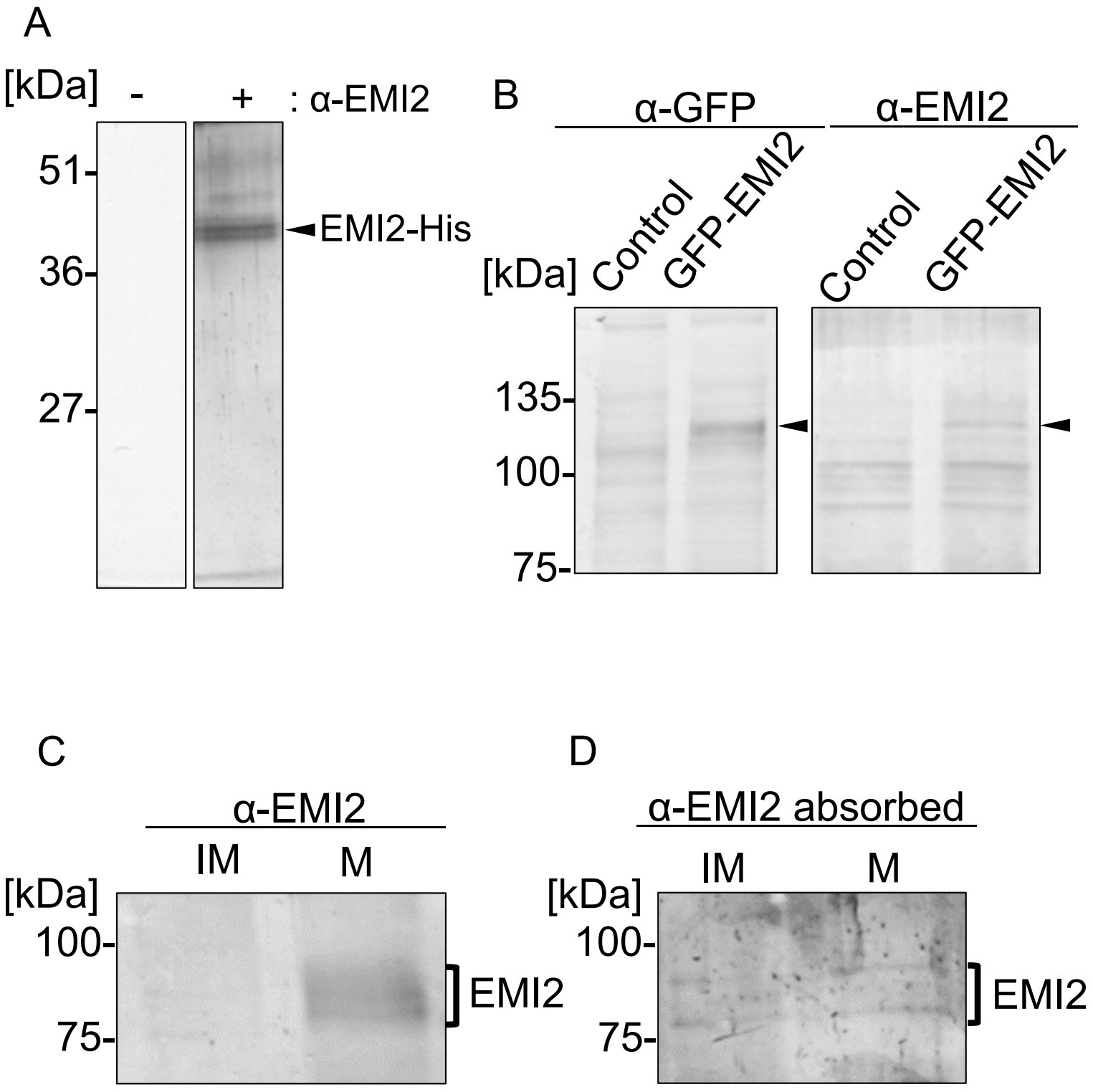
A
[kDa]
-
+
: α-EMI2
51
36
27
EMI2-His
B
α-GFP
α-EMI2
Control
GFP-EMI2
Control
GFP-EMI2
[kDa]
135
100
75
C
α-EMI2
IM
M
[kDa]
100
75
EMI2
D
α-EMI2 absorbed
IM
M
[kDa]
100
75
EMI2

Fig. 19. **Expression and translational regulation of *Emi2* mRNA during oocyte maturation.** (A, left) Immunoblotting of EMI2, cyclin B1 and γ-tubulin in oocytes at 0, 8 and 18 h after resumption of meiosis. (right) Quantitative analysis (means ± standard deviations; n = 3). The statistical significance was analyzed by Tukey-Kramer test. * $P < 0.05$, ** $P < 0.01$. (B) Time course of PAT assay of *Emi2* (left) and cyclin B1 mRNA (right) during oocyte maturation. Similar results were obtained from three independent experiments. Note that poly(A) tails of a fraction of cyclin B1 mRNA were shortened in MII oocytes. (C) RNA-seq-based gene expression values (FPKM) for *Emi2* in GV-stage and MII oocytes (means ± standard deviations; n = 3). *t*-test: * $P < 0.05$.

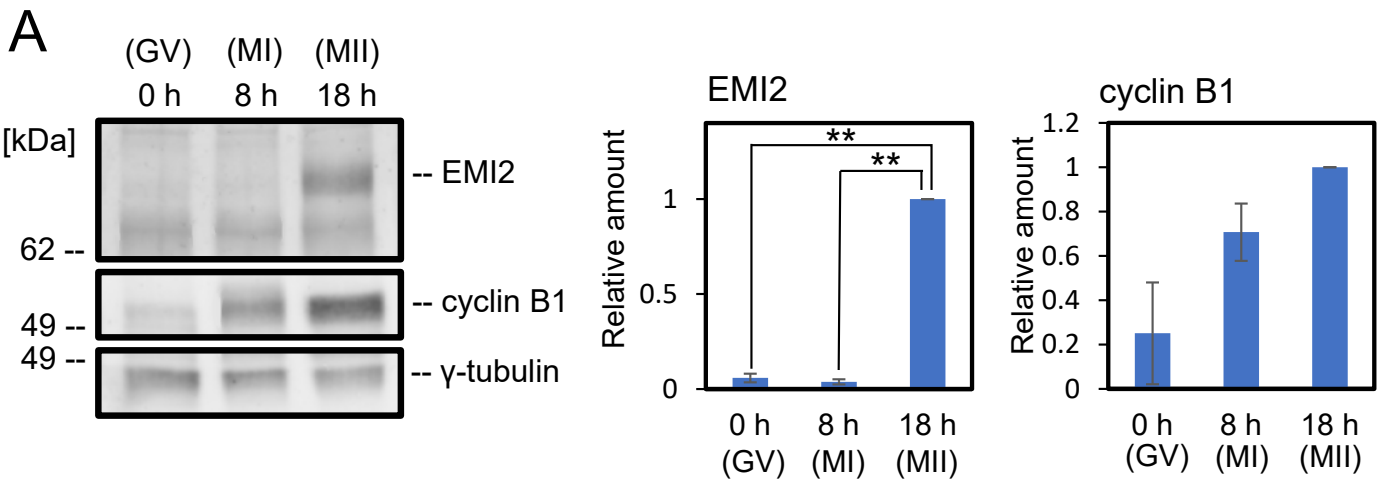
A
(GV)
0 h
(MI)
8 h
(MII)
18 h
[kDa]
62 --
49 --
49 --
-- EMI2
-- cyclin B1
-- γ-tubulin
EMI2
Relative amount
1
0.5
0
**
**
0 h
(GV)
8 h
(MI)
18 h
(MII)
cyclin B1
Relative amount
1.2
1
0.8
0.6
0.4
0.2
0
0 h
(GV)
8 h
(MI)
18 h
(MII)

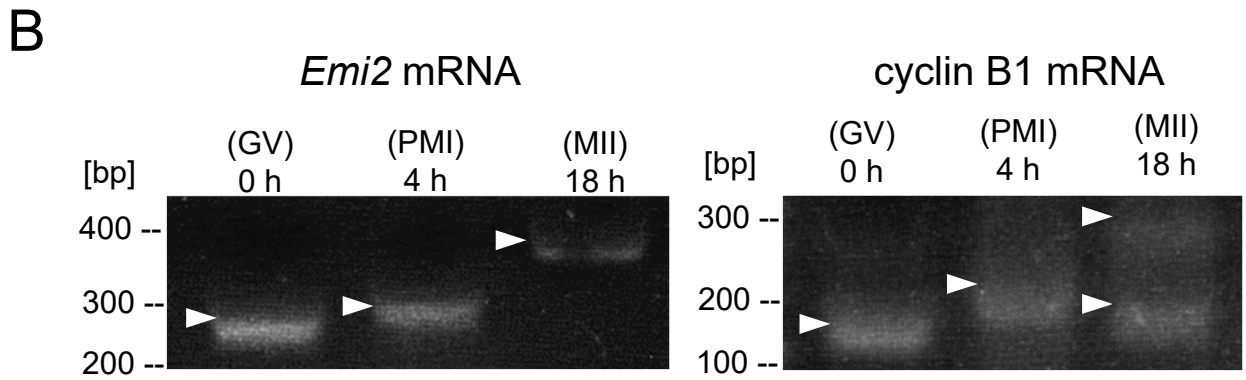
B
Emi2 mRNA
[bp]
(GV)
0 h
(PMI)
4 h
(MII)
18 h
400 --
300 --
200 --
cyclin B1 mRNA
[bp]
(GV)
0 h
(PMI)
4 h
(MII)
18 h
300 --
200 --
100 --

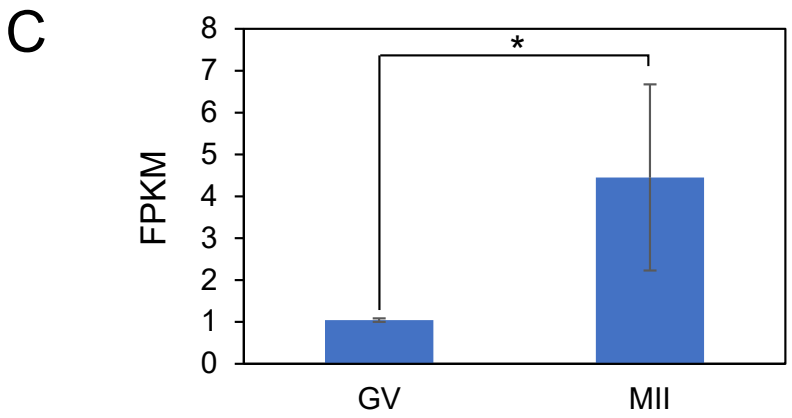
C
FPKM
8
7
6
5
4
3
2
1
0
*
GV
MII

Fig. 20. **Meiotic progression was not arrested at MII in *Emi2*-3'UTR-MO-injected oocytes.** (A) The sequences of the 3'UTR of *Emi2* mRNA that are targeted by *Emi2*-3'UTR-MO. *Emi2*-5mm-MO contains 5 mismatches. (B) Immunoblotting of EMI2 and γ-tubulin in oocytes not injected (-) and injected with *Emi2*-5mm-MO and *Emi2*-3'UTR-MO at 28 h after resumption of meiosis. (C) Immunofluorescence of β-tubulin (red) in oocytes injected with *Emi2*-5mm-MO and *Emi2*-3'UTR-MO at 28 h and 48 after resumption of meiosis. DNA is shown in blue. Bars: 20 μm.

A

Emi2 3'UTR

5'-TCCCCATTTTAAATATTTTGATGTTTTAAATAAAGAATTTTCAGGGTTGTT poly(A)-3'

Emi2-3'UTR-MO 3'-ATTTATTTCTTAAAAGTCCCAACAA-3'

Emi2-5mm-MO 3'-ATTCATTACTTAATAGTCACATCAA-5'

B

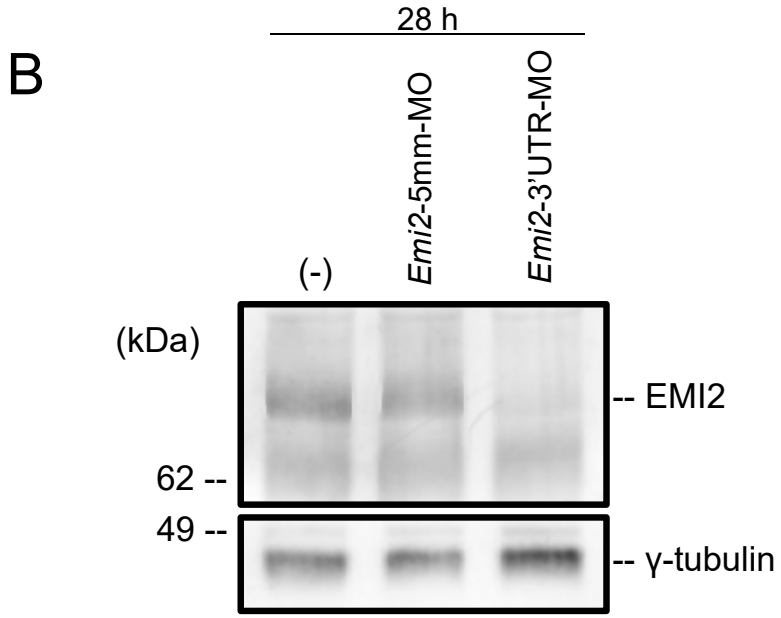

C

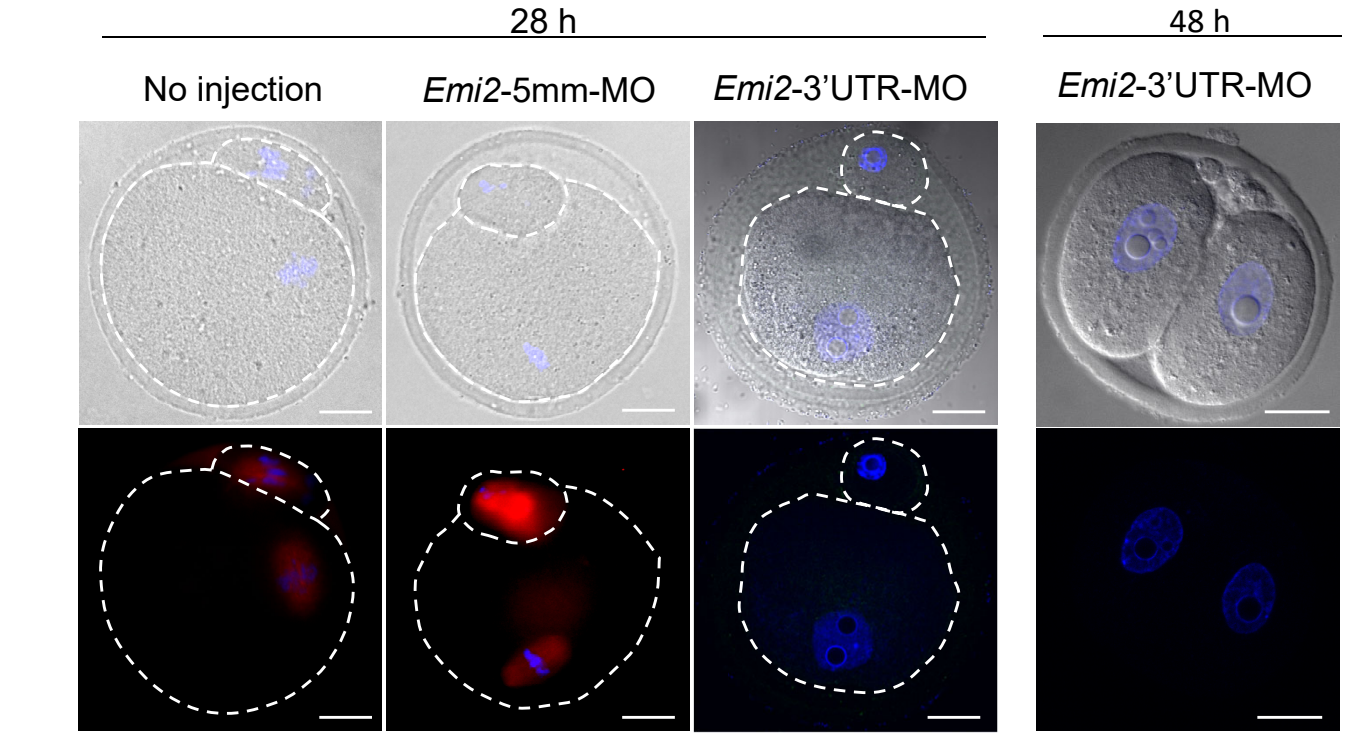

Fig. 21. ***GFP-Emi2*-mRNA injected-oocytes were arrested at MI.**
(A) Immunofluorescence of β-tubulin (red) in MII-stage oocytes injected with *GFP* mRNA at 18 h after resumption of meiosis. Right figure shows bright field. DNA is shown in blue. PB, polar body. (B) Immunofluorescence of α-tubulin (red) in MI-stage oocytes injected with *GFP-Emi2* mRNA at 18 h after resumption of meiosis. Right figure shows bright field. DNA is shown in blue. (C) The rate of MI or MII-stage oocytes at 18 h after resumption of meiosis. The numbers in parentheses indicate the total numbers of oocytes analyzed. (D) Immunofluorescence of Mad2 (green) and CREST (red) in no-injected oocytes, nocodazole-treated oocytes and *GFP-Emi2* mRNA-injected oocytes at 8 h after resumption of meiosis. Lower panels are enlarged views of chromatid. DNA is shown in blue. White arrows indicate the colocalization of Mad2 and CREST. Black arrows indicate the localization of CREST. Bars: 20 μm.

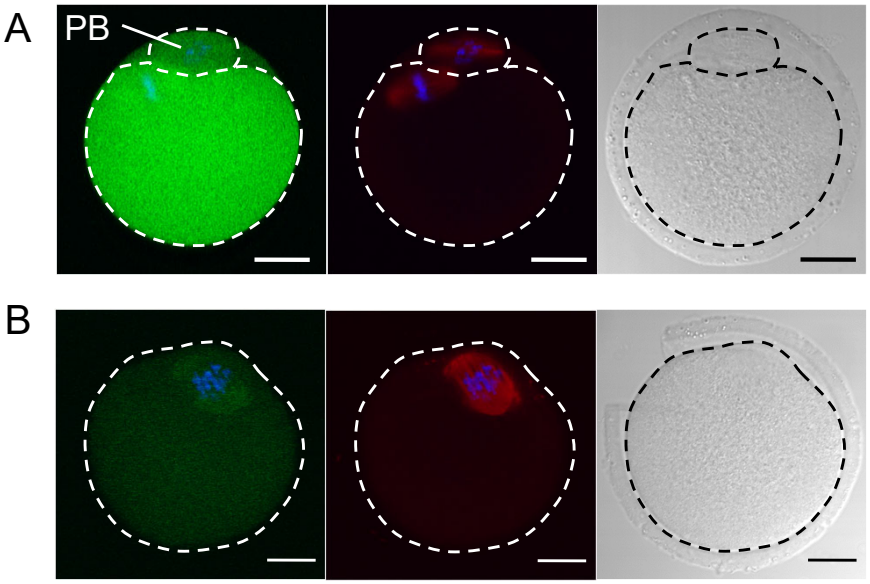
A
PB
B

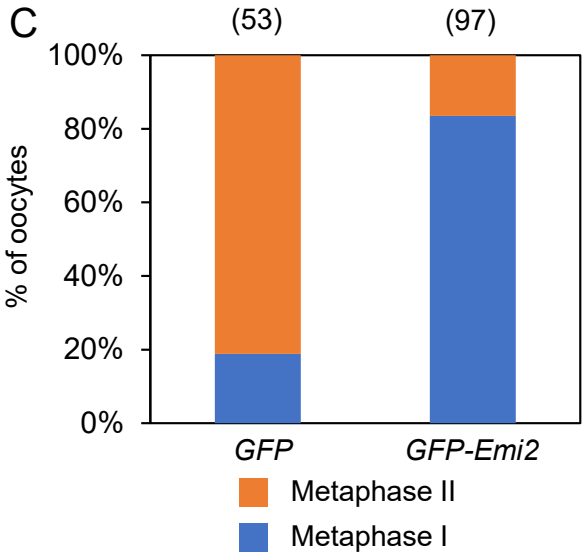
C
(53)
(97)
100%
80%
60%
40%
20%
0%
% of oocytes
GFP
GFP-Emi2
Metaphase II
Metaphase I

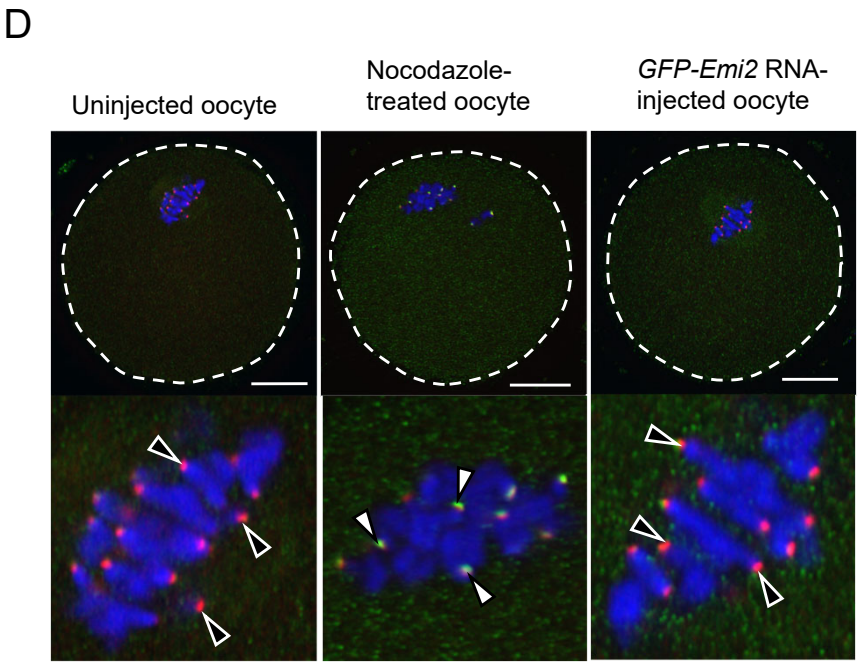
D
Uninjected oocyte
Nocodazole-treated oocyte
GFP-Emi2 RNA-injected oocyte

Fig. 22. **Dormant *Emi2* mRNA formed granules similar to cyclin B1 mRNA in mouse oocyte.** (A) Expression of *Emi2* mRNA in the mouse ovary. A mouse ovary section hybridized with the *Emi2* antisense probe (left) and sense probe (right). (B) FISH analysis of *Emi2* mRNA in GV-stage oocyte. (C) FISH analysis of *Emi2* (green) and cyclin B1 (red) mRNAs in GV-stage oocytes. (insets) Enlarged views of the boxed region. (D) FISH analysis of oocytes at 0, 4, 18 h after resumption of meiosis. (E) The numbers of RNA granules per 100 μm^2 in individual oocytes at 0, 4, and 18 h were counted (mean ± SD). The numbers in parentheses indicate the total numbers of oocytes analyzed. The statistical significance was analyzed by Tukey-Kramer test. **P* < 0.05, ***P* < 0.01. GV, germinal vesicle; PB, polar doby. Bars, 10 μm in A, B and D, 20 μm in C.

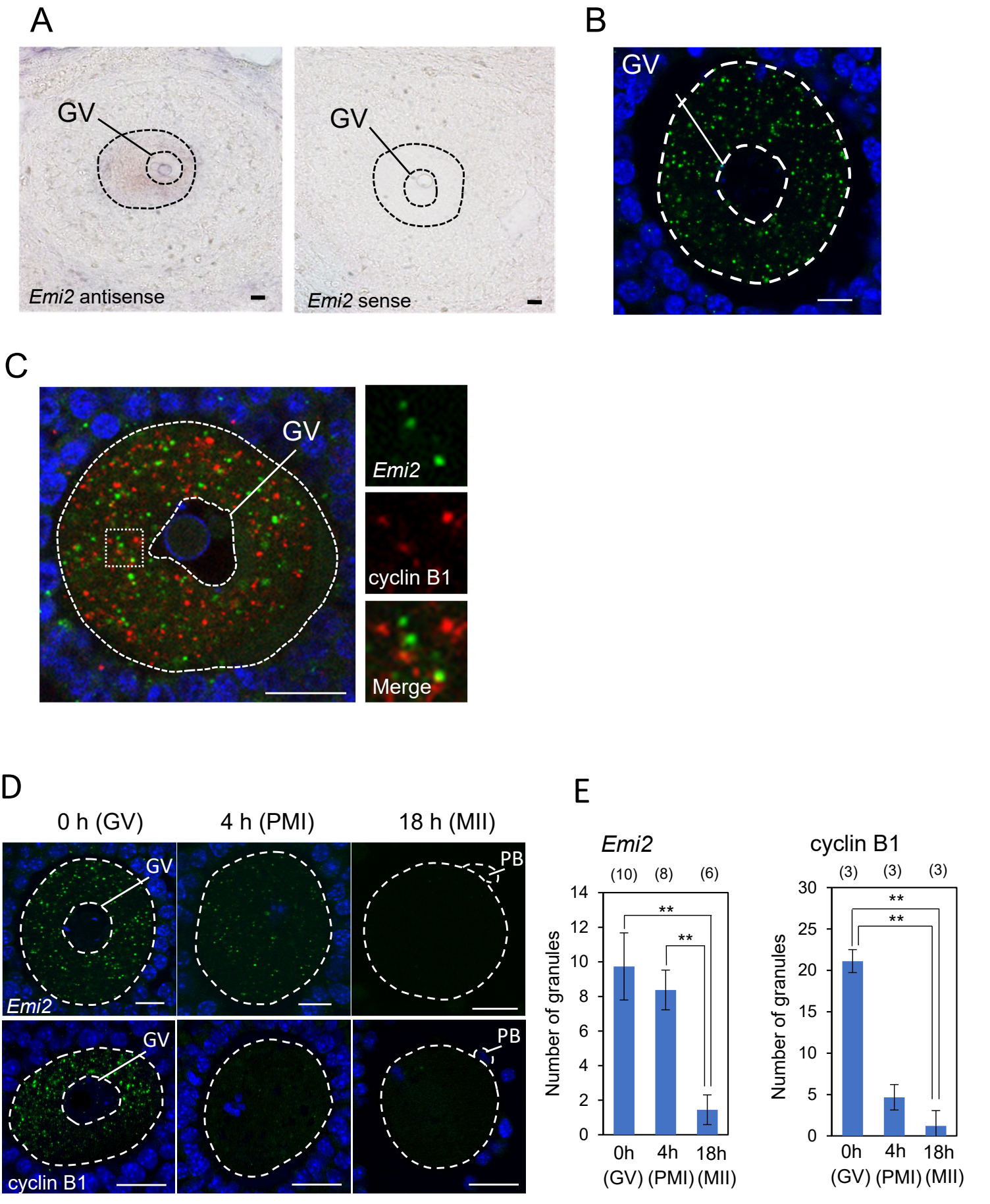
A
GV
Emi2 antisense
GV
Emi2 sense
B
GV
C
GV
Emi2
cyclin B1
Merge
D
0 h (GV)
4 h (PMI)
18 h (MII)
GV
PB
Emi2
GV
PB
cyclin B1
E
Emi2
(10) (8) (6)
Number of granules
0h (GV)
4h (PMI)
18h (MII)
cyclin B1
(3) (3) (3)
Number of granules
0h (GV)
4h (PMI)
18h (MII)

Fig. 23. **Interaction of RNA-binding proteins with *Emi2* mRNA.**
(A-C) Immunoblotting of mouse ovary extracts before IP (Initial) and IP with control IgG (IgG) or anti-Pum1 antibody (α-Pum1) (A), anti-HuR (α-HuR) (B) and anti-HuB (α-HuB) (C). Semi-quantitative RT-PCR amplification for *Emi2,* cyclin B1 *and α-tubulin* transcripts. Graphs show the quantitative of RT-PCR (means ± standard deviations; n = 3 or 4). *t*-test: * $P < 0.05$, ** $P < 0.01$.

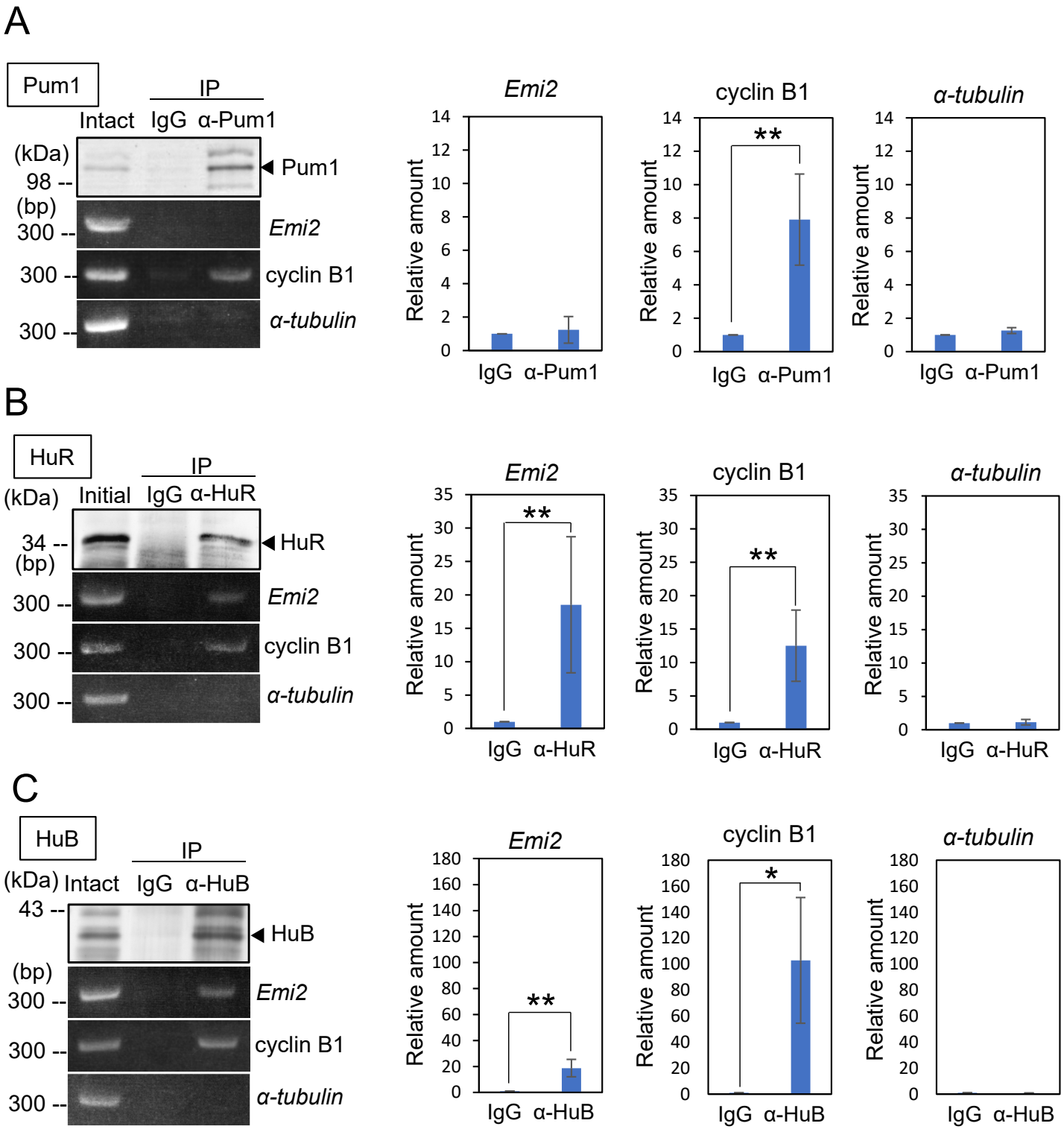
A
Pum1
IP
Intact IgG α-Pum1
(kDa)
98 --
Pum1
(bp)
300 --
Emi2
300 --
cyclin B1
300 --
α-tubulin
Emi2
cyclin B1
α-tubulin
Relative amount
IgG α-Pum1
**
B
HuR
IP
(kDa) Initial IgG α-HuR
34 --
HuR
(bp)
300 --
Emi2
300 --
cyclin B1
300 --
α-tubulin
C
HuB
IP
(kDa) Intact IgG α-HuB
43 --
HuB
(bp)
300 --
Emi2
300 --
cyclin B1
300 --
α-tubulin
IgG α-HuR
IgG α-HuB
*

Fig. 24. **Proteins interacting with *Emi2* and cyclin B1 mRNAs *in vitro*.** Venn diagram depicts the number of proteins isolated as proteins interacting with 3'UTR sequences of x*Emi2* (red), m*Emi2* (blue) and mcyclin B1 (green) with the number of overlapping proteins. Keratin and ribosomal proteins were excluded.

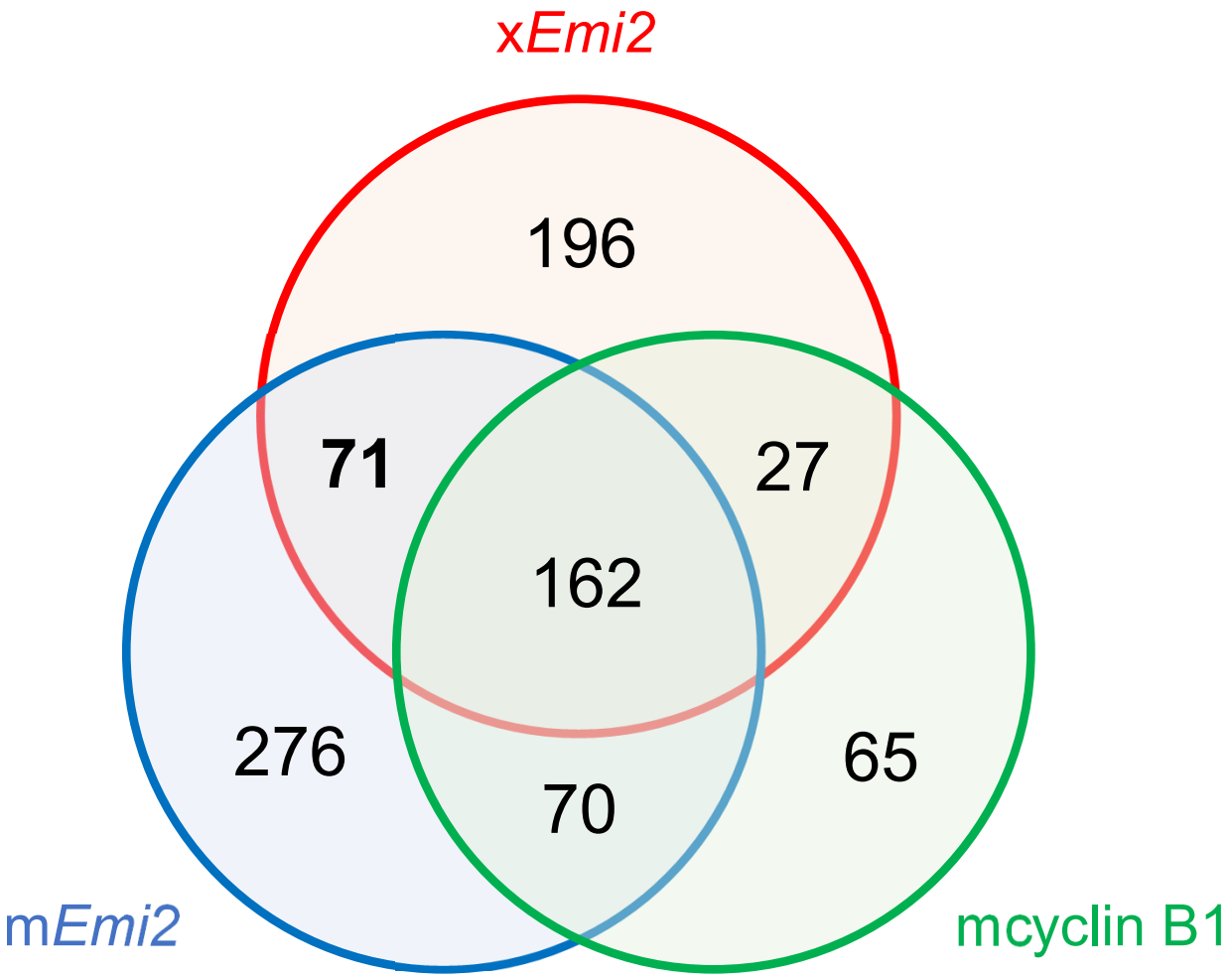
xEmi2
196
71
27
162
276
70
65
mEmi2
mcyclin B1

Fig. 25 **Expression of TDRD3 in mouse ovaries and oocytes, and synthesis of deleted TDRD3 in rabbit reticulocyte lysate.** (A) RT-PCR amplification for *Hdlbp*, *HuB*, *Hnrmpm*, *Ddx4* and *Tdrd3* mRNAs in the mouse ovary. (B) RT-PCR amplification for *Tdrd3* mRNA and immunoblotting of TDRD3 in the extracts of mouse ovary and oocyte. (C) Schematic diagrams of TDRD3, N-terminus of TDRD3 (1-473 aa) and C-terminus of TDRD3 (246-744 aa). (D) Immunoblot analysis for the translation of FLAG-tagged TDRD3 (1-473 aa) and TDRD3 (246-744 aa) in rabbit reticulocyte lysate by anti-FLAG (α-FLAG) and anti-TDRD3 (α-TDRD3) antibodies. Since the anti-TDRD3 antibody recognized the residues near the C-terminus of TDRD3. N-terminus of TDRD3 was not detected by this antibody. (E) Immunoblot analysis for the translation of FLAG-tagged TDRD3 in rabbit reticulocyte lysate with (+) or without (-) anti-FLAG antibody. Arrows and parentheses indicate FLAG-tagged TDRD3 fragments.

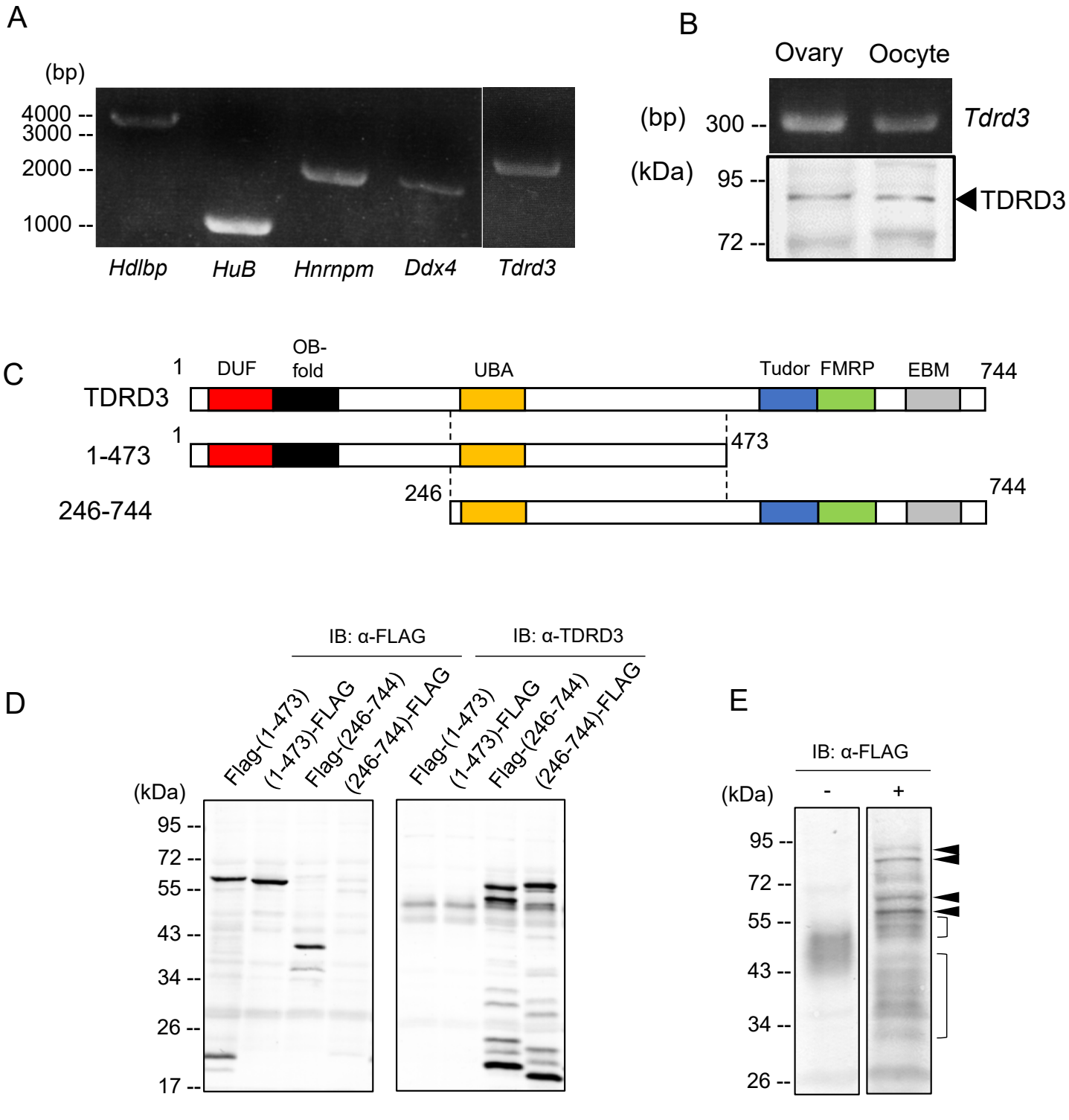
A
(bp)
4000 --
3000 --
2000 --
1000 --
Hdlbp
HuB
Hnrnpm
Ddx4
Tdrd3
B
Ovary
Oocyte
(bp)
300 --
Tdrd3
(kDa)
95 --
72 --
TDRD3
C
TDRD3
1
DUF
OB-fold
UBA
Tudor
FMRP
EBM
744
1-473
473
246-744
246
D
IB: α-FLAG
IB: α-TDRD3
Flag-(1-473)
(1-473)-FLAG
Flag-(246-744)
(246-744)-FLAG
(kDa)
95 --
72 --
55 --
43 --
34 --
26 --
17 --
E
IB: α-FLAG
(kDa)
-
+
95 --
72 --
55 --
43 --
34 --
26 --

Fig. 26. **Detection of interaction between TDRD3 and 3'UTR of *Emi2* mRNA by UV cross-linking.** (A) UV-cross linking assay of 3'UTR of *Emi2* and cyclin B1 mRNA with FLAG-CPEB1. Existence of FLAG-CPEB1 is indicated in upper panel. DIG-labeled probes that interact with FLAG-CPEB1 were detected in lower panel. (B, left) UV-cross linking assay of 3'UTR of *Emi2* and cyclin B1 mRNA with TDRD3-FLAG. Existence of TDRD3-FLAG is indicated in upper panel. DIG-labeled probes that interact with TDRD3-FLAG were detected in lower panel. (B, right) Quantitative analysis for protein-RNA complexes in (B) (means ± standard deviations; n =4). The statistical significance was analyzed by Tukey-Kramer test. $^{**}P < 0.01$. (C, left) UV-cross linking assay of 3'UTR of *Emi2* and cyclin B1 mRNA with TDRD3 (1-473 aa)-FLAG. Existence of TDRD3 (1-473 aa)-FLAG is indicated in upper panel. DIG-labeled probes that interact with TDRD3 (1-473 aa)-FLAG were detected in lower panel. (C, right) Quantitative analysis for protein-RNA complexes in (C) (means ± standard deviations; n =2).

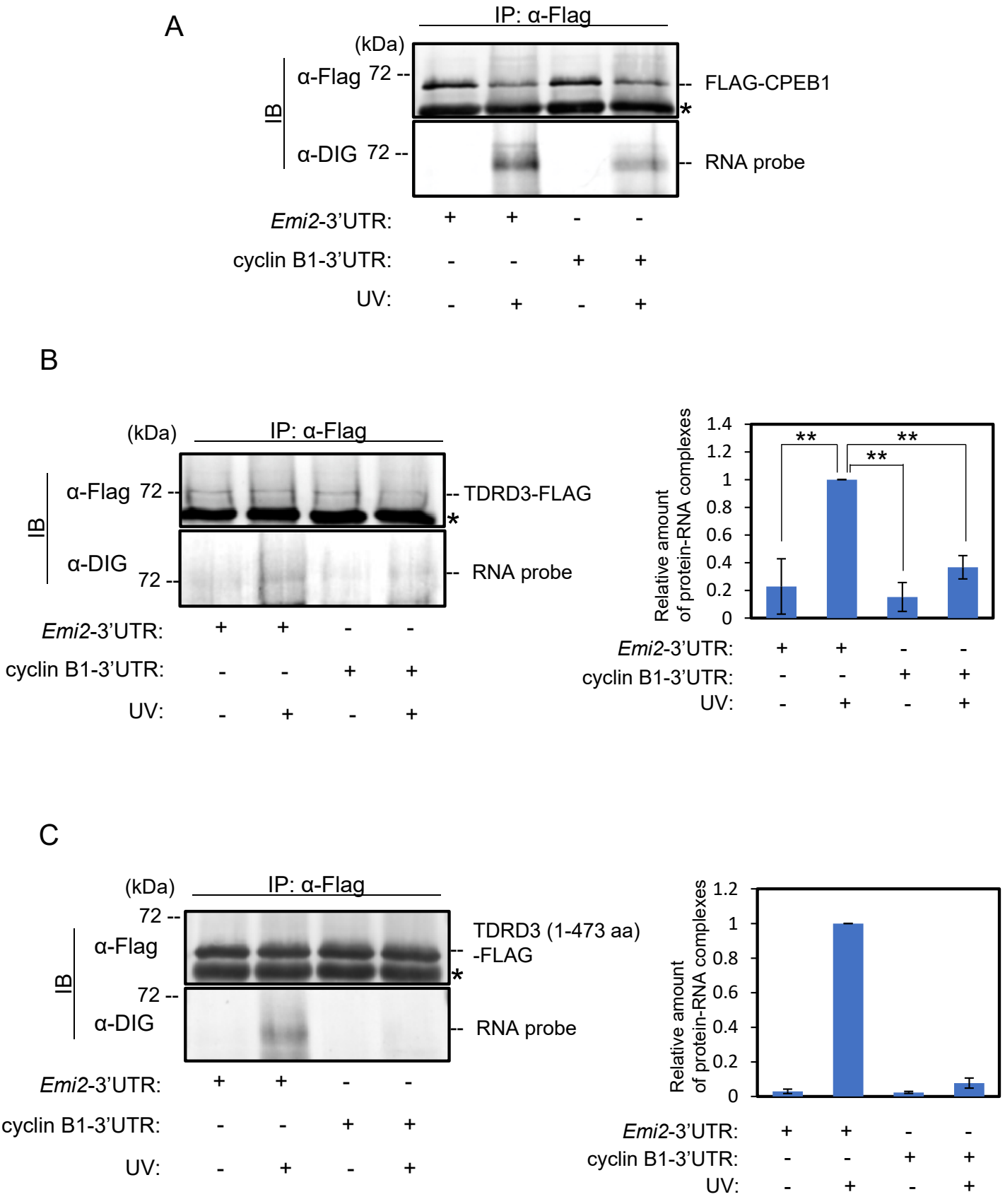
A
IP: α-Flag
(kDa)
IB
α-Flag 72 --
α-DIG 72 --
-- FLAG-CPEB1
*
-- RNA probe
Emi2-3'UTR: + + - -
cyclin B1-3'UTR: - - + +
UV: - + - +
B
(kDa)
IP: α-Flag
IB
α-Flag 72 --
α-DIG 72 --
-- TDRD3-FLAG
*
-- RNA probe
Emi2-3'UTR: + + - -
cyclin B1-3'UTR: - - + +
UV: - + - +
Relative amount of protein-RNA complexes
1.4
1.2
1
0.8
0.6
0.4
0.2
0
**
**
**
Emi2-3'UTR: + + - -
cyclin B1-3'UTR: - - + +
UV: - + - +
C
(kDa)
IP: α-Flag
72 --
IB
α-Flag
72 --
α-DIG
TDRD3 (1-473 aa)
-FLAG
*
-- RNA probe
Emi2-3'UTR: + + - -
cyclin B1-3'UTR: - - + +
UV: - + - +
Relative amount of protein-RNA complexes
1.2
1
0.8
0.6
0.4
0.2
0
Emi2-3'UTR: + + - -
cyclin B1-3'UTR: - - + +
UV: - + - +

Fig. 27. **Simultaneous detection of RNA-binding protein, TDRD3 and Pum1, and mRNA, *Emi2* and cyclin B1.** (A, left) Immunofluorescence of TDRD3 in immature oocytes. (right) An enlarged view of the boxed region. Similar results were obtained from two independent experiments. (B) Double immunofluorescence of TDRD3 (red) and Pum1 (green) in immature oocytes. Similar results were obtained from two independent experiments. (C) FISH analysis of *Emi2* mRNA (green) and TDRD3 (red) (left) or Pum1 (red) (right). Arrows indicate TDRD3 overlapped with *Emi2* RNA granules. (D) FISH analysis of cyclin B1 mRNA (green) and TDRD3 (red) (left) or Pum1 (red) (right). Arrows indicate Pum1 overlapped with cyclin B1 RNA granules. DNA is show in blue. GV, germinal vesicle. Bars: 10 μm in A and B, 2 μm in C and D.

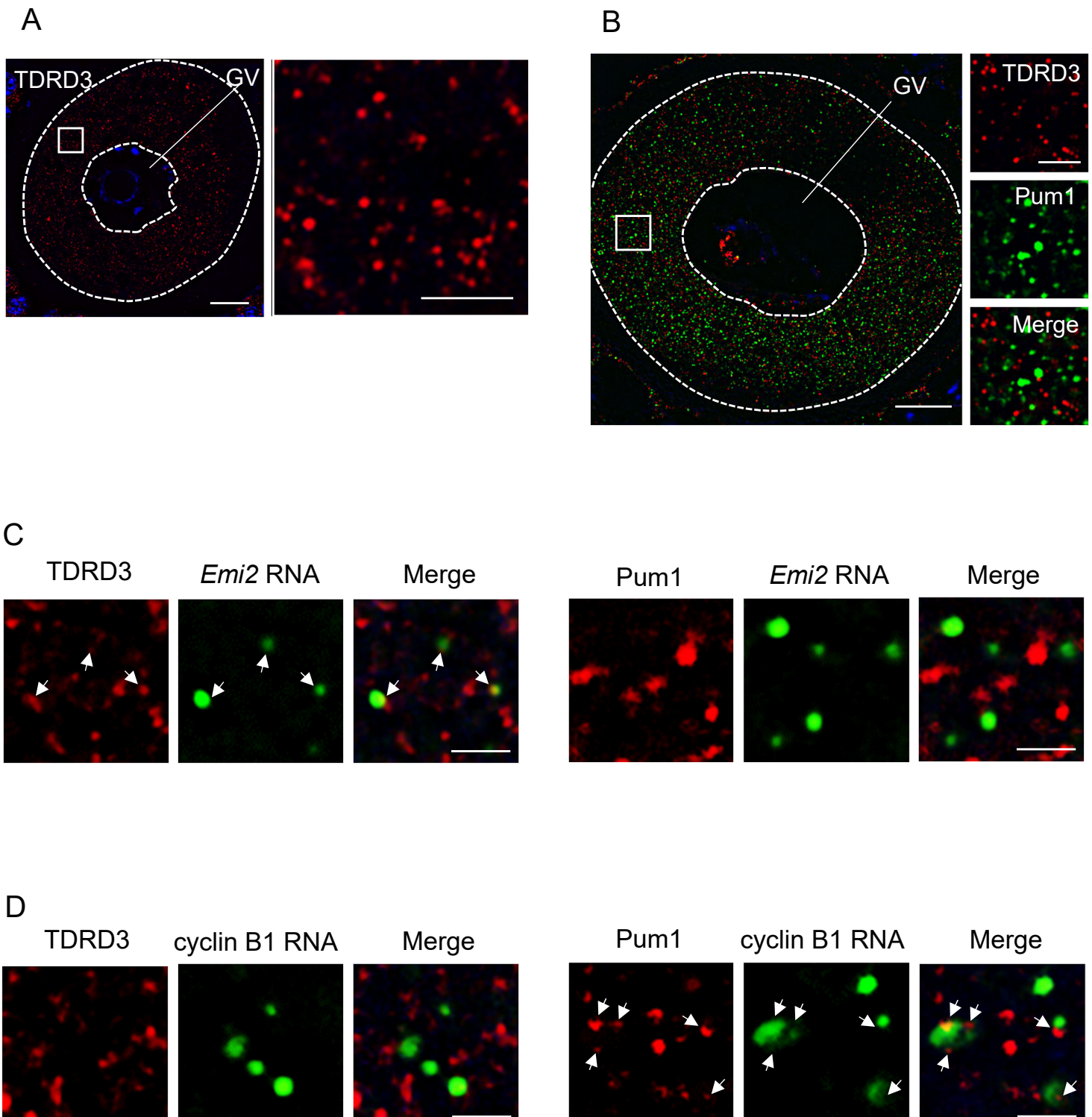
A
TDRD3
GV
B
GV
TDRD3
Pum1
Merge
C
TDRD3
Emi2 RNA
Merge
Pum1
Emi2 RNA
Merge
D
TDRD3
cyclin B1 RNA
Merge
Pum1
cyclin B1 RNA
Merge

Fig. 28. **Inhibition of TDRD3 by anti-TDRD3 antibody delays the timing of translation of EMI2 protein.** (A) Immunoblotting of EMI2, cyclin B1 and Mad2 in anti-TDRD3 antibody and IgG injected oocytes at 0, 8, 12, and 18 h after resumption of meiosis. (B) Quantitative analysis for the amount of EMI2, cyclin B1 and Mad2 in (A) (means ± standard deviations; n =3). *t*-test: * $P < 0.05$, ** $P < 0.01$. (C) Timing of PB1 extrusion in IgG and anti-Tdrd3 antibody-injected oocytes.

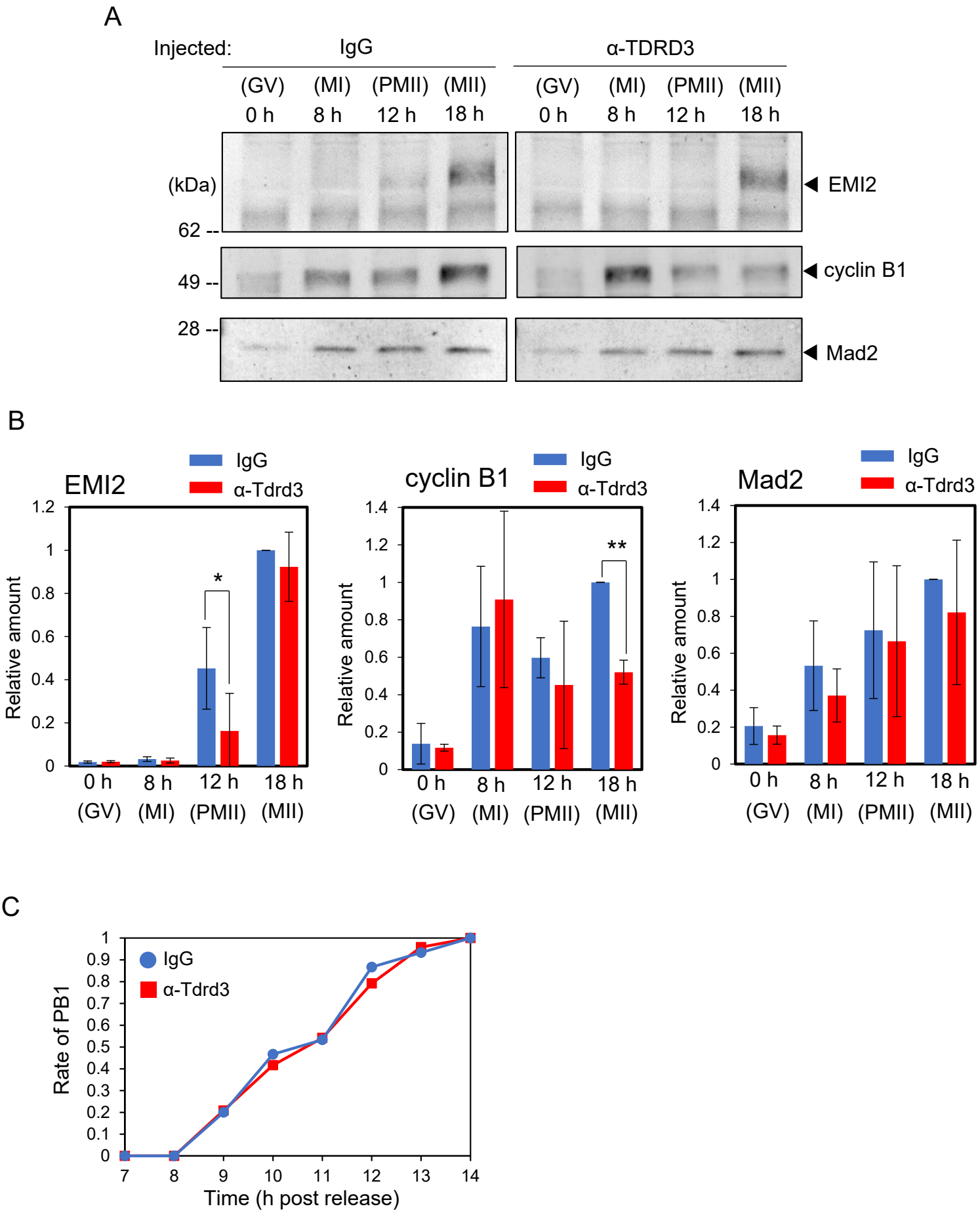
A
Injected:
IgG
α-TDRD3
(GV) 0 h
(MI) 8 h
(PMII) 12 h
(MII) 18 h
(kDa)
62 --
49 --
28 --
EMI2
cyclin B1
Mad2
B
EMI2
cyclin B1
Mad2
IgG
α-Tdrd3
Relative amount
0 h (GV)
8 h (MI)
12 h (PMII)
18 h (MII)
*
**
C
Rate of PB1
Time (h post release)
IgG
α-Tdrd3